

CZECH TECHNICAL UNIVERSITY IN PRAGUE
FACULTY OF ELECTRICAL ENGINEERING
DEPARTMENT OF ELECTROMAGNETIC FIELD



Organic LED-based visible light communications

DOCTORAL THESIS BY ZAHRA NAZARICHALESHTORI

Ph.D. PROGRAMME: ELECTRICAL ENGINEERING AND
INFORMATION TECHNOLOGY [P2612]
BRANCH OF STUDY: RADIOELECTRONICS [2601V010]

SUPERVISOR: Prof. Ing. STANISLAV ZVÁNOVEC, Ph.D.
CO-SUPERVISOR: Prof. Zabih Ghassemlooy

2021

Declaration of Originality

I, the undersigned, hereby declare that this doctoral thesis is the result of my research in our research team and my contribution corresponds to that specified at the beginning of each research chapter. The thesis was written under the professional supervision of Prof. Stanislav Zvánovec and Prof. Zabih Ghassemlooy, using the literature and resources listed in the Bibliography and References.

In Prague, 2021

.....
Ing. Zahra Nazarichaleshtori

Acknowledgement

Firstly, I would like to express my thanks to my supervisor Stanislav Zvanovec, who supported and guided me during my studies and gave me the opportunity to be a part of a great team of people. Many thanks also belong to our optical team, it was my pleasure to collaborate with them on optic topics.

I would like to acknowledge Fary Ghassemlooy for the opportunity to spend 6 months at Northumbria University and his opinions and advice, which have significant impact on the results presented in this thesis. I would like to thank Andrew Burton and Petr Chvojka for their support and advice.

Finally, special thank goes to my family and my husband for their never ending support and patience.

Abstract

Visible light communication (VLC) systems relies on light emitting diodes (LEDs), organic light emitting diodes (OLEDs) and laser diodes to provide illumination and data broadcasting, simultaneously. The thesis focuses on utilization of OLEDs for VLC systems. OLEDs has recently attracted significant attention as offering tremendous advantages such as transparent displays, environmentally friendly, low power consumption, and large active areas. Moreover, the potential of manufacturing OLEDs on flexible substrate offers an attractive feature of having curved OLED panels/displays. The interest into adopting OLEDs in indoor environments have been growing, which provides us with a significant potential of facilitate simultaneously illumination, display, and data communication. Since OLEDs are being producing in different shapes and sizes, the necessity of comprehensive characterization of a range of rigid and flexible OLEDs is obvious if they are going to be fully exploited in VLC. Based on OLED characterization the beam pattern of curved OLED has been derived with a symmetrical and wider than Lambertian characteristic which follows the three-term Gaussian profile. An experimental test-bed which utilize a number of those OLEDs transceiver with a multiband carrierless amplitude and phase modulation (*m*-CAP) has been developed. In addition, the impact of beam pattern of curved OLED on the VLC channel characteristics has been derived in terms of optical path loss and RMS delay spread for the cases when the curved OLED is used as a transmitter in empty and furnished indoor environments, i.e., shopping mall, office, corridor and semi-open corridor, with different scenarios.

Key Words

Optical wireless communication, visible light communication, organic light emitting diodes.

Abstrakt

Komunikační systémy ve viditelném světle (visible light communication, VLC) založené na LED diodách, organických LED (OLED) a laserových diodách, mohou poskytovat jak osvětlení tak i přenos dat zároveň. Disertační práce se zaměřuje na využití OLED pro systémy VLC. OLEDs nedávno přilákaly významnou pozornost, protože nabízejí výhody, jako jsou průhledné displeje, technologie šetrné k životnímu prostředí, nízkou spotřebu energie či velké aktivní oblasti. Navíc, potenciál výroby OLED na pružném substrátu nabízí atraktivní funkce se zakřivenými OLED panely/displeji. Zájem o použití OLED ve vnitřních prostorech roste, což nám poskytuje značný potenciál pro usnadnění současného osvětlení, využití displej tak i datové komunikace. Protože OLED se vyrábějí v různých tvarech a velikostech, je nutná komplexní charakterizace celé řady pevných a flexibilních/ohebných OLED pro plné využití v VLC komunikacích. Na základě charakterizace OLED byl odvozena charakteristika vyzařování ohebného OLED panelu jako symetrická a širší než Lambertianův profil s Gaussovým profilem třetího řádu. Byl vyvinut experimentální spoj s OLED transceiverem využívající *m*-CAP modulaci. Dále byl odvozen vliv ohebné OLED na charakteristiky VLC kanálu (ztráty a RMS rozprostření zpoždění) pro případy, kdy je ohebná OLED použita jako vysílač v prázdných a zařízených vnitřních prostředích, zejména pro nákupní centra, kanceláře, chodby a pootevřené chodby, a různé scénáře pokrytí.

Klíčová Slova

Optické bezdrátové komunikace, komunikační systémy ve viditelném světle, organické LED diody.



Contents

	Page
1 Introduction	1
2 State-of-the-Art	5
2.1 Optical Channel	5
2.2 System Performance	8
2.3 Equalization in visible light communication (VLC)	8
2.4 Modulation Schemes	12
3 Organic-based VLC System	15
3.1 Principle of Organic Devices	15
3.2 Literature Review of organic-based vlc (OVLC)	18
4 Objectives of the Thesis	21
5 Achieved Results	23
5.1 Comprehensive Optical and Electrical Characterization and Evaluation of Organic Light-Emitting Diodes for Visible Light Communication	25
5.2 A Flexible OLED based VLC Link with <i>m</i> -cap Modulation	41
5.3 Performance Evaluation of Various Training Algorithms for artificial neural network equalizer (ANN) Equalization in Visible Light Communications with an Organic LED	48
5.4 Coverage of a Shopping Mall with Flexible OLED-based Visible Light Communications	54
5.5 Utilization of an OLED-Based VLC System in Office, Corridor, and Semi-Open Corridor Environments	67
6 Conclusion and Future Work	83
References	85
Author's Publications	91
Curriculum Vitae	94



Abbreviations

ANN	Artificial Neural Network Equalizer
AWGN	Additive White Gaussian Noise
BER	Bit Error Rate
BLW	Baseline Wander
C2C	Car to Car
CAP	Carrier-less Amplitude and Phase Modulation
CG	Conjugate-Gradient
CGP	Conjugate Gradient Back-Propagation
CIR	Channel Impulse Response
D2D	Device to Device
DFE	Decision Feedback Equalizer
DMT	Discrete Multitone Modulation
FOV	Field of View
FPGA	field programmable gate array
FSO	Free Space Optics
I2D	Infrastructure to Device
IM/DD	Intensity Modulation/Direct Detection
IR	Infrared
ISI	Inter Symbol Interference
IoT	Internet of Things
LCD	Liquid Crystal Display
LD	Laser Diode
LED	Light Emitted Diode
LM	Levenberg-Marquardt Back-Propagation
LMMSE	Linear Minimum Mean-Square-Error
LMS	Least Mean Squares
LOS	Line of Sight
MPPM	Multiple PPM
NLOS	Non Line of Sight
NN	Neural Network
NRZ	Non Return Zero

O-SEFDM	Optical Spectrally Efficient Frequency Division Multiplexing
OE	Optical to Electrical
OFDM	Orthogonal Frequency Division Multiplexing
OLED	Organic Light Emitted Diode
OOK	On-Off Keying
OPD	Organic Photo Detector
OPL	Optical Path Loss
OPV	Organic Photovoltaics
OVLC	Organic-based VLC
OWC	Optical Wireless Communication
PAM	Pulse Amplitude Modulation
PAPR	Peak to Average Power Ratio
PD	Photo Detector
PPM	Pulse Position Modulation
PRBS	Pseudo Random Binary Sequence
PWM	Pulse Width Modulation
QAM	Quadrature Amplitude Modulation
RC	Resistor Capacitor
RF	Radio Frequency
RLS	Recursive Least Squares
RMS	Root mean square
RZ	Return Zero
Rx	Receiver
SCG	Scaled Conjugate-Gradient
SNR	Signal to Noise Ratio
SSL	Solid State Lighting
TIA	Trans-Impedance Amplifier
TV	Television
Tx	Transmitter
UV	UltraViolet
VL	Visible Light
VLC	Visible Light Communication
VOOK	Variable OOK
VPPM	Variable PPM
WDM	Wavelength Division Multiplex
ZF	zero-forcing equalizer
<i>m</i> -CAP	Multi Carrier-less Amplitude Phase Modulation



List of Symbols

Symbol	Description
$y(t)$	regenerated electrical signal
$x(t)$	emitted optical intensity
$h(t)$	CIR
$n(t)$	noise
N_o	one-sided power spectral density
A_{PD}	effective area of PD
d_{LOS}	distance between Tx and Rx
T_s	optical filter gain
g	optical concentrator gain
m_L	Lambertian emission
$H(0)$	channel DC gain
$dH_{LOS}(0)$	DC channel gain of the LOS path
$dH_{NLOS}(0)$	DC channel gain of the NLOS path
d_1	distances between Tx and wall
d_2	distances between wall and a point on the receiving surface
dA_{wall}	size of the reflective area
P_R	total received power
P_E	emitted optical power
P_R	received optical power
R_b	data rate
B_C	channel capacity
W	available bandwidth in the channel
w_j	tap weight coefficients of ZF equalizer
y_n	ZF equalizer inputs
q_n	ZF equalizer outputs
Z^{-1}	delay in ZF equalizer
T_b	symbol period
a	slope parameter of the log-sigmoid function
f_c	cut-off frequency of the low-pass filter
R	effective resistance of OLED

C_o	plate capacitance of OLED
A_t	OLED photoactive area
d_t	OLED thickness
B_{mod}	modulation bandwidth
γ	PD responsivity
\otimes	convolution
η	LOS path gain
$\delta(t)$	Dirac delta function
Δt	time delay of the LOS path
θ	irradiance angle
Ψ	incident angle
Ψ_{FOV}	field of view (FOV) of Rx
β	angle of irradiance from the reflective area of the wall
α	angle of irradiance to the wall
ρ	surface reflection coefficient
τ	channel mean excess delay
τ_{RMS}	RMS delay spread
ξ	filter oversampling rate
μ	step-size parameter in LMS algorithm
∇	gradient descent
$\varphi(v)$	log-sigmoid function
ϵ_0	permittivity of free space
ϵ_r	relative dielectric constant of the organic layer

One of a branch of communication is optical wireless communication (OWC) operating in both the indoor and outdoor environments; with split into three categories based on their operating wavelength; ultraviolet (UV), visible light (VL) and infrared (IR), see [Figure 1.1](#). The invention of the laser by T. H. MainamIn in 1960, caused a new are of OWC [1]. As the 6328-Å helium-neon laser was discovered in 1962, the first OWC link employing laser to send data through the air channel with span of 30 km was performed by a Hughes group [1]. The era of indoor free space optics (FSO) communication was initiated in 1979 by F. R. Gfeller and U. Bapst as they suggested the utilization of diffuse emissions in the IR band for indoor communications [2]. Following, Kanh and Barry represented a indoor wireless IR channel characterization in [3].

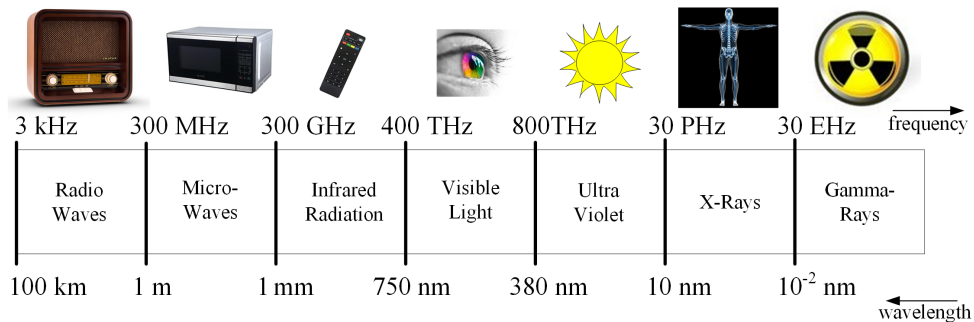


Figure 1.1: Electromagnetic spectrum

The next candidate from OWC is VLC, which has gained huge attention among researchers and industrial companies due to the rapid development of solid state lighting (SSL). VLC offers advantages over the radio frequency (RF) technologies such as inherent security, immunity to RF-based electromagnetic interference, license-free spectrum, being a green technology, and high scalability [4]. VLC relies conventional silicone based light emitted diode (LED)s, organic light emitted diode (OLED)s as well as white laser diodes as a light source to provide illumination and data communication, simultaneously [4]. LEDs offer several benefits over existing lighting infrastructures, such as lower power consumption, longer life expectancy, higher energy efficiency, reduced maintenance, lower heat generation characteristics and fast switching [4]. VLC systems must provide illumination for a SSL environment such as a home or office; the light spectrum produced must encompass the entire visible spectrum to produce white light. LEDs produce white

light with either a package that contains individual red, green, and blue (RGB) LEDs or a blue LED that has a yellowish phosphor encompassing the photoactive area, known as WPLEDs. The most common choice represent WPLEDs for two reasons; (i) no colour balancing is required to achieve a constant white hue and therefore the signal processing requirements are less, (ii) WPLEDs are cheaper than their RGB counterparts [5]. The gallium-based LED based VLC systems, which utilize blue light to excite yellowish phosphors to synthesize white light, have been extensively investigated in the literature [6–8]. Whereas the RGB and phosphor laser diode (LD)s based VLC require higher thermal stability of the phosphor due to a much greater optical power density [9]. Compared with the phosphor-based LD, the RGB LD is safer to the human eye due to low blue light component [10]. Moreover, VLC has vast untapped potential, given the millions of LED lamps already installed in streets, private houses, public buildings and offices which encouraged the VLC development. Thus, VLC has potential applications in a number of areas including smart lighting, indoor localization [11], vehicles and transportation, the internet of things (IoT) [12], underwater communication [13] and electromagnetic interference-sensitive or security-sensitive scenarios [14, 15]. In 1979, F. R. Gfeller and G. Bapst demonstrated the technical feasibility of indoor OWC using infrared LEDs [16]. In [17], VLC at low data rates was investigated as built upon fluorescent lamps. The fast switching feature of LEDs prompted researches on high-speed VLC. A concept of using the traffic light LED as the optical signal transmitter was proposed by Pang et al. in 1999. Next, at Keio University in Japan, the use of white LED for access networks were carried out by S. Haruyama and M. Nakagawa proposed [18]. The effects of light reflection and shadowing on the system performance were analyzed, and VLC applications at relatively low rates were explored. The first IEEE standard for visible light communication was proposed in 2011 in the form of IEEE 802.15.7 [19] and one year later standard supplement for modulation scheme and dimming was published in [20].

In this work, we focus on the use of OLEDs for VLC systems. The emissive electroluminescent layer in OLED is a film of organic compounds which makes OLEDs lighter, more flexible, and thinner with small total stack thickness of between 100 and 500 nm than the crystalline layers in LEDs or liquid crystal display (LCD) devices [21]. OLEDs offer more attractive advantages, including transparent displays, environmentally friendly, biodegradable, rich color, low power consumption, large active areas, and bright with no need for backlight as in LCD. Resulting in growing interest into adopting OLEDs over the conventional SSL in indoor environments for soft lighting and display applications as well as using in wearable products (i.e., smart watches and wearable computers). That leads to providing the potential of infrastructure to device (I2D) and device to device (D2D) communications.

In the first part of the doctoral thesis, state-of-the-art VLC is presented in [chapter 2](#) focusing on channel characterization, system performance, equalization theory and mod-

ulation schemes. In [chapter 3](#) the principle of organic devices, and a survey containing an overview and application of OLEDs in VLC technologies are discussed. The objectives of the thesis are given in [chapter 4](#). Then, the thesis core is demonstrated in [chapter 5](#) by a collection of journal papers presenting a description of their contributions and relevance to the thesis topic. In the end, the achieved results and future research topics are summarized.

A typical VLC link transfers data via modulation of LED/OLED through an optical channel towards a receiver. In this chapter, the basic principles of a VLC systems as well as the theory of modulation schemes, and equalization are outlined. In addition, characterizing a VLC channel in term of channel impulse response (CIR), channel delay spread and channel capacity is presented. Finally, the receiver part is discussed with emphasis on system performance evaluation. The following subsections describe the state-of-the-art as it relates to the goals of this thesis.

2.1 Optical Channel

The physical indoor VLC channel includes the effects of both components line of sight (LOS), where the LED is aligned directly with the receiver (Rx), and non line of sight (NLOS), where the signal is captured via walls and ceiling reflections [4]. Figure 2.1 illustrates a block diagram of a typical (O)VLC link. The desired modulation format can be created either by MATLAB or by a field programmable gate array (FPGA) using shift registers. The data generated by a pseudo random binary sequence (PRBS) is modulated prior to intensity modulation of the light source via the driving circuit. To meet the optical power constraint a DC bias can be adopted. Following, the optical signal transmitted over the wireless channel is captured by a photo detector (PD), and the regenerated electrical signal is given as [4]:

$$y(t) = \gamma \cdot x(t) \otimes h(t) + n(t) \quad (2.1)$$

where $x(t)$ is the emitted optical intensity, γ is the PD responsivity in (A/W), $h(t)$ is the CIR and \otimes denotes convolution. $n(t)$ represents the noise, which is modeled as the signal independent additive white gaussian noise (AWGN) with one-sided power spectral density N_0 . If the NLOS component is neglected, the CIR of the indoor channel can be written as $h(t) = \eta\delta(t - \Delta t)$ where $\delta(t)$ is Dirac delta function, Δt is the time delay of the LOS path, and η is the LOS path gain [4]. We consider three criteria to quantify the limitation on the transmission rate through free space; channel gain and corresponding optical path loss (OPL), channel mean excess delay and root mean square (RMS) delay spread.

- **Channel DC Gain**

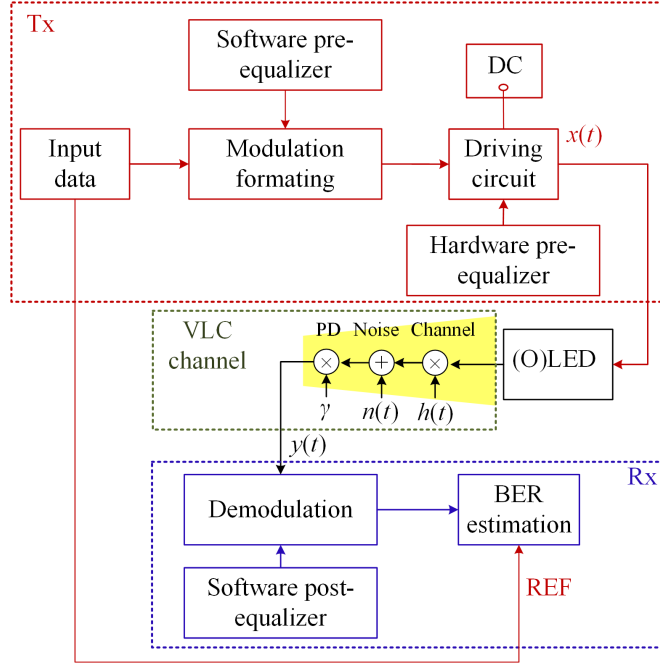


Figure 2.1: A block diagram of a typical (O)VLC link

The essential parameter characterizing an optical propagation channel is the channel impulse response, which is given as a superposition of LOS and NLOS signal components at the detector as $h(t) = h_{\text{LOS}}(t) + h_{\text{NLOS}}(t)$. The channel can be described either in terms of frequency response as $H(f) = \int_{-\infty}^{\infty} h(t)e^{-j2\pi ft} dt$. One of the most important features of a CIR is channel DC gain which defines the achievable signal to noise ratio (SNR) and is given as:

$$H(0) = \int_{-\infty}^{\infty} h(t)dt \quad (2.2)$$

The geometry of the transmitter (Tx), Rx, and surface reflectors for a typical indoor VLC system is shown in Figure 2.2. The LOS link gain, where Tx is considered to be a monochromatic point source with a Lambertian radiation pattern, can be expressed according to a model shown in Figure 2.2 is given by [22]:

$$H_{\text{LOS}}(0) = \begin{cases} \frac{A_{\text{PD}}(m_L+1)}{2\pi d_{\text{LOS}}^2} \cos^{m_L}(\theta) \cos(\Psi) g(\Psi) T_s(\Psi) & , 0 \leq \Psi \leq \Psi_{\text{FOV}} \\ 0 & , \Psi > \Psi_{\text{FOV}} \end{cases} \quad (2.3)$$

where A_{PD} is the effective area of the Rx photodiode, d_{LOS} represents the distance between the Tx and the Rx, θ stands for the irradiance angle with respect to n_s , and Ψ is the incident angle with respect to n_r (see Figure 2.2). $T_s(\Psi)$ is the optical filter gain, $g(\Psi)$ the optical concentrator gain, Ψ_{FOV} is the field of view (FOV) of the Rx

and m_L represents Lambertian emission, which is given by:

$$m_L = -\frac{\ln(2)}{\ln[\cos(\theta_{1/2})]} \quad (2.4)$$

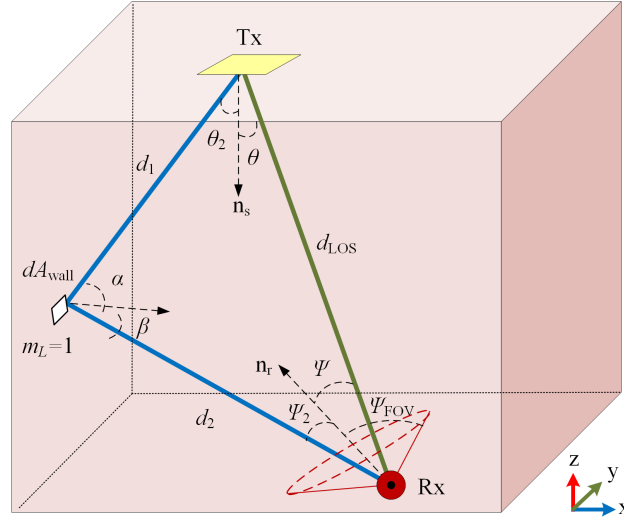


Figure 2.2: VLC link configuration for LOS and NLOS

The optical irradiation pattern profile determines the spatial intensity distribution of light emitted from the light source, which is a key feature to analyze the coverage of signal distributed in VLC links. A directed LOS link will provide the best signal quality where luminous intensity is maximized; (i.e., $\theta = 0^\circ$). Considering power due to the NLOS paths, the DC channel gain of the reflected path is given by [23]:

$$dH_{\text{NLOS}}(0) = \begin{cases} \frac{A_{\text{PD}}(m_L+1)}{2\pi d_1^2 d_2^2} \rho dA_{\text{wall}} \cos^{m_L}(\theta_2) \cos(\alpha) \cos(\beta) \\ \cos(\Psi_2) g(\Psi_2) T_s(\Psi_2) \\ 0 \end{cases}, \begin{cases} 0 \leq \Psi_2 \leq \Psi_{\text{FOV}} \\ \Psi_2 > \Psi_{\text{FOV}} \end{cases} \quad (2.5)$$

where β represents the angle of irradiance from the reflective area of the wall, α is the angle of irradiance to the wall, d_1 and d_2 are the distances between the Tx and the wall, and the wall and a point on the receiving surface, respectively, and dA_{wall} is the size of the reflective area with surface reflection coefficient defined as ρ . If we consider both multipath propagation and the LOS component, for the more general case, the total received power P_R is given by:

$$P_R = P_E H_{\text{LOS}}(0) + \int_{\text{walls}} P_E dH_{\text{NLOS}}(0) \quad (2.6)$$

- **OPL**

The optical signal attenuation caused by reflections and transmission in the free space is quantified by OPL. The OPL in dB can be given as:

$$\text{OPL} = -10 \log_{10}(H(0)) \quad (2.7)$$

- **Channel Delay Spread**

The RMS delay spread is commonly used to define time dispersion in wireless channels. The channel mean excess delay τ and the RMS delay spread τ_{RMS} are given as [8]:

$$\tau = \frac{\int_0^{\infty} t \times h(t) dt}{\int_0^{\infty} h(t) dt} \quad (2.8)$$

$$\tau_{\text{RMS}} = \sqrt{\frac{\int_0^{\infty} (t - \tau)^2 \times h(t) dt}{\int_0^{\infty} h(t) dt}} \quad (2.9)$$

2.2 System Performance

For intensity modulation/direct detection (IM/DD) optical transmission systems, the electrical SNR is defined as:

$$\text{SNR} = \frac{(\gamma P_R)^2}{R_b N_o} = \frac{(\gamma H(0) P_E)^2}{R_b N_o} \quad (2.10)$$

where P_E and P_R are the emitted and received optical power, respectively, and R_b is data rate. Considering a channel with non return zero (NRZ)-on-off keying (OOK) and return zero (RZ)-OOK modulation, bit error rate (BER) is given as, respectively [24]:

$$\text{BER} = \frac{1}{2} \text{erfc}\left(\frac{1}{2\sqrt{2}} \sqrt{\text{SNR}}\right) \quad (2.11)$$

$$\text{BER} = \frac{1}{2} \text{erfc}\left(\frac{1}{2} \sqrt{\text{SNR}}\right) \quad (2.12)$$

The channel capacity B_C is defined in b/s based on the available bandwidth in the channel W and SNR (in linear scales) using the Shannon-Hartley theorem [25]:

$$B_C = W \log_2(1 + \text{SNR}) \quad (2.13)$$

2.3 Equalization in VLC

Equalizers represent one of the most effective techniques to compensate multipath induced inter symbol interference (ISI) in band-limited communication systems. When data rate transmission exceeds the system bandwidth leads to ISI. The equalizer employ a linear transversal filter to inverse the undesirable effects of the system response. Generally, equalizers can be classified into two categories; analog and digital with different complexity and performance. Although an analog domain equalizer is simple, based on a high pass resistor capacitor (RC) filter [26] can result in attenuation of low frequency components, and hence, the baseline wander (BLW) phenomenon. On the other hand, digital equalizers such as least mean squares (LMS) or recursive least squares (RLS)-based

zero-forcing equalizer (ZF), decision feedback equalizer (DFE) and ANN offer significant system performance improvement at the cost of increased complexity [27].

- **ZF equalizer with adaptive algorithm**

The linear filter most often used for equalization is the transversal filter shown in Figure 2.3 as it tries to force a flat magnitude response by removing the ISI. The ZF is a linear equalizer with a number of adjustable tap coefficients w_j , as illustrated in Figure 2.3. Its input is the sequence y_n given in Equation 2.1 and its output is the estimate of the information sequence q_n . The estimate of the n th symbol may be expressed as:

$$q_n = \sum_{j=0}^K w_{n+j} y_{n-j} \quad (2.14)$$

where w_j are the tap weight coefficients of the filter. The delay given by Z^{-1} is inversely proportional to the filter oversampling rate ξ and is either selected equal to the symbol period or at a frequency higher than the symbol rate, typically $\xi = T_b/2$ where T_b is symbol period). The estimate q_n is quantized to the nearest (in distance) information symbol. Considerable research has been performed on the criterion for optimizing the filter coefficients w_j . A desirable coefficient is chosen to minimize the average probability of error. Note, the probability of error as a performance index for optimizing w_j is computationally complex since the probability of error is a highly non-linear function of w_j . An increase in performance can be obtained if an adaptive algorithm is introduced to find the tap weights as illustrated by Figure 2.3. There are several adaptive algorithms, most notable are the LMS and RLS.

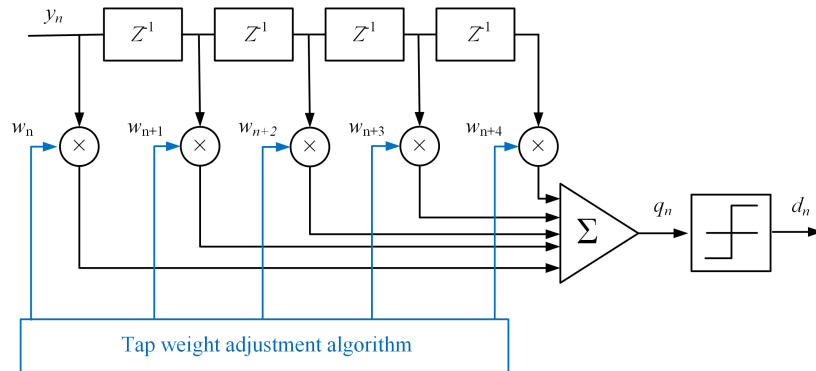


Figure 2.3: The Adaptive linear transversal equalizer

- **LMS algorithm**

In order to find the tap weights the adaptive algorithm requires training against a header sequence of data symbols that is known at the receiver. The LMS algorithm is a gradient vector descent (based on the minimum square error criterion) on an error cost function $J(n) = E\{e^2(n)\}$ and is very simple to implement due to the lack

of matrix inversions or correlation function calculations. The tap weights are given by:

$$w(n+1) = w(n) + \frac{1}{2}\mu[-\nabla J(n)], \quad 0 < \mu < 1 \quad (2.15)$$

where μ is the step-size parameter that controls the rate of convergence to the minimum square error and the dell operator ∇ indicates a gradient descent. A strategy that then can be used is to uses estimates of the auto-correlation matrix \mathbf{R} and the cross correlationen vector \mathbf{p} . If instantaneous estimates are chosen $\mathbf{R}(n) = x(n)x^H(n)$ and $\mathbf{p}(n) = x(n)d(n)$; the resulting method is the LMS algorithm, see [Figure 2.4](#). The gradient descent is an estimate given by $\nabla J(n) = -2\mathbf{p} + 2\mathbf{R}w(n)$. The update of the filter weights is given by:

$$w(n+1) = w(n) + \mu x(n)e(n) \quad (2.16)$$

where $e(n) = d(n) - y(n)$ and $y(n) = x^H(n)w(n)$.

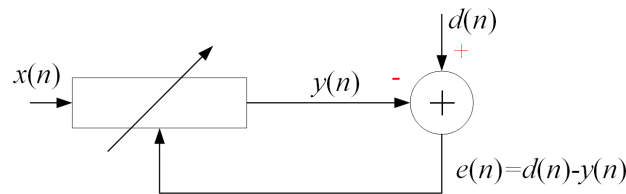


Figure 2.4: The LMS algorithm

- **ANN Equalizer**

The ANN takes loose inspiration from the human brain, which uses synapses and neurons to learn and compute. ANNs retain the neurons for computation and use tapped delay lines (in a transversal configuration) as the inputs. ANNs solve nonlinear problems via the neurons, which are divided into a parallel structure where the inputs to each neuron are scaled by an adaptive adjustable contribution of the synaptic weights of each input. Increasing the number of neurons boosts the ANN learning capacity while increasing complexity [28]. The structure of the model, the type of activation function, and the learning algorithm affect neural-network model implementation [29]. The block diagram in [Figure 2.5](#) illustrates the fundamental model of a neuron, which forms the basis for designing a large family of neural network (NN)s [30]. The neural model includes an externally applied bias b_k , which has the effect of increasing or lowering the contribution of each weighted input to the activation function. The output of the k_{th} neuron is given by $y_k = \varphi(v)$ where $v = u_k + b_k$ and u_k is the summed weighted contribution of the inputs defined as:

$$u_k = \sum_{j=1}^n w_{kj}x_j \quad (2.17)$$

where x_1, x_2, \dots, x_n are the input signals, and $w_{k1}, w_{k2}, \dots, w_{kn}$ are the weights of neuron k . Several activation functions are introduced in [30] including threshold function, piecewise linear function, and log-sigmoid function, however, any differentiable formulation may be used. In the following, a log-sigmoid function is considered for the hidden layer output and a linear function at the ANN output as is typical in the literature. An example of the log-sigmoid function, employed in this work, is defined by [30]:

$$\varphi(v) = \frac{1}{1 + e^{(-av)}} \quad (2.18)$$

where a is the slope parameter of the log-sigmoid function.

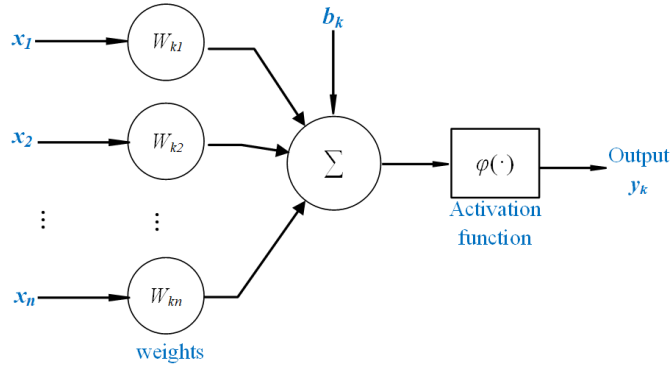


Figure 2.5: The neural network model

In general, there are four fundamentally different network architectures that can be used as an equalizer (i) feedforward single-layer; (ii) feedforward multilayer; (iii) feedback singlelayer; and (iv) feedback multilayer networks. In a multi-layer configuration, the neurons are organized as follows; an input layer consisting of an observation vector of incoming samples, a hidden layer where the processing occurs and an output layer. A recurrent (feedback) ANN is different to a feedforward NN in that has at least one feedback loop, see [30], which generally results in improvement in non-linear mapping at the cost of potential error propagation.

ANNs require a training sequence to adjust the neuron weights in order to map the input-output sequence of the system under test. For early stopping, algorithms update the neuron weights until the error between the equalized data and the target data does not exceed an objective error. It is also possible to allow ANN to run its training algorithm for objective epochs or seconds. There are a number of training algorithms (see Table 2.1) that could be used, which are also available in the Matlab [31, 32]. One of the most popular ones is levenberg-marquardt back-propagation (LM) [33]. The conventional form of the conjugate-gradient (CG) training algorithm requires a time-consuming line search but a modified version of it (i.e., scaled conjugate-gradient (SCG)) introduced by Møller [34] avoids the use of a line search. When comparing against other digital equalisation techniques,

ANNs offer several advantages: (i) generalization -due to input-output mapping, as opposed to ISI estimation, complex decision boundaries are created and hence, even when an error or bit sequence not included in the training sequence can be estimated [33]; and (ii) evidential response - to reject ambiguous patterns in classification, where a NN can provide information of particular pattern selected as well as the confidence in the decision made. ANNs have been palpable in communication systems as a result of their flexibility and learning capability. There are a large number of algorithms, which could be used for determining the network parameters and for training NNs. It is noticeable that the training algorithm and the network topology affect the performance of the NN. Therefore in this paper, we investigate the effect of the various network types and number of neurons in the hidden layer on the learning performance of the NN using LM, SCG, and conjugate gradient back-propagation (CGP) algorithms for feedforward networks. The training algorithms and their main features are summarized in Table 2.1 [32].

Table 2.1: The training algorithms [32]

Algorithm	Feature - Method used to update weight and bias values
Levenberg–Marquardt	
LM	Levenberg-Marquardt optimization
Conjugated gradient descent	
CGB	Conjugate gradient backpropagation
SCG	Scaled conjugate gradient method
CGP	Gradient backpropagation with Polak-Ribière updates
Resilient backpropagation	
RP	Resilient backpropagation algorithm
Quasi-Newton algorithm	
OSS	One-step secant method
BFG	BFGS quasi-Newton method

2.4 Modulation Schemes

There are two typical groups of modulation schemes for optical communications: (i) base-band modulations; and (ii) multi-carrier modulations. The most popular baseband schemes are OOK, pulse position modulation (PPM) or pulse amplitude modulation (PAM) [8]. The multi-carrier modulations include orthogonal frequency division multiplexing (OFDM) and carrier-less amplitude and phase modulation (CAP) modulation [35]. Since OVLC systems are highly bandlimited, a modulation scheme is desirable that can transmit more symbols-per-bit within a small modulation bandwidth B_{mod} . In addition, since LEDs have

dual functionality of illumination and data communications, then modulation schemes adopted should also offer dimming control. A number of modulation schemes have been developed with this features such as multiple PPM (MPPM) [36]. Furthermore, analysing the communications link performance in terms of power requirement and spectral efficiency η_s is essential. The most power efficient scheme is the high order L -PPM, but requires the largest bandwidth. In [37] it is shown that variable OOK (VOOK) requires the same power as variable PPM (VPPM) while its η_s is better than VPPM. In addition, under 50 % brightness, RZ-OOK should require 3 dB less power than VOOK with η_s of 1 b/s/Hz; however, RZ-OOK provides at most 50% brightness. The technique of optical-fast OFDM (O-FOFDM) reported in [38] aims to improve η_s by using half the bandwidth of OFDM, with the caveat that it is limited to one dimensional modulation formats. To achieve optical bandwidth saving, a dense OFDM (DOFDM) is employed by narrowing the spacing between two optical sub-channels in [39], while [40] proposed a higher number of sub-channels using Nyquist wavelength division multiplex (WDM) techniques. In [41] 50% electrical bandwidth saving is achieved using a mix of electrical and optical single sideband signal manipulation techniques. In addition, an optical spectrally efficient frequency division multiplexing (O-SEFDM) system was proposed in [42] to provide higher η_s relative to O-OFDM, where non-orthogonal and overlapping sub-carriers are employed so that the performance is the same as O-OFDM for bandwidth saving up to 25%. The O-SEFDM technique can also increase η_s in both electrical and optical domains. The CAP scheme was shown to outperform OFDM in terms of R_b using the same physical link in VLC [43]. CAP systems have several advantages over OFDM, a single carrier modulation is utilized rather than Fourier transform [44, 45]. In multi carrier-less amplitude phase modulation (m -CAP) the signal bandwidth is split into several subcarriers, where the attenuation caused by an LED frequency response is decreased. Therefore, VLC links by allocating different bandwidths for individual subcarriers, with high η_s (i.e., up to 36% improvement in R_b for 6-CAP) can be supported [46]. The first VLC experiment utilizing m -CAP was reported in [45] with R_b of 31.5 Mb/s using 10-CAP; thus resulting in η_s of 4.85 bps/Hz, which offers huge potential for a future research. Since the nonlinearity of the source degrades the system OVLC performance, therefore transmitting an OFDM signal results in intermodulation products between the subcarriers. In addition, giving that OFDM signals have a relatively high dynamic range, which is described often in the terms of the peak to average power ratio (PAPR), subcarriers can add constructively or destructively, thus leading to a large variation in the transmit signal power level. High PAPR means large saturation power for power amplifiers, which results in reduced power efficiency. To combat this, PAPR reduction techniques of signal scrambling and signal distortion (i.e., companding, signal clipping, peak windowing, envelope scaling, and peak reduction carrier) can be adopted. E.g., for OFDM-VLC in [47] an exponential nonlinear companding transformation techniques and in [48] an advanced A-law companding al-

gorithm were proposed. Alternative, in [49] a hybrid modulation scheme was proposed where the OFDM signal is converted to a pulse width modulation format prior to intensity modulation of the light source in order to mitigate the requirement for higher PAPR.

Organic-based VLC System

Semiconductor is considered organic if the materials are mainly carbon or nitrogen. Organic materials possess similar characteristics to metallic semiconductors and polymers concurrently [50]. These features are attractive for the emerging new type of electronics industry - organic electronics. The most popular devices are OLEDs and organic solar cells known as organic photovoltaics (OPV).

3.1 Principle of Organic Devices

- **OLEDs**

OLED display devices use organic carbon-based films, sandwiched together between two charged electrodes; one is a metallic cathode (aluminum or silver) and the other is a transparent anode (indium tin oxide (ITO)), see [Figure 3.1](#). The organic materials can be long-chain polymers (i.e., PLEDs) or small organic molecules (i.e., SMOLEDs) in a crystalline phase. The [Figure 3.2](#) shows a PLED structure along with a top view photograph of a single photoactive area PLED (3.5 mm²) as an inset, presented in [51]. When polymer semiconductors exposed to oxygen and water molecules in air undergo severe degradation. That introduce defects in the polymer acting as charge carrier traps [51]. Based on the PLED processing presented in [51], after oxygen plasma treatment of the cleaned ITO substrates, a hole-injection layer of PEDOT:PSS was deposited on top of the ITO. The emissive layer of poly was deposited from solution in toluene. In order to increase the inter-molecular interaction through the reorganization of the polymer chains which results in a higher bandwidth, the samples were annealed for 10 minutes above the glass transition temperature, at 150°C under nitrogen atmosphere. On top of the emissive layer a 30 nm of metallic calcium is evaporated as a cathode, covered by a protective layer of aluminum. PLEDs were encapsulated with a glass cover to prevent degradation as a result of air exposure.

The potential to be flexible as well as dropping the production cost bring a benefit of non-rigid OLEDs over LEDs and other lighting technologies. The curved or rolled OLED panels/displays can be used in wearable products (such as wearable smart watches and computers), mobile phones, and television (TV)s. OLEDs have a

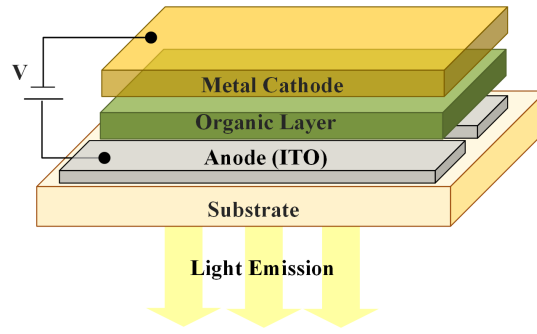


Figure 3.1: OLED structure

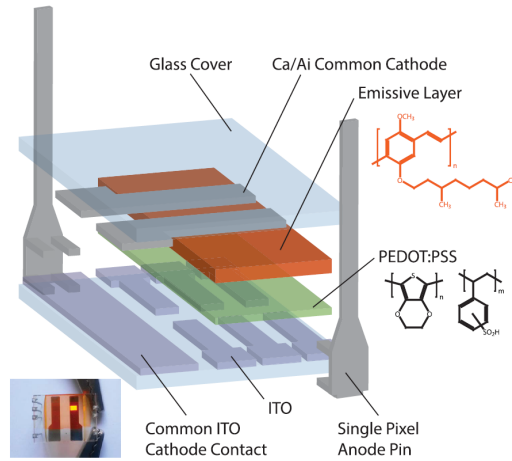


Figure 3.2: PLED structure [51]

low-pass filter transfer function with the cut-off frequency given by [4]:

$$f_c = \frac{1}{2\pi RC_o} \quad (3.1)$$

where R is the effective resistance of the OLED, and C_o is the plate capacitance expressed by:

$$C_o = \frac{A_t \epsilon_0 \epsilon_r}{d_t} \quad (3.2)$$

where A_t is the OLED photoactive area, d_t is the OLED thickness, ϵ_0 and ϵ_r are the permittivity of free space and relative dielectric constant of the organic layer, respectively. Several important materials have been used for the electron injection layer of OLEDs such as LiF, NaCl, NaF and their dielectric constants are 9.036, 5.895 and 5.072, respectively at the temperature of 300 K [52]. Obviously, having a larger photoactive area decreases achievable modulation bandwidth of OLED and hence a restriction in R_b is imposed on OVLC systems. Additionally, bandlimited systems experience degradation in the BER performance due to ISI. The BLW phenomenon is another challenge in OVLC systems, where the signal randomly deviates from the DC level due to high pass filtering or capacitive coupling. A number of methods have been proposed to overcome the small B_{mod} and ISI including (i)

high-level modulation schemes with no equalization or raised cosine filtering, which are the most popular methods of mitigating ISI; and (ii) equalization such as the ANN based equalizer to maximize R_b by undoing the detrimental effect of the ISI [53]. In [54] it was experimentally demonstrated that the radiation pattern of a bent OLED panel is not Lambertian, and an improved analytic mixed Gaussian model was proposed to describe the rotational radiation asymmetry, where parameters values were found by using an expectation-maximization algorithm for curve fitting with the measured data. Compared with Lambertian source, OLED sources are more flexible in radiation pattern control showing advantages in terms of lower OPL. In addition, its impact on the VLC channel characteristics is investigated in the [section 5.4](#) and [section 5.5](#).

- **Organic Photodiodes**

An PD is a semiconductor device that converts light into an electrical current. PDs may contain optical filters, built-in lenses, amongst other optics. Organic PDs are particularly well suited for VLC technology as they enable chemically tailored optoelectronic performance and fabrication by printing techniques on thin and flexible substrates [55, 56]. In many organic optoelectronic devices, including OLEDs, OPVs and organic photo detector (OPD)s, a hole injection layer (interlayer) is usually inserted between the transparent anode and the active layer as electron blocker. Several strategies are reported in the literature to improve hole extraction from the photoactive layer. The most popular is incorporation of several different types of hole extraction layers in the device stack such as conductive polymeric materials, selfassembled molecules and metal oxides, surface treatment of the positive electrodes and the conductive polymeric layers. The interlayer at the negative electrode can improve the OPD performance, transferring electrons more efficiently and blocking the movement of holes from the active layer to the cathode. Furthermore, although the local vacuum reference energy level is assumed to be constant at each interface in the organic device, it seems that the use of an interlayer can result in a device with interface dipoles at the organic/metal and organic/organic interfaces, thus resulting in a shift of the vacuum level [56]. This indicates that, the interlayer plays an important role in the charge injection/extraction control, since it can set the work function of the electrode.

Due to the aforementioned advantages of OPDs, they have gained attention using in VLC systems. For instance, in [57] an all-organic flexible VLC system was shown, where a flexible OPVs manufactured in a roll-to-roll process was used as a receiver. Adopting an organic bulk heterojunction OPVs based on P3HT:PCBM as photodetectors in VLC was investigated in [58]. [55] demonstrated the color selectivity and high performance of an OPD in a VLC system which is capable of demultiplexing intermixed optical signals. This work introduces a solution for

printing bulk-heterojunction photodetectors regarding wavelength selectivity. In this approach, a narrow and tune the response in the visible range without optical filters or light-management techniques can be achieved using incorporating nonfullerene acceptors in a transparent polymer donor matrix. That results in an excellent charge-carrier dynamics enabling state-of-the-art responsivities $> 102 \text{ mA W}^{-1}$ and cut-off frequencies $> 1.5 \text{ MHz}$.

There are further works which demonstrate OPDs can be used as fast receivers, however the OPDs were not used as detectors in VLC data links, yet. For instance, due to shorter average exciton lifetime in the presence of many donor–acceptor interfaces at the thin multilayers device, a bandwidth of 430 MHz was achieved [59]. In addition, there are several works reporting OPDs, which operate in the region of 50–80 MHz [60–62]. In [63], PDs with 30 MHz bandwidth was reported, taking advantage of the high vertical carrier mobility.

3.2 Literature Review of OVLC

Figure 3.3 shows the achieved R_b in OVLC for different optical components, modulation schemes and equalizers. A review of OVLC systems shows that using different organic devices, modulation schemes and digital signal processing techniques the achievable data rate R_b can be increased significantly from 550 kb/s [64] to $> 50 \text{ Mb/s}$ [65]. In [64] an experimental OOK-OVLC link using a SMOLED (B_{mod} of 93 kHz) and a silicon PIN-PD as the Tx and the Rx, respectively with an ANN equalizer at R_b of 550 kb/s was reported. A 1.4 Mb/s OVLC system using an OLED (B_{mod} of 93 kHz) with discrete multitone modulation (DMT) was experimentally demonstrated in [66]. In [67] an OVLC using an OLED with B_{mod} of 150 KHz and an RC equalizer R_b was increased to 2.15 Mb/s. In [5] it was demonstrated that by isolating the AC data source using a high impedance NAND gate (i.e., no low frequency restrictions and therefore no BLW effect) R_b can be increased. In addition, the modulation depth was increased from < 10 using a bias-tee up to ~ 100 , thus significantly improving the SNR. In [5] it was shown that R_b can be increased significantly using the multi-layer perceptron (MLP)-ANN to 2.7, 2.2, and 1.25 Mb/s for 4-PPM, OOK, and 2-PPM, respectively compared to the non-equalized system.

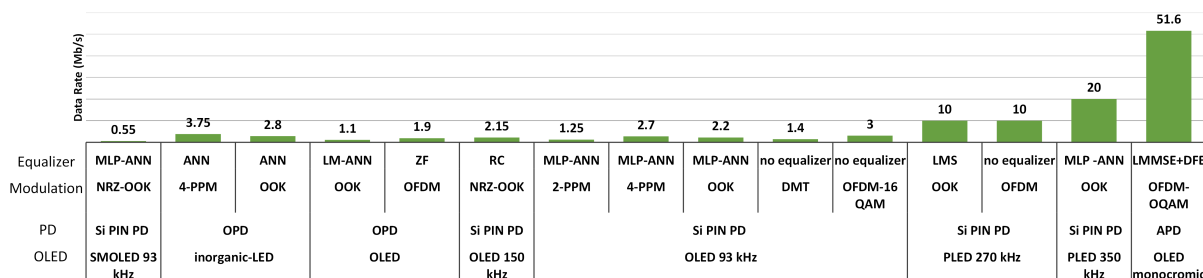


Figure 3.3: The evaluation of the achieved data rates in OVLC

Alternatively, multi-carrier modulation techniques such as OFDM have been adopted to increase the R_b . In [68] it was shown that, 3 Mb/s can be achieved using OFDM-quadrature amplitude modulation (QAM) based OLED with a 93 kHz bandwidth. In several recent works, new experimental results on PLED-based VLC have been reported. For instance, the first notable R_b of 10 Mb/s was achieved by adopting a PLED with a B_{mod} of 270 kHz using OOK in combination with a LMS equalizer [69]. The same R_b was achieved using OFDM in [53], the system block diagram is shown in Figure 3.4. Next, through low-temperature thermal annealing and crystallisation of the polymer, a slight marginal improvement in B_{mod} (i.e., 350 kHz) was reported, which was used in OVLC in combination with an ANN to achieve a R_b of 20 Mb/s [51]. Furthermore, in [70] based on wavelength-division multiplexing (WDM) using three individual RGB pixels of a PLED and an ANN equalizer R_b per PLED chips of 27.9, 18.6 and 8.4 Mb/s for the red, blue and green components, respectively (i.e., an aggregate link capacity of ~ 55 Mb/s) were reported.

OPDs are adopted in VLC systems, since they can offer superior responsivity in comparison to Si-PDs in the visible spectrum. E.g., in [71] a VLC system employing an inorganic-LED, OPD of 160 kHz, and an ANN equalization achieved R_b of 2.8 and 3.75 Mb/s for NRZ-OOK and 4-PPM, respectively. In [72], an all-organic-based VLC employing an ANN equalizer with LM demonstrated a R_b of 1 Mb/s over a short transmission span. Whereas, in [73] an OFDM-based all-organic VLC link with a bit/power loading algorithm to combat the system frequency selectivity reported R_b of 1.9 Mb/s. In [74] it was demonstrated that setting a specific carrier frequency f_c can affect the system performance. The achieved R_b of 220, 640 and 260 kb/s for f_c of 100, 200 and 300 kHz, respectively was reported. Also investigated was the angular dependence of the system performance showing R_b of 160 kb/s with a tilt angle up to 48° . Thus, opening up the possibility of adopting advanced techniques, e.g., the angle diversity. In [57], a fully organic flexible VLC system using off-the-shelf components, flexible circuits and flexible commercial OLED and an OPD, manufactured in a roll-to-roll process, was reported. This all-organic flexible VLC system is capable of transmitting an audio file in real-time. And their future goal is to design the driving circuits operating over hundreds of MHz, both in emission and transmission, and to build an OPD that could support this operating frequency.

Recently, 51.6 Mb/s OLED based VLC employing a monochromic OLED fed by an OFDM signal with offset QAM (OQAM) has been reported which is the highest single-wavelength transmission speed reported in OVLC so far [65]. The experimental system diagram is shown in Figure 3.5. In this work, the bit and power loading technique and a joint linear minimum mean-square-error (LMMSE) and a DFE were used at the Rx to combat ISI, and a cyclic prefix (CP) to improve spectral efficiency. The work in [75] investigated the OLED nonlinearity using Volterra series and a Volterra-based nonlinear

equalizer in order to mitigate both ISI and nonlinearity more effectively than other equalizers over a link span of 3 m. Recently, organic solar cells have been used as high-speed detectors for VLC as well as supplying the power needed for the Rx circuit [76].

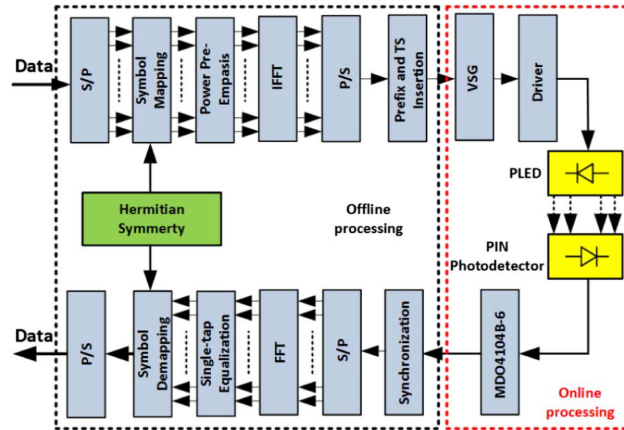


Figure 3.4: The system block diagram in [53]

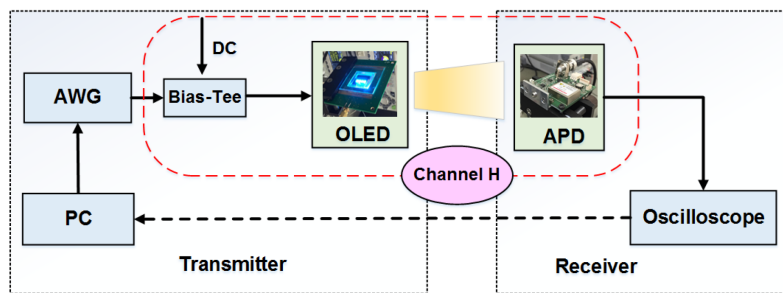


Figure 3.5: The experimental system diagram in [65]

Objectives of the Thesis

There is a growing interest in utilization of OLEDs for soft lighting and display applications. There will be a high demand on to design VLC transceivers utilizing OLEDs for communications due to their inherent advantages such as flexible substrates, low-cost manufacturing, bright and soft light. However, the carrier mobility of organic semiconductors is much slower than the devices composed of metal alloys, such as gallium nitride, thus leading to a restriction in the OLED modulation bandwidth. The manufacturing processes, materials and the photoactive size of the devices can affect the raw modulation bandwidth of OLEDs. To increase the transmission bandwidth (i.e., data throughput), novel approaches have been proposed including equalization techniques, signalling schemes and the optimum driver circuits which are mentioned in [chapter 2](#) and [chapter 3](#). Nevertheless, there are still many challenges awaiting theoretical, analytical and experimental verification. Therefore, the dissertation thesis has the following main goals:

- To propose equalizations for OLED-based VLC
- To develop analytical and simulation models of OLED-based VLC for different scenarios
- To develop an experimental test-bed for measurement
- experimentally evaluation of the proposed systems and to compare with the predicted and simulated systems

To meet the main goals of the thesis, the following specific milestones have been set:

- To characterize OLEDs with different sizes in term of optical and electrical specifications.
- To experimentally evaluate a number of OLEDs for the VLC system.
- To investigate the candidate modulation schemes (m -CAP) for a number of OLEDs in the VLC system.
- To adopt a flexible OLED based VLC system with m -CAP for different angle of incidence on the PD.

-
- To investigate equalization techniques for OVLC.
 - To simulate VLC link in an empty room implemented using OpticStudio® to be confirmed in comparison to the results reported in the literatures.
 - To investigate the impact of the symmetry beam pattern of OLED, which is wider than Lambertian, in VLC systems including by considering reflections from wavelength-dependent surfaces within the indoor environments. To model the flexible OVLC system for the shopping mall, office, corridor and semi-open corridor using OpticStudio®. The analytical models is based on the real parameters and statistics of flexible OLED devices, characterization of OVLC channel in term of optical path loss and the delay spread as well as system performance.
 - To simulate OVLC for D2D communications including by user mobility and rotation angles.

The core of this thesis is based on published papers in scientific journals with impact factor and papers in international conference proceedings. The original papers with bibliographic citations contributing to the thesis are provided in the following sections.

Section 5.1 provides experimental investigation of optical and electrical characteristics of a number of rigid and flexible (or curved) OLEDs in terms of the threshold voltage, bias current, linear dynamic range, optical spectrum, optical radiation patterns and output optical power–current–voltage ($L-I-V$) curves. In addition, the VLC system performance in terms of the measured BER was evaluated where these OLEDs were adopted as a light source.

Section 5.2 focuses on evaluation of the exciting feature of OLED panels which is being curved, rolled or folded light source. The effect of curved OLED radiation pattern, which is wider than Lambertian, for VLC system were experimentally evaluated. In addition, investigation of an OVLC system performance using a curved and flat OLEDs with m -CAP modulation for $m = 2$. The optical receiver move along a circular path which leads to variety of incidence angles. The link performance is quantified in terms of BER. It is shown that curved OLED offers lower BER for the viewing angles greater 40° compared to the flat OLED.

Section 5.3 presents evaluation of the effect of training algorithms in an ANN equalizer for a feedforward multi-layer perceptron configuration in VLC systems where a low bandwidth OLED is used. We tested several algorithms which are the scaled conjugate-gradient, conjugate-gradient backpropagation and LM algorithms for a range numbers of neurons. I showed that, LM offers superior BER performance based on the mean square error in comparison to other training algorithms evaluated in this work.

section 5.4, provides unique characteristics of a flexible OLED-based VLC for coverage of a shopping mall environment. A number of scenarios of VLC system with flexible OLED were analyzed. Based on the obtained simulation data, a new expressions of the VLC channel characteristics in case of full and half-circular OLED based transmitter for both empty and furnished shopping malls were derived in terms of optical loss and channel delay spread. In addition, system performance was investigated in terms of BER and channel capacity.

section 5.5 presents the impact of a symmetry beam pattern of OLED, which is wider

than Lambertian, on the VLC system by considering wavelength-dependent surface materials reflections. A VLC system using flat and half-circular flexible OLEDs for use in an office environment for a number of scenarios was simulated. Furthermore, I investigated the use of OLED-based VLC in corridor and semi-open corridor in shopping malls. We considered two scenarios; (i) where the OLED panel is located on the inner shop wall behind the glass window and (ii) on the wall or shop window inside the corridor. The channel characteristics is shown in term Of RMS delay spread and OPL.

As a summary, an experimentally investigation of optical and electrical characteristics of a number of rigid and flexible OLEDs is carried out. Following, an experimental test-bed which utilize a number of different OLEDs transceiver with m -CAP modulation is developed. The effect of curved OLED radiation pattern on the VLC link has been examined for the first time. Additionally, due to low modulation bandwidth of the OLED, the ANN equalizer are investigated. A simulation of OLED-based VLC system for indoor environments are presented in which the results show the channel characteristics and the BER with respect to spatial parameters to derive a novel methodology.

5.1 Comprehensive Optical and Electrical Characterization and Evaluation of Organic Light-Emitting Diodes for Visible Light Communication

This chapter is a version of the published manuscript:

Z.N. Chaleshtori, A. Burton, S. Zvanovec, Z. Ghassemlooy, P. Chvojka, “Comprehensive optical and electrical characterization and evaluation of organic light-emitting diodes for visible light communication,” *Optical Engineering*, Vol. 59(4), pp. 046106, 2020.

Connection to my Ph.D. thesis:

Recently, OLEDs have potential of using for *(i)* illumination or visual displays in public places and *(ii)* flexible panel display for use in wearable biomedical devices. Hence, characterization of different types of OLEDs is essential when these used in VLC. Therefore, optical and electrical characteristics of a number of rigid and flexible OLEDs within the context of VLC systems have been experimentally investigated. In addition, the use of OLEDs in VLC is mostly limited to tiny OLEDs, indeed more research utilizing large OLEDs with much lower bandwidth in VLC needed to be done.

Optical Engineering

OpticalEngineering.SPIEDigitalLibrary.org

Comprehensive optical and electrical characterization and evaluation of organic light-emitting diodes for visible light communication

Zahra Nazari Chaleshtori
Andrew Burton
Stanislav Zvanovec
Zabih Ghassemlooy
Petr Chvojka

Zahra Nazari Chaleshtori, Andrew Burton, Stanislav Zvanovec, Zabih Ghassemlooy, Petr Chvojka, "Comprehensive optical and electrical characterization and evaluation of organic light-emitting diodes for visible light communication," *Opt. Eng.* **59**(4), 046106 (2020), doi: 10.1117/1.OE.59.4.046106

SPIE.

Comprehensive optical and electrical characterization and evaluation of organic light-emitting diodes for visible light communication

Zahra Nazari Chaleshtori,^{a,*} Andrew Burton,^b Stanislav Zvanovec,^a
Zabih Ghassemlooy,^b and Petr Chvojka^a

^aCzech Technical University in Prague, Faculty of Electrical Engineering,
Department of Electromagnetic Field, Prague, Czech Republic

^bNorthumbria University, Faculty of Engineering and Environment,
Optical Communications Research Group, Newcastle-upon-Tyne, United Kingdom

Abstract In recent years, we have seen an increased use of organic light-emitting diodes (OLEDs) for illumination in indoor environments due to their softer light compared with the conventional inorganic LEDs. In addition, OLEDs have been reported in visible light communication (VLC) systems, specifically for applications with lower data rates, such as information boards, camera communications, and positioning. However, OLEDs need extensive electrical and optical characterization if they are going to be fully exploited in VLC. We investigated characteristics of a range of flexible and rigid OLEDs and compared them with inorganic LEDs. We show that OLEDs have highly linear power–current characteristics, and compared with rigid OLEDs with beam patterns closely matching the Lambertian profile, the flexible OLED’s radiation pattern is wider. Based on the measured experimental data, a new expression for the OLED’s beam pattern, which follows the three-term Gaussian profile, is proposed. Moreover, we show that using larger size OLEDs in VLC links offers improved bit error rate performance over a wide tilting angle of up to 80 deg and a transmission path length of up to 60 cm. © 2020 Society of Photo-Optical Instrumentation Engineers (SPIE) [DOI: [10.1117/1.OE.59.4.046106](https://doi.org/10.1117/1.OE.59.4.046106)]

Keywords: organic LEDs; radiation pattern; spectrum; visible light communications.

Paper 191065 received Aug. 2, 2019; accepted for publication Apr. 8, 2020; published online Apr. 21, 2020.

1 Introduction

Visible light communications (VLC) is seen as a viable complementary technology to radio frequency (RF) wireless communications in mostly indoor environments to meet the growing demands for high-speed wireless data transmission.^{1,2} VLC has the advantages of being high energy efficiency (i.e., a green technology), having no RF electromagnetic interference, being license-free, and having inherent security and privacy compared with the RF technologies.³ In VLCs, both conventional gallium-based light-emitting diodes (LEDs) and organic LEDs (OLEDs) as well as white laser diodes (LDs) are being used as a light source.^{1,4} The gallium-based LED-based VLC systems, which utilize blue light to excite yellowish phosphors to synthesize white light, have been extensively investigated in the literature.^{1,5} Whereas the red, green, and blue (RGB) and phosphor LDs-based VLCs require higher thermal stability of the phosphor due to a much greater optical power density.⁶ Compared with the phosphor-based LD, the RGB LD is safer to the human eye due to the low illumination level blue light component.⁷

OLEDs have interesting features over conventional and mainstream solid-state lighting and flat panel displays such as energy efficiency (i.e., they are environmentally friendly), brightness with no need for backlight as in LCD, sunlight style color-temperature tenability, very high color rendering index, small total stack thickness of an OLED being between 100 and 500 nm,⁸ and flexibility (i.e., can be fabricated on plastics substrates or used in wearable clothes).^{8–11}

*Address all correspondence to Zahra Nazari Chaleshtori, E-mail: nazarzah@fel.cvut.cz

In addition, OLEDs with large photoactive areas are being used as pixels in smartphones, TVs, and wearable devices, which offers the potential of infrastructure-to-device (I2D) and device-to-device (D2D) communications.¹² The latter is performed by transmitting and receiving the information data via the smartphone's OLED-based display pixels^{13,14} and the built-in cameras.^{15,16}

OLEDs work in a similar manner to LEDs and use organic carbon-based molecules to generate electron-hole pairs, but they have different characteristics. There are two different types of OLEDs based on (i) small organic molecules deposited on a glass and (ii) polymer (i.e., large plastic molecules) to produce light.^{17,18} However, the modulation bandwidth B_{mod} of OLEDs is orders of magnitude smaller compared with inorganic LEDs (i.e., in the kHz range compared with MHz in inorganic LEDs). The bandwidth limitation is due to the carrier lifetime and the parasitic resistor-capacitor (RC) effects, thus limiting their use in medium- to high-speed data communications.¹⁹ However, OLED properties (i.e., B_{mod}) have been improved using new materials with higher charge mobility.²⁰ In addition, a number of advanced communications and signaling schemes as well as optimum driver circuits have been proposed to increase the transmission data rate.^{21,22} Future OLED applications will be in (i) medium to large panels for use in public places such as airports, shopping centers, train, and bus stations^{23,24} and (ii) flexible or flat panel display technology for use in wearable biomedical devices in hospitals,²⁵ which provide visual display, data communications, and indoor localization. The devices of nano-OLEDs and microfluidic OLEDs are promising, providing for new applications.²⁶ However, very little work has been reported on the optical and electrical characterization of different types of standard OLEDs used for illumination, which are essential when these devices are used in VLC. In this paper, we first experimentally investigate optical and electrical characteristics in terms of the threshold voltage, bias current, linear dynamic range, optical spectrum, optical radiation patterns, and output optical power-current-voltage ($L-I-V$) of a number of rigid and flexible (or curved) OLEDs within the context of VLC systems. In addition, the characterization of organic devices is mostly limited to $L-I-V$ or the frequency response measurements. In this work, the focus is also on other features of OLEDs (particularly large area flexible and rigid devices), such as dynamic resistance, linearity, and radiation patterns, which are important in VLC and are compared with the conventional inorganic sources. Large OLED panels compared with tiny OLEDs have lower modulation bandwidth, thus supporting a reduced level of throughputs in VLC.^{21,22} Therefore, more research utilizing large OLEDs with much lower bandwidth needs to be done. A number of schemes, including multicarrier and multi-level modulation schemes, have been proposed to increase the data throughput. Here, we demonstrate the use of large size OLEDs as a transmitter in VLC systems employing a multiband carrierless amplitude and phase (m -CAP) modulation, which offers similar spectrum efficiency as orthogonal frequency division multiplexing (OFDM) but at much reduced implementation complexity. Hence, we evaluate the system performance in terms of the measured bit error rate (BER).

The rest of the paper is organized as follows. In Sec. 2, the structure of a typical OLED is described. In Sec. 3, the characterization of OLEDs is given, followed by the experimental investigation of the OLED-based VLC link in Sec. 4, and finally, conclusions are drawn in Sec. 5.

2 Structure of OLEDs

The principal material in an organic semiconductor is either carbon or nitrogen.²⁷ The organic materials can be long-chain polymers (i.e., PLEDs) or small organic molecules (i.e., SMOLEDs) in a crystalline phase.^{19,27} The organic devices are based on the thin-film technology (see Fig. 1), where the general structure consists of two or more organic semiconductor materials sandwiched between oppositely polarized electrodes. OLEDs have a low-pass filter transfer function with the cut-off frequency given as²⁸

$$f_{3\text{-dB}} = \frac{1}{2\pi(\tau_s + \tau_c)}, \quad (1)$$

where τ_s is the differential carrier lifetime, which is inversely proportional to the drive current.²⁸ $\tau_c \sim RC$, where R is the effective resistance of the OLED and C is the plate capacitance, which is defined as¹

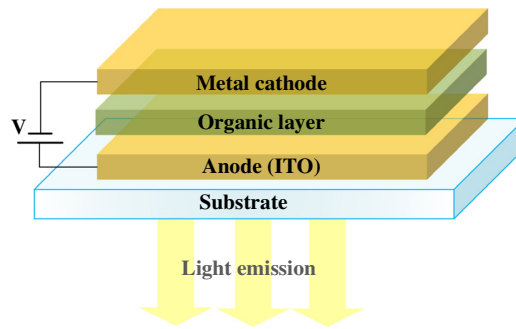


Fig. 1 The OLED structure.

$$C = \frac{A\epsilon_0\epsilon_r}{d}, \quad (2)$$

where A is the OLED photoactive area, d is the OLED thickness, and ϵ_0 and ϵ_r are the permittivity of free space and the relative dielectric constant of the organic layer, respectively.

Note that, as in LEDs, B_{mod} of OLEDs is inversely proportional to A ; hence the bandwidth is much lower than in small area gallium-based LEDs.⁴ In addition, in highly bandlimited organic VLC systems, the intersymbol interference leads to significant BER degradation. A number of schemes have been proposed to overcome both lower B_{mod} and the ISI including: high-level modulations,^{29,30} equalization schemes such as the artificial neural network,^{21,22} specially designed receivers,^{31–35} single-input multiple-output or multiple-input multiple-output configuration,^{36,37} bit/power loading,^{22,38} and power pre-emphasis.^{30,39}

3 Characterization of OLEDs

3.1 Experimental Test-Bed

To carry out comprehensive tests and measurements for characterization of the OLEDs, we have developed an experimental test-bed, as shown in Fig. 2. The test-bed includes an arbitrary function generator AFG Agilent 3252, driving circuits, OLEDs, optical receiver (ORx) Thorlabs PDA100A2 [consisting of a photodiode (PD) and a transimpedance amplifier], spectrometer Thorlabs CCS200 with CCSB1 cosine corrector with a diameter of 8.5 mm and the digital LED lux meter DT-3809.

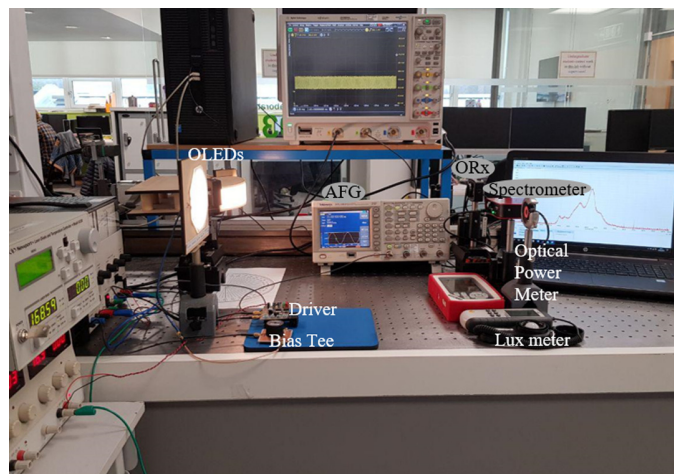


Fig. 2 An experimental test-bed for characterization of OLEDs.

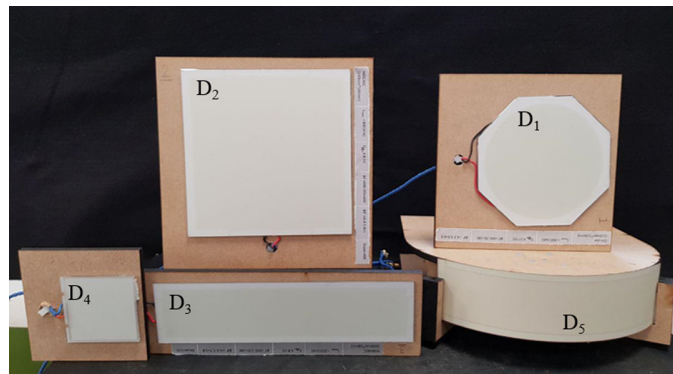

Fig. 3 Different OLEDs (D1 to D5) under test.

Table 1 The OLEDs under test.

OLED	Size (mm)	Device thickness (mm)	Luminous efficiency (lm/W) [bias current I_B (mA)]	Luminous flux (lm) [I_B (mA)]
Rigid				
D ₁ : N6OA40C	48.7 (radius)	1	55 (230)	75 (230)
D ₂ : N6SC40C	140 × 140	0.88	55 (480)	150 (480)
D ₃ : N6BA40C	200 × 50	1.77	53 (230)	73 (230)
D ₄ : N6SB40	55 × 53	1.97	55 (62)	20 (62)
Flexible				
D ₅	200 × 50	0.41	53 (230)	75 (230)

Five OLEDs, four different rigid OLEDs from LG (i.e., N6OA40C, N6SC40C, N6BA40C, and N6SB40 denoted as D₁ to D₄) and a single flexible OLED from UNISAGA (denoted as D₅), see Fig. 3, were investigated in terms of their optical and electrical characteristics including the optical spectrum, $L-I-V$ curves, optical radiation pattern, and B_{mod} . All experiments were carried out under the same controlled environments (within a dark room), and for each set-up, five sets of measurements were taken to ensure repeatability and correctness. The main parameters of the tested OLEDs are given in Table 1.

3.2 Optical and Electrical Characterization

3.2.1 OLED's spectrum

To measure the spectrum profiles of OLEDs, a spectrometer with a cosine corrector capturing light over a 180-deg angle was used. The measured normalized optical spectrum (averaged over five sets of measurements) for a range of I_B for D₁ is shown in Fig. 4(a), showing the R, G, and B components at the peak wavelengths of 613, 555, 450, and 480 nm, respectively. OLEDs D₁ to D₅ and an inorganic white LED [LUXEON cool white rebel star LED (5650K) sr-01] display broad-spectrum profiles with RGB components; see Fig. 4(b). For the flexible OLED, the R component is at a slightly higher wavelength of 620 nm, whereas the B and G components have lower intensities compared with the rigid OLEDs. This is attributed to the lower conversion efficiency of B and G materials in D₅. Whereas, for the inorganic LED, the dominant color is B.

Next, we investigate the spectrum (i.e., the color) of D₁ under different dimming levels (i.e., $10 \text{ mA} < I_B < 300 \text{ mA}$) as shown in Fig. 4(c). Note that the normalized intensity profiles are almost the same with low intensity variation of the peak intensities, thus indicating no significant changes in the color of OLEDs in contrast to the inorganic LEDs reported in Ref. 40.

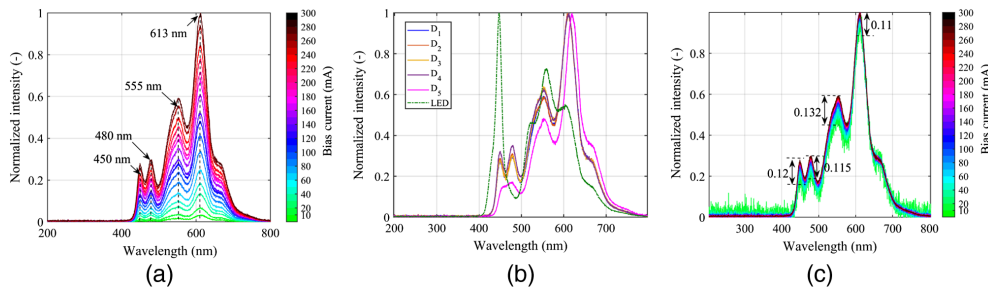


Fig. 4 (a) The optical spectrum of D_1 is normalized to the maximum I_B with peak wavelengths marked where the legend color scale represents I_B , (b) all devices outputs and a gallium-based white LED at their corresponding maximum I_B , and (c) the optical spectrum of D_1 for a range of I_B where each of the spectral responses were normalized to unity and then superimposed on top of each other.

3.2.2 OLED $L-I-V$ curves

The $I-V$ curves of the OLED panels under test were measured using a source meter (Keithley SourceMeter Series 2400), and their illuminance was measured using a lux meter, where the distance between the OLED and the lux meter was fixed at $15 \times$ the horizontal dimension of the OLED (as recommended by the lux meter manufacturer). The measured $L-I-V$ curves of the OLEDs are shown in Fig. 5, showing linear characteristics with sufficient dynamic ranges. Table 2 summarizes the measured maximum current I_{B-Max} , threshold voltage V_{th} , range of I_B in the linear part ΔI , the range of voltage in the linear part ΔV , and the slope of the $V-I$ curve (i.e., inverse of the dynamic resistance for all OLEDs at I_B). Note that, with a wide linear range,

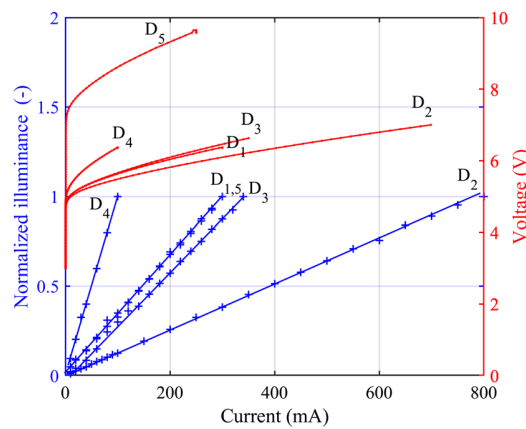


Fig. 5 The $L-I-V$ curves for OLEDs where $V-I$ and $L-I$ curves are associated to each device marked as D_1 to D_5 .

Table 2 The parameters of OLEDs under test.

OLED	I_{B-Max} (mA)	V_{th} (V)	Slope ($\Delta I / \Delta V$)	Dynamic resistance (Ω) [I_B (mA)]
D_1	300	4.6	0.263	3.8 (160)
D_2	800	4.8	0.400	2.5 (400)
D_3	350	4.8	0.225	4.4 (160)
D_4	100	5.0	0.083	12.0 (60)
D_5	300	7.0	0.033	4.3 (180)

Table 3 The parameter of linearity of inorganic LEDs and OLEDs.

OLED	RMSE	Ga LED	RMSE		
			R	G	B
D ₁	2 × 10 ⁻¹⁴	RGB	0.004	0.07	0.008
D ₂	3 × 10 ⁻¹⁴	RAGB	0.0036	0.0025	0.0032
D ₃	1.1 × 10 ⁻¹⁴	5 mm RGB	0.0016	0.0027	0.0047
D ₄	1.3 × 10 ⁻⁷	COBLED		0.5114	
D ₅	1.2 × 10 ⁻¹⁴				

the $L-I$ range around I_B higher signal levels can be used for intensity modulation of the OLED, thus having a higher signal-to-noise ratio and lower BER. Using linear regression curve-fitting, the plots in Fig. 5 show a highly linear $L-I$ relationship. To compare the linearity of inorganic LEDs with OLEDs, we used root mean square error (RMSE) i.e., $RMSE = \sqrt{(\sum P_I - P_{mod})^2/n}$, where P_I and P_{mod} are the measured and linear modelled optical powers, respectively, and n is the number of measured samples; see Table 3. Note that OLEDs tested in this work show a considerably lower RMSE compared with the inorganic LEDs [i.e., RGB, 5 mm RGB, RAGB (RGB + amber LEDENGIN LZ4-00MA00), and a COBLED (LUSTREON 4W 48led COBLED Chip)].

3.2.3 Optical radiation pattern

The optical radiation pattern describes the spatial intensity distribution of light emitted from the OLEDs, which is important, especially when analyzing the coverage and signal distribution in VLC links. The light intensity of LEDs defined in terms of the angle of irradiance θ is given as^{1,2}

$$I(\theta) = \frac{m_L + 1}{2\pi} I(0) \cos^{m_L}(\theta), \quad \theta = \left[-\frac{\pi}{2}, \frac{\pi}{2}\right], \tag{3}$$

where $I(0)$ is the center luminous intensity of an LED and m_L is the Lambertian order given as¹

$$m_L = -\frac{\ln(2)}{\ln[\cos(\theta_{1/2})]}, \tag{4}$$

where $\theta_{1/2}$ is the semiangle at half illuminance.

To empirically derive the beam patterns of rigid OLEDs and determine the Lambertian order of emission, a lux meter was used to measure the luminance, as shown in Fig. 6(a). As expected, the profiles are complete hemispheres close to the Lambertian emitter with $m_L = 1$ in contrast to the intensity profile of a COBLED with $m_L = 0.66$ as shown in Fig. 6(b).

With reference to Fig. 7(a), the irradiance angle θ is given as

$$\theta = \arccos \frac{\vec{d}_{Rx} \cdot \vec{r}_{OLED}}{|\vec{d}_{Rx}| |\vec{r}_{OLED}|}, \tag{5}$$

where \vec{r}_{OLED} and \vec{r}_{Rx} are the norm vectors of the OLED and the ORx, respectively, and d_{Rx} is the distance between the OLED and ORx. The positions of the OLED and the ORx are considered as (r, φ, x_1) and (r', φ', x_2) in the cylindrical coordinate, respectively, where r is the OLED curvature radius, $0 < \varphi < 180$ deg, and x_1 refers to the OLED's width. Thus, we have

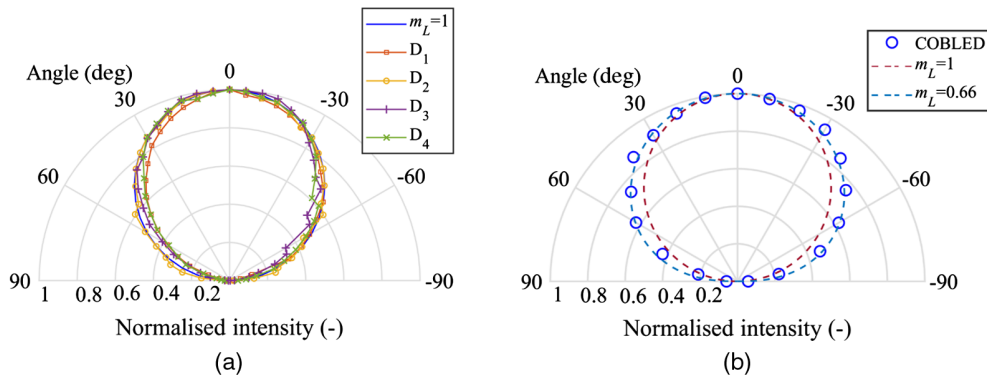


Fig. 6 The polar dimensional radiation patterns for (a) rigid OLEDs for D_1 , D_2 , D_3 , and D_4 and (b) a COBLED.

$$\cos(\theta) = \frac{r' \cos \varphi' \cos \varphi - r \cos^2 \varphi + r' \sin \varphi' \sin \varphi - r \sin^2 \varphi}{r' - r}. \quad (6)$$

To investigate the intensity profiles of flexible OLEDs, the device was bent with different radii of curvature r of 11 and 8 cm to have quadrature and half-circle light sources, as shown in Fig. 7(a). The measured radiation pattern shows a symmetry about the origin 0 deg not fitting the Lambertian radiation pattern; see the solid blue line for $m_L = 1$ in Fig. 7(b). Note that the OLED with a higher r displays a radiation beam profile closer to Lambertian with $m_L = 1$. The radiation angle ranges for $\theta_{1/2}$ for the flat and 11 and 8 cm curved OLEDs are 58 deg, 65 deg, and 75 deg, respectively.

A numerical fitting method was used to estimate the radiation pattern parameters of flexible OLEDs. The three-term Gaussian model provided the best fit to describe the radiation patterns of OLEDs, which is given as

$$I(\theta) = \sum_{k=1}^q a_k \times \exp\{-[(\theta - b_k)/c_k]^2\}, \quad (7)$$

where a_k , b_k , and c_k are the parameters estimated by the curve fitting tool, k is the order, and q is the term of the Gaussian model, which is considered to be 3 for the best match with the empirical

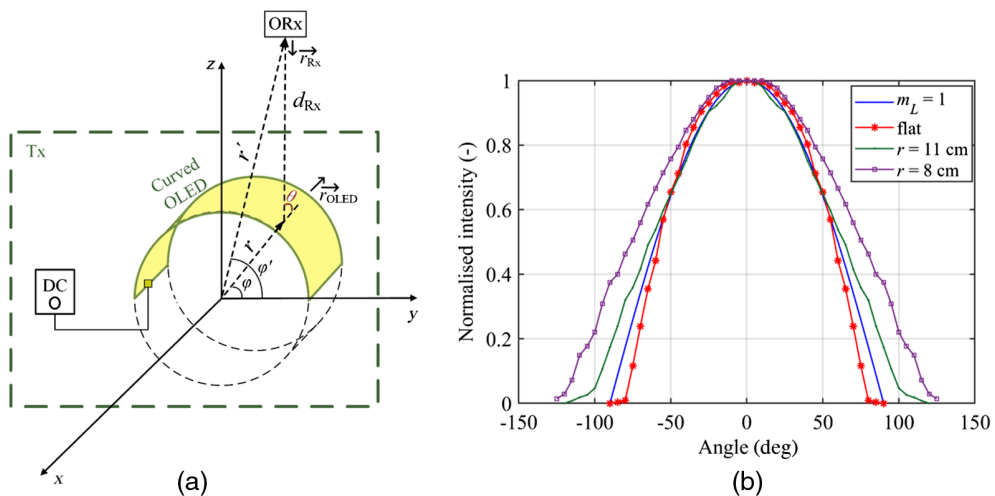


Fig. 7 (a) OLED panel bent in different curvature radii r of 11 and 8 cm and (b) two-dimensional intensity pattern.

Table 4 Three-term Gaussian model parameter for spatial intensity distribution for curvature with radii of 11 and 8 cm.

k	1	2	3
$r = 11$ cm			
a_k	0.9878	0.3054	0.2875
b_k	-0.7595	58.1	-59.42
c_k	51.59	32.99	31.94
$r = 8$ cm			
a_k	0.9814	0.3733	0.2721
b_k	4.832	-63.31	70.73
c_k	60.17	42.31	36.66

data. The RMSE analysis has been carried out on the modeled and measured intensity profiles to assess the accuracy of the model. For the curved OLED, the RMSE values are 0.016 and 0.018 for r of 11 and 8 cm, respectively, which are less than the standard error limit of 0.05.⁴¹ The numerical fitting parameters are shown in Table 4 for OLEDs with an r of 11 and 8 cm. Note that a_k is the peak of the k 'th term of the three-term Gaussian (i.e., $a_1 \sim 1$) and b_k is the angular position of the peak referred to each Gaussian as $b_1 \sim 0$. c_k is the standard deviation of the k 'th term of the three-term Gaussian with higher values representing a wider profile.

3.2.4 OLED bandwidth

To measure B_{mod} of the OLEDs, the devices were biased in the linear region of respective $L-I$ curves; see Fig. 5. The measured frequency responses for D_1 – D_5 over a range of I_B are as shown in Fig. 8, where U is the peak-to-peak received voltage and U_0 is the peak-to-peak voltage of the first sample. For comparison, the maximum and minimum bandwidth values as well as the difference between them (i.e., ΔB) are given in Table 5. The results for the devices tested show that B_{mod} increases with I_B as in agreement with Eq. (1). We also investigated the effect of bending the flexible OLED on B_{mod} and observed no changes in B_{mod} . This is because the cut-off frequency of OLED is defined by its physical parameters. This feature makes the OLED a perfect optical antenna, where the same SNR is maintained over a given transmission radius.

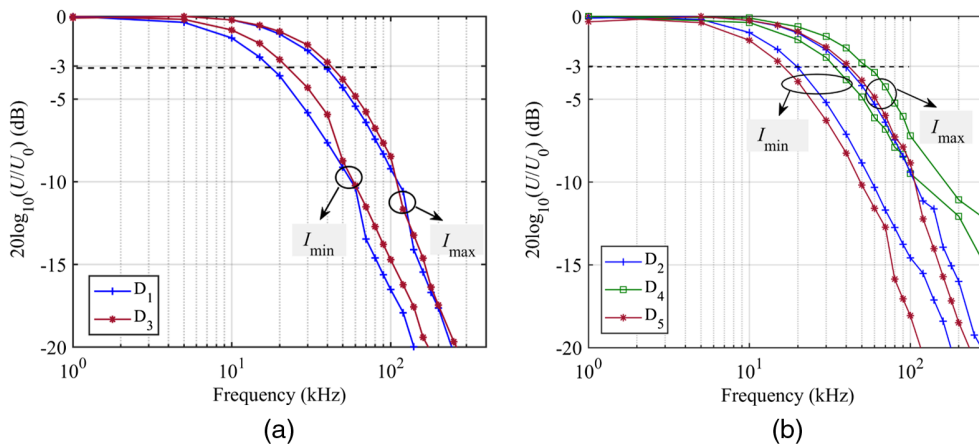


Fig. 8 The measured B_{mod} of (a) $D_{1,3}$ and (b) $D_{2,4,5}$.

Table 5 Bandwidth of OLEDs.

Device	$B_{\text{mod-Min}}$ (kHz) [$I_{B\text{-Min}}$ (mA)]	$B_{\text{mod-Max}}$ (kHz) [$I_{B\text{-Max}}$ (mA)]	ΔB (kHz)
D ₁	15 (40)	38 (250)	23
D ₂	20 (100)	40 (600)	20
D ₃	20 (100)	42 (280)	22
D ₄	34 (30)	54 (60)	20
D ₅	15 (40)	42 (250)	27

4 Experimental OVLC Link Results

4.1 Experimental Test-Bed for OVLC Link with *m*-CAP

OLEDs with both high linearity and dynamic range can be used to support higher-order multi-level and multicarrier modulation schemes. However, in this work, to simply demonstrate the potential of the OLEDs as the transmitter in a VLC system, we have developed an experimental test-bed to assess the link performance. We have adopted an *m*-CAP modulation scheme due to its ability to (i) reduce the effect of the highly bandlimited frequency response of OLEDs acting as a low-pass filter,^{42–44} (ii) be used as a multiuser scheme (e.g., personalized advertising),⁴⁵ and (iii) be implemented more simply compared with the OFDM.

A block diagram of the experimental *m*-CAP OVLC link is shown in Fig. 9. First, *m* independent pseudorandom data streams $d_m(t)$ of length 12,000 bits (memory depth limitation of the AFG) are generated and mapped onto the *M*-QAM (quadrature amplitude modulation) constellation where *M* is the order of the QAM. Note that *M* and *m* are selected as 16 and 2, respectively, in this work. During the experiment, a sufficient number of bits were transmitted to allow for the measurement of the BER at 10^{-6} . The linearity of OLEDs and their high dynamic range offer the potential for choosing a number of carriers. Following upsampling, the real and the imaginary parts of the signal a_i and b_i , respectively, are applied to the in-phase and quadrature pulse shaping transmit filters, and their impulse responses form a Hilbert pair (i.e., they are orthogonal in the time domain). The transmit filters are formed as a product of the square root raised cosine (SRRC) filter pulse shapes and the sine and cosine waves for the quadrature and in-phase part of the signal, respectively. The carrier frequencies given by the transmit filters are set to 10 and 30 kHz for first and second subcarriers (s_1 and s_2), respectively, in this work. The roll-off factor β used for the transmit pulse shapes is chosen as 0.15, given that the minimum bandwidth requirement is proportional to $1 + \beta$. Note that higher β leads to more protection against ISI for consistency with the literature.⁴⁶ The combined output from filters, i.e., *m*-CAP signal $x(t)$, is applied to AFG and used via a driver for intensity modulation of the OLEDs. Following transmission over a short free space (up to 60 cm) line of sight (LoS) channel, the signal is detected using an ORx Thorlabs PDA100A2. Subsequently, the output of ORx is captured using a digital storage oscilloscope Keysight DSO9254A with the sampling frequency of 400 kS/s for

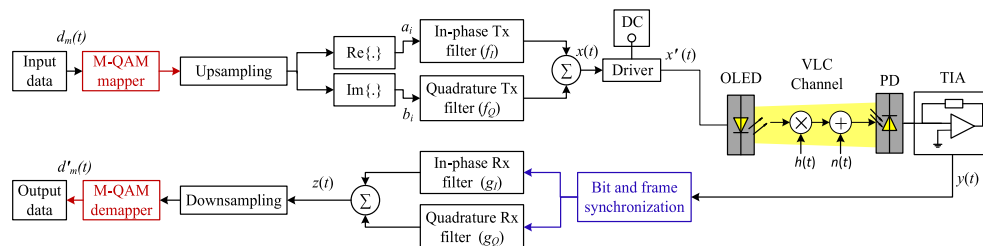


Fig. 9 The block diagram of the proposed OVLC system with *m*-CAP modulation.

Table 6 The system parameters.

OLED	I_B (mA)	B_{mod} (kHz)	Luminous flux (lm)	Area (cm ²)
D ₁	160	28	58.5	74.5
D ₂	450	30	115.0	196.0
D ₃	160	32	52.0	100.0
D ₄	60	54	19.4	29.2
D ₅	180	34	68.4	100.0

ORx	Parameter	Value
	Type of PD	Si-PIN
	Active area of PD	75.4 mm ²
	Bandwidth	1.4 MHz at a 10 dB gain
	Output voltage	0 to 10 V
	Noise of amplifier	195 μ V (RMS)
	NEP	6.75×10^{-12} (W/ $\sqrt{\text{Hz}}$) at $\lambda = 960$ nm
	Responsivity	0.2 (A/W) at $\lambda = 400$ nm
		0.5 (A/W) at $\lambda = 700$ nm

further off-line data processing. The regenerated electrical signal is given as $y(t) = (t)x' \otimes h(t) + n(t)$, where $h(t)$ is the channel impulse response, the \otimes symbol denotes convolution, and the noise $n(t)$ is mainly due to the ambient light and in the form of shot noise. $y(t)$ is resampled to the transmitted signal by original sampling frequency prior to being applied to two time-reversed filters g_I and g_Q matched to the transmit filters. The combined filter output $z(t)$ followed downsampling is applied to the M -QAM demapper to regenerate the estimated transmitted data $d'_m(t)$. All of the key system parameters are shown in Table 6.

4.2 Experimental Results

In this section, we evaluate the LoS OLED VLC link based on the BER for a range of transmission spans from 10 to 60 cm and the OLED tilt angles α from -90 deg to 90 deg. The BER results versus the path length for the OLED VLC for s_1 and s_2 are shown in Figs. 10(a) and 10(b), respectively, along with the 7% forward error correction (FEC) BER limit of 3.8×10^{-3} . Examples of measured constellation diagrams are shown as insets for D₂ with two distances d of 40 and 50 cm and 30 and 50 cm for s_1 and s_2 , respectively. At the FEC BER limit, the transmission path lengths for s_1 are 36, 50, and ~ 60 cm for D₄, D_{1,3} and D_{2,5}, respectively, which are sufficient for D2D communications. In the case of s_2 , we observe a small decrease in the transmission spans by 2, 15, and 10 cm for D₄, D_{1,3} and D_{2,5}, respectively, compared with s_1 . Although the path length of 60 cm was obtained from our experiment, even longer distances can be achieved using OLED panels made of materials with higher charge mobility giving higher B_{mod} ^{20,47} or larger panels with higher output optical power. To meet a given BER target and increase the transmission span, the same SNR at a receiver and thus higher output optical power are required. Therefore, organic devices with larger areas (note decreased 3 dB bandwidth) or an array of OLEDs can be utilized to follow these requirements. For instance, an OLED panel with a luminous flux of ~ 3000 lm can support data transmission for distances of up to 3 m.

For D₂, the BER plots in polar formats against α are shown in Fig. 11 for s_1 and s_2 . Also shown for comparison is the plot for the FEC BER limit. Note that the path length is fixed at 30 cm [i.e., a BER $< 10^{-6}$ when $\alpha = 0$ deg; see Fig. 10(a)]. Note that the BER profiles display a symmetry about the origin (i.e., the ORx is facing the OLED at α of 0 deg) offering improved

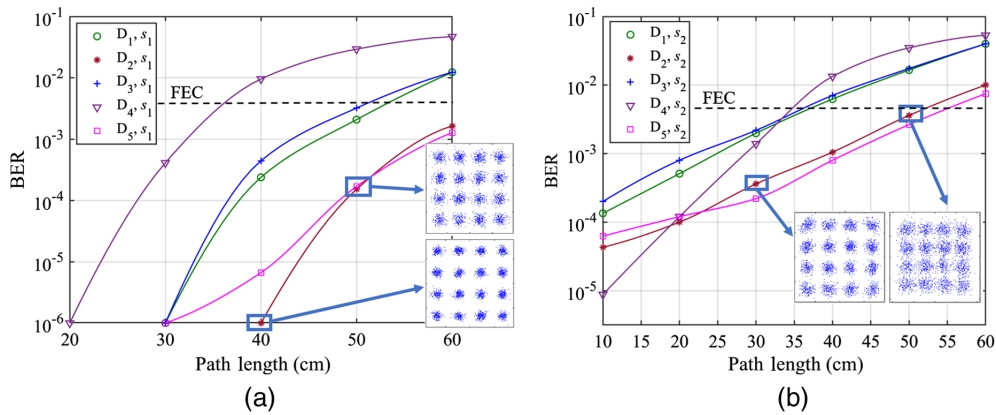


Fig. 10 The BER versus the path length for OLEDs with m -CAP for (a) s_1 with the consolation diagrams for two distances of 40 and 50 cm for D_2 and (b) s_2 with the consolation diagrams for two distances of 30 and 50 cm for D_2 .

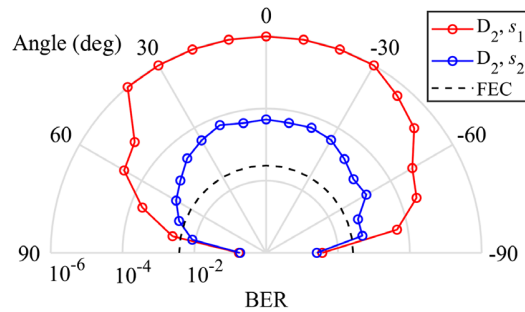


Fig. 11 The polar plot of BER for tilted OLED (D_2) with m -CAP for s_1 and s_2 .

performance over a wide tilting angle. To meet the FEC limit, D_2 can operate with α of up to ± 80 deg and ± 70 deg for s_1 and s_2 , respectively.

5 Conclusions and Future Outlook

In this paper, we carried out a characterization for a range of fixed and flexible OLEDs in terms of their optical spectrum, power–current, and illumination profiles. We showed that OLEDs offer a stable illumination profile regardless of the bias current and a highly linear power–current characteristic compared with the inorganic LEDs. We also showed that the rigid OLEDs beam pattern closely matches Lambertian with $m_L = 1$, whereas for curved OLED, the radiation pattern displays a symmetry that is wider than Lambertian for curved OLED with a curvature radius of 8 cm and a radiation angle of 75 deg. Based on the measured experimental data for the curved OLED, we showed a new expression for the OLED’s beam pattern, which follows the three-term Gaussian profile with an RMSE value of less than a standard error limit of 0.05 to assess the accuracy of the model. In addition, we evaluated OLED-based VLC systems for low data rate transmissions as in D2D communications. We showed that the BER results of a tilting OLED displayed a symmetry about the origin, with larger size OLEDs showing improved BER (i.e., below the FEC limit) over a wider tilting angle (up to 80 deg, which is considerably large for D2D communications) and a longer transmission length (i.e., up to 60 cm).

Acknowledgments

This work was supported by the European Union’s Horizon 2020 research and innovation program under the Marie Skłodowska-Curie grant agreement no 764461 (VISION) and the Czech Rep. funded project GACR 17-17538S.

References

1. Z. Ghassemlooy et al., *Visible Light Communications: Theory and Applications*, CRC Press (2017).
2. Z. Ghassemlooy, W. Popoola, and S. Rajbhandari, *Optical Wireless Communications: System and Channel Modelling with Matlab®*, 2nd ed., CRC Press (2019).
3. P. H. Pathak et al., "Visible light communication, networking, and sensing: a survey, potential and challenges," *IEEE Commun. Surv. Tutorials* **17**(4), 2047–2077 (2015).
4. P. A. Haigh et al., "Organic visible light communications: recent progress," in *16th Int. Conf. Transparent Opt. Networks*, IEEE, pp. 1–5 (2014).
5. P. Binh and N. Hung, "High-speed visible light communications using ZnSe-based white light emitting diode," *IEEE Photonics Technol. Lett.* **28**(18), 1948–1951 (2016).
6. J. Yang et al., "Highly uniform white light-based visible light communication using red, green, and blue laser diodes," *IEEE Photonics J.* **10**(2), 8200508 (2018).
7. T.-C. Wu et al., "Tricolor R/G/B laser diode based eye-safe white lighting communication beyond 8 Gbit/s," *Sci. Rep.* **7**(1), 11 (2017).
8. P. A. Haigh et al., "Visible light communications using organic light emitting diodes," *IEEE Commun. Mag.* **51**(8), 148–154 (2013).
9. P. Haigh, "Using equalizers to increase data rates in organic photonic devices for visible light communications systems," Doctor of Philosophy, University of Northumbria (2014).
10. J. Ràfols-Ribé et al., "High-performance organic light-emitting diodes comprising ultra-stable glass layers," *Sci. Adv.* **4**(5), eaar8332 (2018).
11. J. Clark and G. Lanzani, "Organic photonics for communications," *Nat. Photonics* **4**(7), 438 (2010).
12. P. Luo et al., "Undersampled-based modulation schemes for optical camera communications," *IEEE Commun. Mag.* **56**(2), 204–212 (2018).
13. Y. Li et al., "A VLC smartphone camera based indoor positioning system," *IEEE Photonics Technol. Lett.* **30**(13), 1171–1174 (2018).
14. R. Boubezari et al., "Smartphone camera based visible light communication," *J. Lightwave Technol.* **34**(17), 4121–4127 (2016).
15. B. Lin et al., "An indoor visible light positioning system based on optical camera communications," *IEEE Photonics Technol. Lett.* **29**(7), 579–582 (2017).
16. Q. Wang et al., "Light positioning: a high-accuracy visible light indoor positioning system based on attitude identification and propagation model," *Int. J. Distrib. Sens. Networks* **14**(2), 1550147718758263 (2018).
17. J. H. Burroughes et al., "Light-emitting diodes based on conjugated polymers," *Nature* **347**(6293), 539 (1990).
18. C. W. Tang and S. A. VanSlyke, "Organic electroluminescent diodes," *Appl. Phys. Lett.* **51**(12), 913–915 (1987).
19. Z. H. Kafafi, *Organic Electroluminescence*, CRC Press (2018).
20. W. Zhu et al., "Graphene radio frequency devices on flexible substrate," *Appl. Phys. Lett.* **102**(23), 233102 (2013).
21. P. A. Haigh et al., "A 20-Mb/s VLC link with a polymer LED and a multilayer perceptron equalizer," *IEEE Photonics Technol. Lett.* **26**(19), 1975–1978 (2014).
22. H. Chen et al., "A 51.6 Mb/s experimental VLC system using a monochromic organic LED," *IEEE Photonics J.* **10**(2), 7901312 (2018).
23. T. Yamada, "Latest development of soluble-OLED material and its application to mid-to large-sized panel production," in *26th Int. Workshop Active-Matrix Flatpanel Displays and Devices*, IEEE, Vol. 26, pp. 1–4 (2019).
24. H. J. Shin and T. W. Kim, "Ultra-high-image-density, large-size organic light-emitting device panels based on highly reliable gate driver circuits integrated by using InGaZnO thin-film transistors," *IEEE J. Electron Devices Soc.* **7**, 1109–1113 (2019).
25. J. Smith et al., "Application of flexible flat panel display technology to wearable biomedical devices," *Electron. Lett.* **51**(17), 1312–1314 (2015).
26. T. Kasahara, H. Kuwae, and J. Mizuno, "New era of device science," in *Pan Pacific Microelectron. Symp.*, IEEE, pp. 1–6 (2019).

27. J. Kalinowski, *Organic Light-Emitting Diodes: Principles, Characteristics and Processes*, CRC Press (2018).
28. P. Deng, M. Kavehrad, and M. A. Kashani, "Nonlinear modulation characteristics of white LEDs in visible light communications," in *Opt. Fiber Commun. Conf.*, Optical Society of America, p. W2A.64 (2015).
29. P. A. Haigh et al., "Wavelength-multiplexed polymer LEDs: towards 55 Mb/s organic visible light communications," *IEEE J. Sel. Areas Commun.* **33**(9), 1819–1828 (2015).
30. S. T. Le et al., "10 Mb/s visible light transmission system using a polymer light-emitting diode with orthogonal frequency division multiplexing," *Opt. Lett.* **39**(13), 3876–3879 (2014).
31. A. Burton et al., "Optoelectronic modelling, circuit design and modulation for polymer-light emitting diodes for visible light communication systems," in *26th Int. Conf. Telecommun.*, IEEE, pp. 55–59 (2019).
32. A. Burton et al., "Smart receiver for visible light communications: design and analysis," in *8th Int. Symp. Commun. Syst., Networks and Digital Signal Process.*, IEEE, pp. 1–5 (2012).
33. Z. Zeng et al., "Angle diversity receiver in LiFi cellular networks," in *IEEE Int. Conf. Commun.*, IEEE, pp. 1–6 (2019).
34. C. Chen et al., "An omnidirectional user equipment configuration to support mobility in LiFi networks," in *IEEE Int. Conf. Commun. Workshops*, IEEE, pp. 1–6 (2019).
35. M. D. Soltani et al., "Bidirectional optical spatial modulation for mobile users: toward a practical design for LiFi systems," *IEEE J. Sel. Areas Commun.* **37**(9), 2069–2086 (2019).
36. N. V. Khanh et al., "Investigation on MIMO OLED VLC system performance," in *Novel Opt. Mater. and Appl.*, Optical Society of America, p. JTU5A. 61 (2018).
37. P. A. Haigh et al., "A MIMO-ANN system for increasing data rates in organic visible light communications systems," in *IEEE Int. Conf. Commun.*, IEEE, pp. 5322–5327 (2013).
38. H. Chen et al., "A 1.9 Mbps OFDM-based all-organic visible light communication system," in *IEEE Int. Conf. Commun. Syst.*, IEEE, pp. 1–6 (2016).
39. P. Haigh et al., "Organic visible light communications: methods to achieve 10 Mb/s," in *IEEE Photonics Conf.*, IEEE, pp. 553–554 (2017).
40. M. Dyble et al., "Impact of dimming white LEDs: chromaticity shifts due to different dimming methods," *Proc. SPIE* **5941**, 59411H (2005).
41. J. W. Gorman and R. Toman, "Selection of variables for fitting equations to data," *Technometrics* **8**(1), 27–51 (1966).
42. P. A. Haigh et al., "Multi-band carrier-less amplitude and phase modulation for bandlimited visible light communications systems," *IEEE Wireless Commun.* **22**(2), 46–53 (2015).
43. P. A. Haigh et al., "A multi-CAP visible-light communications system with 4.85-b/s/Hz spectral efficiency," *IEEE J. Sel. Areas Commun.* **33**(9), 1771–1779 (2015).
44. P. Chvojka et al., "On the m-CAP performance with different pulse shaping filters parameters for visible light communications," *IEEE Photonics J.* **9**(5), 1–12 (2017).
45. M. M. Merah, H. Guan, and L. Chassagne, "Experimental multi-user visible light communication attocell using multiband carrierless amplitude and phase modulation," *IEEE Access* **7**, 12742–12754 (2019).
46. M. I. Olmedo et al., "Multiband carrierless amplitude phase modulation for high capacity optical data links," *J. Lightwave Technol.* **32**(4), 798–804 (2014).
47. K. Yoshida et al., "245 MHz bandwidth organic light-emitting diodes used in a gigabit optical wireless data link," *Nat. Commun.* **11**, 1171 (2020).

Zahra Nazari Chaleshtori received her MSc degree from Isfahan University of Technology, Iran, in 2016. Currently, she is a PhD candidate at Czech Technical University (CTU) in Prague, Czech Republic. She is focused on the utilization of organic LED-based visible light communications for device-to-device. She is involved in EU H2020 Marie Skłodowska-Curie Innovative Training Network (VisIoN 764461) and is a member of Wireless and Fiber Optics team at CTU.

Andrew Burton received his BEng (Hons.), MSc degrees (distinction), and PhD from Northumbria University, United Kingdom. Since graduation he worked as a research fellow

at Northumbria University until 2019, when he joined ISOCOM company as a technical manager. His research interests include electronics, optical communications, and visible-light communications.

Stanislav Zvanovec received his MSc degree and PhD from the CTU in Prague, in 2002 and 2006, respectively. He is a full professor, the deputy head of the Department of Electromagnetic Field, and the leader of Wireless and Fiber Optics team at CTU. His current research interests include FSO and fiber optical systems, VLC, and RF over optics. He is the author of two books and more than 250 journal articles and conference papers.

Zabih Ghassemlooy FOSA, FIET, SMIEEE, received his BSc (Hons.) degree in EE Engineering from Manchester Metropolitan University in 1981 and his MSc degree and PhD from Manchester University, United Kingdom, in 1984 and 1987, respectively. From 1987 to 88, he was a postdoctoral research fellow in the City University, United Kingdom. From 2004 to 14, he was an associate dean researcher, Faculty of Engineering and Environmental, Northumbria University, head of the Optical Communications Research Group, research fellow in 2016, and distinguished professor in 2015, Chinese Academy of Science. He has published 850 publications. His research interests are optical wireless communications, free-space optics, and visible light communications. He is the chief editor of the *British Journal of Applied Science and Technology*.

Petr Chvojka received his MSc degree and PhD from the Faculty of Electrical Engineering, CTU in Prague, in 2013 and 2018, respectively. He is currently working as a research fellow at the Department of Electromagnetic Field, CTU, in Prague, where he is a member of the Wireless and Fiber Optics Group. His research focuses on optical systems design and modeling, including inorganic and organic devices and digital signal processing techniques for visible light communications.

5.2 A Flexible OLED based VLC Link with *m-cap* Modulation

This chapter is a version of the published manuscript:

Z.N. Chaleshtori, A. Burton, Z. Ghassemlooy, S. Zvanovec, “A Flexible OLED based VLC Link with *m-cap* Modulation,” In 2019 15th International Conference on Telecommunications (ConTEL), pp. 1–6, 2019, IEEE.

Connection to my Ph.D. thesis:

CAP modulation has been the focus of increasing research in recent years due to a number of advantages including high spectral efficiency. The *m*-CAP modulation scheme is adopted in this research due to (i) its ability to reduce the effect of the highly bandlimited frequency response of OLEDs acting as a low-pass filter; (ii) be used as a multiuser scheme (e.g., personalized advertising); and (iii) be implemented more simply compared with the OFDM. Therefore, a flexible OLED is proposed as a light source for *m*-CAP VLC, where the effect of the beam pattern of curved OLED is investigated experimentally as well.

A Flexible OLED based VLC Link with m -CAP Modulation

Zahra Nazari Chaleshtori¹, Andrew Burton², Zabih Ghassemlooy², Stanislav Zvanovec¹

¹Department of Electromagnetic Field, Faculty of Electrical Engineering, Czech Technical University in Prague, Prague, Czech Republic, 16627

²Optical Communications Research Group, Faculty of Engineering and Environment, Northumbria University, Newcastle-upon-Tyne, NE1 8ST, UK

{nazarzah; xzvanove}@fel.cvut.cz, {z.ghassemlooy; andrew2.burton}@northumbria.ac.uk

Abstract—In recent years there has been a growing interest in using organic light emitting diodes (OLEDs) for illumination in indoor environments. They offer attractive features such as flexibility and large active areas at a low cost; they are energy efficient and have higher illumination levels compared to silicone based LEDs. In addition, the utilization of OLEDs have increased in devices such as smart mobile phones and TVs because of their low thickness. This paper investigates the performance of an OLED based visible light communications (OVLC) system, using a curved and flat OLED with multiband carrierless amplitude and phase (m -CAP) modulation for $m = 2$ at different angles of incidence on the optical receiver. It is shown that the BER performance is improved (i.e., below the forward error correction (FEC) limit of 3.8×10^{-3}) with the curved OLED when the optical receiver moving along a circular path for the viewing angles greater 40° compared to the flat OLED, which is advantageous in device to device communications.

Keywords- flexible organic LEDs; m -CAP modulation; visible light communications.

I. INTRODUCTION

Visible light communications (VLC) simultaneously provides illumination and wireless data transmission using the visible spectrum of 380 nm to 750 nm [1, 2]. VLC is a green technology and can offer advantages over the radio frequency (RF) communication systems such as immunity to RF electromagnetic interference, a license-free spectrum, inherent security, and lower power consumption [1, 3]. VLC systems employ either conventional silicone based light emitting diodes (LEDs), organic based LEDs (OLEDs) or even white laser diodes (LDs) as light sources [4]. The applications of VLC has been increasing due to the widespread use of LEDs as the light sources in indoor and outdoor environments. For example, indoor positioning systems [5], aviation [6], underwater communications [6], intelligent transportation systems [7], internet of things (IoT) [8] and camera communications [9].

There has been a growing interest into adopting OLEDs over the conventional solid-state lights. Flat panel OLED displays are attractive due to properties such as the possibility of fabricating the device on flexible substrates, achieving larger active areas using low-cost solution processing techniques and environmentally friendly (i.e., a green technology) [4]. Organic electronics are able to use plastics as the substrates, hence can be made to be mechanically flexible and with arbitrary shapes.

This allows for the production of curved or rolled OLED panels/displays, which can also be employed in wearable products (i.e., smart watches and wearable computers). In addition, the maximum thickness of an OLED is 500 nm [4], which is ideal for thin film devices (such as mobile phones, computers, and TVs), thus providing the potential of infrastructure-to-device (I2D) and device-to-device (D2D) communications [9]. In D2D communications, the data can be transmitted via pixels of the mobile phones display [10] and is captured using the camera(s) in smartphones [11].

However, the reported modulation bandwidth B_{mod} of OLEDs is lower than silicone LEDs (i.e., kHz compared to MHz), which is limited by the carrier lifetime [12]. Recent improvements of the OLEDs properties are showing that with new materials increased charge mobility can be achieved [13]. The performance of organic devices is dependent on the charge mobility, i.e., as charge carrier mobility determines how fast the device can be turned on and off. Recently, a number of advanced communication techniques and signalling schemes have been proposed to increase the transmission data rates R_b . A significant enhancement in R_b from 550 kb/s [14] to more than 50 Mb/s was reported for OLED-based visible light communication (OVLC) [15]. An almost 55 Mb/s OLED link was reported in [16] where wavelength-division multiplexing (WDM) (using red/orange, blue and green wavelengths) and an artificial neural network (ANN) equalizer was used. In [17], a 51.6 Mb/s experimental monochromatic OLED based VLC system was demonstrated; where the OLED modulated by offset-quadrature amplitude modulation-based orthogonal frequency division multiplexing (OFDM) was employed with a joint linear minimum mean-square-error (LMMSE) based decision feedback equalizer (DFE). Furthermore, employing polymer LEDs (PLEDs) in the VLC systems has shown a notable enhancement in R_b , as reported in [18]. For instance, 10 Mb/s was achieved using PLED (having B_{mod} of 270 kHz) and on-off keying (OOK) in combination with a least mean square (LMS) equalizer [19], reaching the same R_b as OFDM organic VLC system [20]. Next, through low-temperature thermal annealing and crystallisation of the polymer, a marginal improvement in B_{mod} up to 350 kHz has been reported in [18] with R_b of 20 Mb/s using an ANN equalizer. In [21], a fully organic flexible VLC system using off-the-shelf components, flexible circuits and flexible commercial OLED and an organic photodiode (PD) - manufactured in a roll-to-roll process - was reported. This all-organic flexible VLC

system is capable of transmitting an audio file in real-time. And their future goal is to design the driving circuits operating over hundreds of MHz, both in emission and transmission, and to build an OPD that could support this operating frequency.

The use of advanced modulation schemes to improve the spectral efficiency of bandlimited VLC systems are being investigated [20]. OFDM has the potential for supporting high order modulation formats such as quadrature amplitude modulation (QAM), where both amplitude and phase components were used to achieve spectrum efficiency [22]. Multiband carrierless amplitude and phase (*m*-CAP) also employs QAM, and is based on a combination of two pulse amplitude modulation (PAM) signals to form a QAM signal and their impulse responses form a Hilbert pair. CAP modulation has been the focus of increasing research in recent years due to a number of advantages including high spectral efficiency. In this paper a flexible OLED is proposed as a light source for *m*-CAP VLC, which can be used in short range device to device communications in a number of indoor applications. We characterize the OLED to determine the illumination profile and power current relationship. The link performance is quantified in terms of the bit error rate (BER).

The rest of the paper is organized as follows. In Section II, the structure of OLEDs is described. Section III discusses the experimental set-up. Section IV experimental results. Finally, conclusions are given in Section IV.

II. THE STRUCTURE OF OLEDS

The structure of an OLED consists of a substrate (glass, metal or plastic) to which all other layers are deposited, metal cathodes and anode, the organic photoactive layers and an external light extraction film, see Fig. 1 [1]. The organic layers are sandwiched between a transparent anode (indium tin oxide (ITO)) and a metal cathode (aluminium or silver) [1]. The organic materials can be long-chain polymers (i.e., PLEDs) or small organic molecules (i.e., SMOLEDs) in a crystalline phase [12]. Using flexible substrates, such as polyethylene terephthalate, provides OLED panels or displays that can be curved or rolled. These are used in wearable products, mobile phones, and TVs. As the production cost drops, non-rigid OLED lighting products begin to offer a competitive advantage over LED and other lighting technologies.

OLEDs have a low-pass filter transfer function with the cut-off frequency given by [1]:

$$f_c = \frac{1}{2\pi RC}, \quad (1)$$

where R is the effective resistance of the OLED and C is the plate capacitance expressed by [1]:

$$C = \frac{A\epsilon_0\epsilon_r}{d}, \quad (2)$$

where A is the OLED photoactive area, d is the OLED thickness, and ϵ_0 and ϵ_r are the permittivity of free space and relative dielectric constant of the organic layer, respectively.

According to (1) and (2), f_c is inversely proportional to the photoactive area; consequently, a larger photoactive area decreases the achievable B_{mod} and a restriction in R_b is imposed

on OVLC systems. Moreover, in bandlimited systems, inter-symbol interference (ISI) leads to BER degradation. In addition, high pass filtering or capacitive coupling leads to deviating the signal randomly from the DC level called the baseline wander (BLW), which is another challenge in OVLC systems. A number of techniques have been proposed to improve OVLC systems performance. For instance, high-level modulation schemes [20] and equalization using ANN [18].

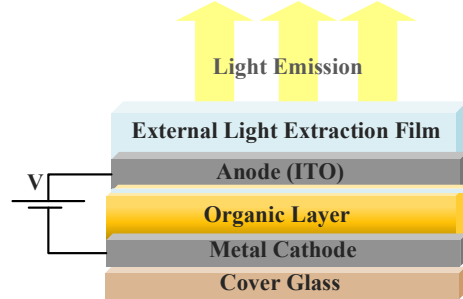


Fig. 1. An OLED structure

III. EXPERIMENTAL SET-UP

A block diagram of a *m*-CAP OVLC link is shown in Fig. 2. First, m independent pseudo-random data streams $d_m(t)$ (where $m = 2$) with the length of 12,000 bits are generated and mapped onto the QAM constellation. Note, in this work 16-QAM is considered. The real $\Re(a_i)$ and imaginary $\Im(b_i)$ components of the upsampled data are applied to their corresponding filters. Here we use square root raised cosine (SRRC) filters with carrier frequencies of 10 kHz (s_1 the first subcarrier) and 30 kHz (s_2 the second subcarrier) with the corresponding in-phase and quadrature components modulated onto the sine and cosine waves, respectively. The roll-off factor used for the root-raised the sine and cosine pulses is 0.15, as to stay with the literature. The filters outputs are summed, which represent the *m*-CAP signal $x(t)$ and is used for intensity modulation of the OLED via the output driver. At the receiver, following optical detection and amplification the regenerated electrical signal $y(t)$ is applied to the bit and frame synchronization module, and the output of the module is applied to two filters of g_I and g_Q which are the time-reversed SRRC filters used at the transmitter. The summed filters output signal $z(t)$ is downsampled and is fed to the M-QAM demapper to obtain the estimates transmitted data $d'_m(t)$.

The experimental test-bed for the proposed link uses a flexible OLED, which is depicted in Fig. 3. The *m*-CAP signal was supplied using an Agilent arbitrary function generator (AFG 3252). The *m*-CAP signal was generated in the Matlab domain. The required sampling frequency and a number of samples per symbol can be determined following the procedures outlined in [23] and the references within. The optical receiver (ORx) consists of a PD and a transimpedance amplifier (TIA) (Thorlabs PDA100A2). The flexible OLED panel has been bent with a curvature radius r of 11 cm, see Fig 4. Here we considered two cases for system evaluation: (i) the ORx moving along a fixed radius of $h = 30$ cm around the light source, (case1) see Fig. 4(a);

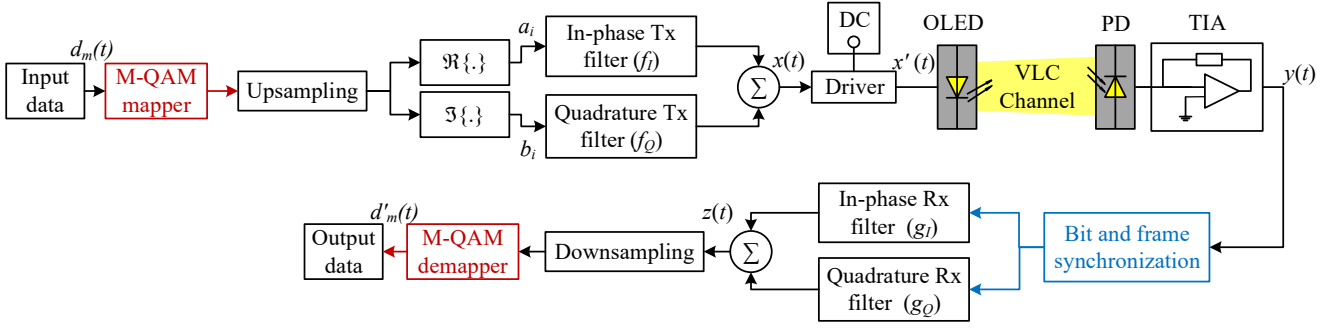


Fig. 2. The block diagram of the proposed system with m -CAP modulation.

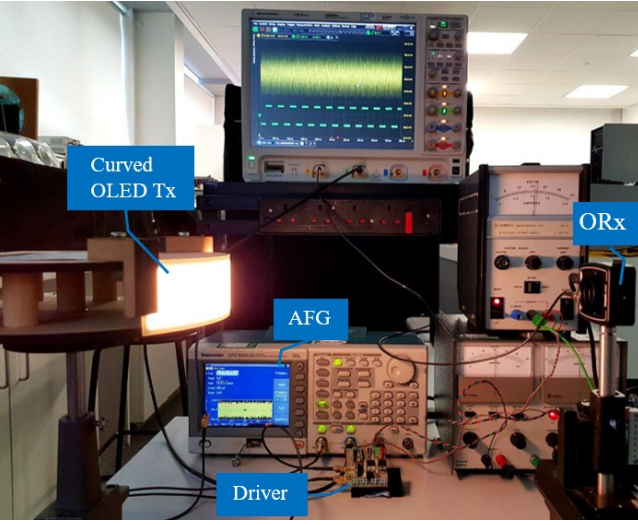


Fig. 3. An OVLC experimental test-bed with a curved OLED

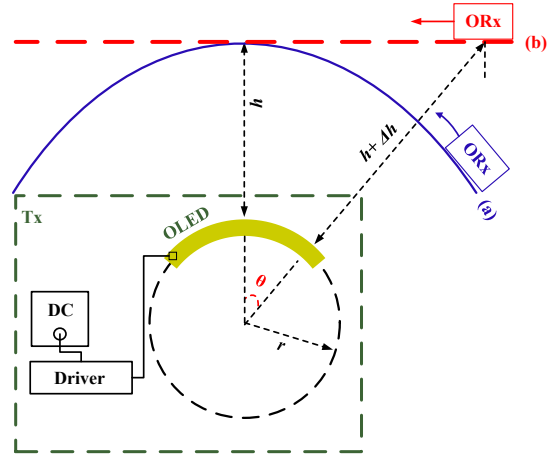


Fig. 4. The block diagram of the experimental set-up with the ORx moving along: (a) a circular path (case1) and (b) a straight path (case2).

and (ii) the Rx was placed on the axis in parallel to the light source, (case2) see Fig. 4(b). We measured the BER for both curved and flat OLEDs over the two scenarios. All the key system parameters are shown in Table I.

IV. EXPERIMENTAL RESULTS

A. Characterization of flexible OLED

The measured normalized optical spectrum (normalized to the maximum achieved intensity associated with the highest I_B) of the OLED at different bias currents I_B is depicted in Fig. 5(a), which shows the individual red, green and blue (RGB) components at the peak wavelengths of 620 nm (R), 555 nm (G), 450 nm and 480 nm (B). Next, we normalised the intensity plots shown in Fig. 5(a) to unity and then superimposed on top of each other with the result shown in Fig. 5(b). The plot reveals that the OLED has the same spectral distribution over a wide range of I_B

TABLE I. THE SYSTEM PARAMETERS

Equipment	Parameter	Value
OLED	Dimension	200 × 50 mm ²
	Type	flexible
	Bandwidth	43 (kHz)
	Maximum current	300 (mA)
	Bias current	160 (mA)
	Voltage amplitude	600 (mV)
	Threshold voltage	7 (V)
	Flux	75 (lm)
Luminous efficacy	50 to 55 (lm/W)	
Channel	Length	30 cm
ORx	Active area	75.4 mm ²
	Bandwidth	1.4 MHz at a 10 dB gain
	Output voltage	0 to 10 V
	Noise of amplifier	195 μV (RMS)
	NEP	6.75 × 10 ⁻¹² (W/√Hz) at λ = 960 nm

(i.e., 10-300 mA), thus, the emitted spectrum is independent of I_B and the dimming levels.

The measured $L-I-V$ curve of OLED is shown in Fig. 6, and the optical power displays a highly linear response over a wide current dynamic range of 22 dB (between 10-300 mA). Using linear curve-fitting the power $P_I = 2.4 I_B + 20$, which gives optical power (mW) associated with each I_B (mA), is defined. To measure the output optical power of OLED, an optical power meter (PM100D Thorlabs, S120VC 200-1100 nm 50 mW) with a narrow band optical blue filter with a transmissivity of > 0.96 , which was positioned at a distance 15 times greater than the OLED length in order to ensure a point source light at the far field was used. To determine the optical power P_I at specific values of I_B , we used $P_I = \alpha P_m$, where P_m is the measured power and α can be given by $\alpha = P_t/P_o$. P_t and P_o are the total area under the spectrum profile associated to I_B and area under the blue component, respectively. In Fig. 6, the inset shows a uniform illumination profile for the OLED along its length.

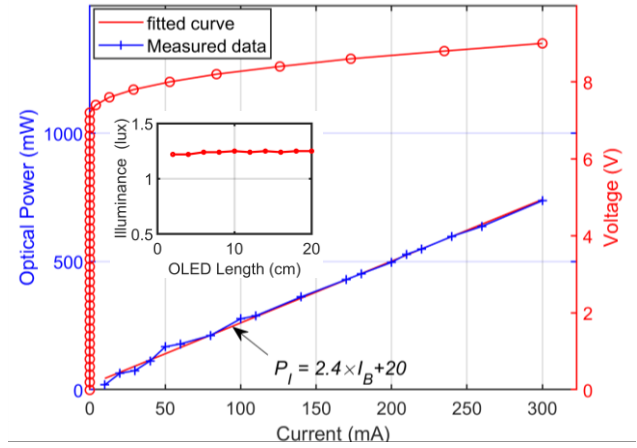


Fig. 6. The $L-I-V$ curves for flexible OLED. The illumination profile along the OLED length is shown in inset.

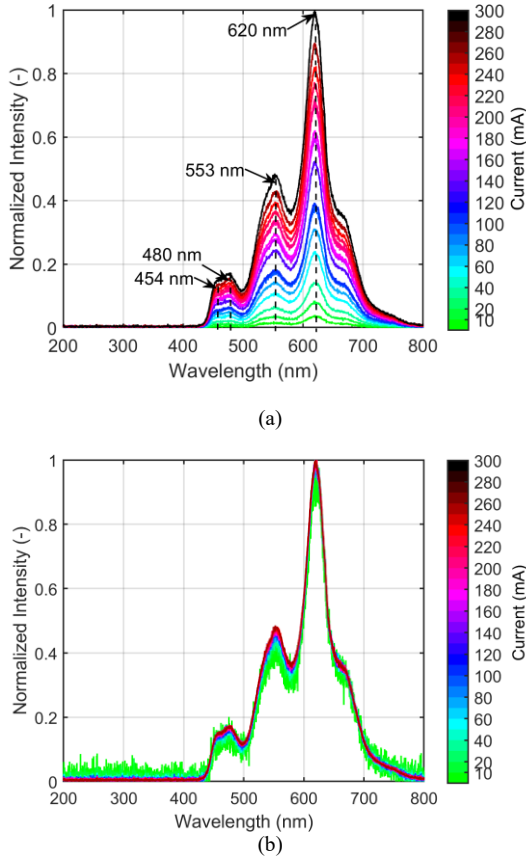


Fig. 5. (a) The optical spectrum of the flexible OLED under test with peak wavelengths marked where the legend color scale represents I_B , and (b) the spectrum of the OLED at different I_B corresponding to different dimming levels. Each of the spectral responses were normalized to unity and then superimposed on top of each other.

B. m -CAP modulation for OVLC link with flexible OLED

Fig. 7 demonstrates the polar plots of the BER for the proposed m -CAP OVLC system for s_1 and s_2 for both the flexible and flat OLEDs and for the circular path (see Fig. 4(a)). Also shown for reference is the forward error correction (FEC) BER limit of 3.8×10^{-3} . As illustrated, the BER display a symmetry about the origin (i.e., The ORx is facing the OLED at θ of 0°) due to uniform illumination profile of OLED referred to the inset plot in Fig. 6 (i.e., the same signal to noise ratio (SNR) across the entire face of OLED). As can be seen, the BER for the curved OLED is improved over a wider θ compared to the flat OLED because of fixed transmission range between the ORx and the OLED. Note, for the circular path the BER remains just below the FEC limit for θ within the range of $\pm 78^\circ$ and $\pm 50^\circ$ for the curved and flat OLEDs, respectively and for s_1 . However, for s_2 , θ drops by 17° and 8° for the curved and flat OLED, respectively.

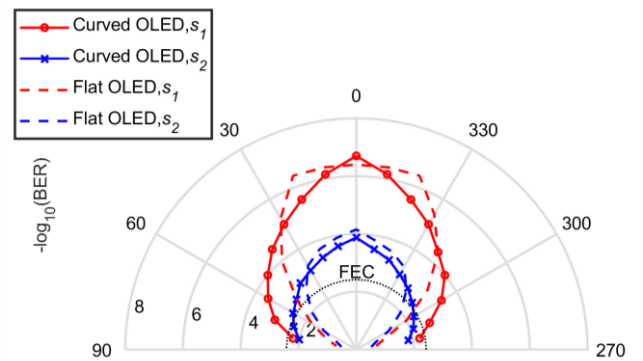


Fig. 7. The polar curve of BER for m -CAP with s_1 and s_2 for case1 (i.e., when the circular paths of ORx with respect to the OLED) for curved and flat OLED.

The BER versus the angle θ for the straight path for s_1 and s_2 are shown in Fig. 8. In this case, θ are 30° and 42° to meet the FEC limit for the curved and flat OLEDs, respectively for s_1 . Note that, for the straight path the transmission distance between the ORx and the transmitter increase by Δh when moving away from the centre point (i.e., $\theta = 0$). To consider this, Fig. 9 depicts the BER versus Δh for curved and flat OLED (note, $\Delta h = 0$ corresponds to the centre point of OLED). As shown, for the flat OLED and for s_1 , the BER remains below the FEC limit for $-7 \text{ cm} < \Delta h < 10 \text{ cm}$, while for the curved OLED the distance of ORx is in the range of $-5 \text{ cm} < \Delta h < 5 \text{ cm}$. The results show that, the potential of using the flexible OLEDs in D2D communications, display-based communications, etc., where the viewing position is not problematic.

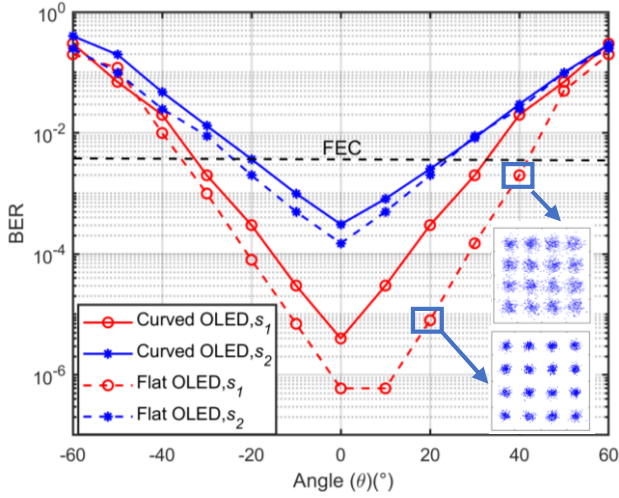


Fig. 8. The BER versus the angle θ for the case2 for curved and flat OLED with m -CAP and for s_1 and s_2 . Note, the straight paths of ORx with respect to the OLED are referred to as case2.

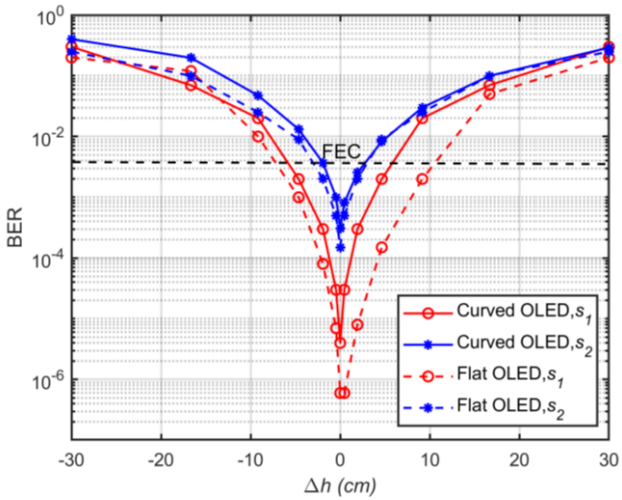


Fig. 9. The BER versus the Δh for m -CAP with s_1 and s_2 ; for curved and flat OLED for the case2. Note, the straight path of ORx with respect to the OLED is referred to as case2.

V. CONCLUSION AND FUTURE OUTLOOK

In this paper, we proposed m -CAP VLC using a flexible OLED as the transmitter. We carried out the characterization of the OLED and showed that, it has a highly linear power-current relationship and there were no changes in the colour as a function of the current over a wide range (i.e., 10-300 mA). The link BER performance was measured and compared with a flat OLED based m -CAP VLC. It was shown that the curved OLED with the optical receiver moving along a circular path offered improved BER performance (i.e., below the FEC limit) over a wide viewing angle for a single subcarrier based m -CAP VLC. This work demonstrated the potential of utilizing flexible OLED based VLC in short range device to device communications.

ACKNOWLEDGEMENT

The work is supported by the European Union's Horizon 2020 research and innovation programme under the Marie Skłodowska-Curie grant agreement no 764461 (VISION) and the Czech Rep. funded project GACR 17-17538S and the UK EPSRC grant EP/P006280/1: MARVEL.

REFERENCE

- [1] Z. Ghassemlooy, L. N. Alves, S. Zvanovec, and M.-A. Khalighi, *Visible Light Communications: Theory and Applications*. CRC Press, 2017.
- [2] Z. Ghassemlooy, W. Popoola, and S. Rajbhandari, *Optical wireless communications: system and channel modelling with Matlab®*. 2nd Edition. CRC press, NY, 2019.
- [3] B. Lin, X. Tang, Z. Ghassemlooy, C. Lin, and Y. Li, "Experimental demonstration of an indoor VLC positioning system based on OFDMA," *IEEE Photonics Journal*, vol. 9, no. 2, pp. 1-9, 2017.
- [4] P. A. Haigh, Z. Ghassemlooy, S. Rajbhandari, and I. Papakonstantinou, "Visible light communications using organic light emitting diodes," *IEEE Communications Magazine*, vol. 51, no. 8, pp. 148-154, 2013.
- [5] H. Lv, L. Feng, A. Yang, P. Guo, H. Huang, and S. Chen, "High accuracy VLC indoor positioning system with differential detection," *IEEE Photonics Journal*, vol. 9, no. 3, pp. 1-13, 2017.
- [6] D.-R. Kim, S.-H. Yang, H.-S. Kim, Y.-H. Son, and S.-K. Han, "Outdoor visible light communication for inter-vehicle communication using controller area network," in *2012 Fourth International Conference on Communications and Electronics (ICCE)*, 2012: IEEE, pp. 31-34.
- [7] T. Nguyen, A. Islam, and Y. M. Jang, "Region-of-interest signaling vehicular system using optical camera communications," *IEEE Photonics Journal*, vol. 9, no. 1, pp. 1-20, 2017.
- [8] S. Schmid, T. Richner, S. Mangold, and T. R. Gross, "EnLighting: An indoor visible light communication system based on networked light bulbs," in *2016 13th Annual IEEE International Conference on Sensing, Communication, and Networking (SECON)*, 2016: IEEE, pp. 1-9.
- [9] Y. Li, Z. Ghassemlooy, X. Tang, B. Lin, and Y. Zhang, "A VLC smartphone camera based indoor positioning system," *IEEE Photonics Technology Letters*, vol. 30, no. 13, pp. 1171-1174, 2018.
- [10] R. Boubezari, H. Le Minh, Z. Ghassemlooy, and A. Bouridane, "Smartphone camera based visible light communication," *Journal of Lightwave Technology*, vol. 34, no. 17, pp. 4121-4127, 2016.
- [11] B. Lin, Z. Ghassemlooy, C. Lin, X. Tang, Y. Li, and S. Zhang, "An indoor visible light positioning system based on optical camera communications," *IEEE Photonics Technology Letters*, vol. 29, no. 7, pp. 579-582, 2017.
- [12] C.-H. Hsiao, C.-F. Lin, and J.-H. Lee, "Driving voltage reduction in white organic light-emitting devices from selectively doping in ambipolar blue-emitting layer," *Journal of Applied Physics*, vol. 102, no. 9, p. 094508, 2007.
- [13] W. Zhu *et al.*, "Graphene radio frequency devices on flexible substrate," *Applied Physics Letters*, vol. 102, no. 23, p. 233102, 2013.

- [14] P. A. Haigh *et al.*, "Exploiting equalization techniques for improving data rates in organic optoelectronic devices for visible light communications," *Journal of lightwave technology*, vol. 30, no. 19, pp. 3081-3088, 2012.
- [15] Z. N. Chaleshtori, P. Chvojka, S. Zvanovec, Z. Ghassemlooy, and P. A. Haigh, "A Survey on Recent Advances in Organic Visible Light Communications," in *2018 11th International Symposium on Communication Systems, Networks & Digital Signal Processing (CSNDSP)*, 2018: IEEE, pp. 1-6.
- [16] P. A. Haigh *et al.*, "Wavelength-multiplexed polymer LEDs: Towards 55 Mb/s organic visible light communications," *IEEE Journal on Selected Areas in Communications*, vol. 33, no. 9, pp. 1819-1828, 2015.
- [17] H. Chen, Z. Xu, Q. Gao, and S. Li, "A 51.6 Mb/s Experimental VLC System Using a Monochromic Organic LED," *IEEE Photonics Journal*, vol. 10, no. 2, pp. 1-12, 2018.
- [18] P. A. Haigh *et al.*, "A 20-Mb/s VLC link with a polymer LED and a multilayer perceptron equalizer," *IEEE Photonics Technology Letters*, vol. 26, no. 19, pp. 1975-1978, 2014.
- [19] P. A. Haigh *et al.*, "Visible light communications: real time 10 Mb/s link with a low bandwidth polymer light-emitting diode," *Optics express*, vol. 22, no. 3, pp. 2830-2838, 2014.
- [20] S. T. Le *et al.*, "10 Mb/s visible light transmission system using a polymer light-emitting diode with orthogonal frequency division multiplexing," *Optics letters*, vol. 39, no. 13, pp. 3876-3879, 2014.
- [21] C. Vega-Colado *et al.*, "An All-Organic Flexible Visible Light Communication System," *Sensors*, vol. 18, no. 9, p. 3045, 2018.
- [22] M. S. Islim *et al.*, "Towards 10 Gb/s orthogonal frequency division multiplexing-based visible light communication using a GaN violet micro-LED," *Photonics Research*, vol. 5, no. 2, pp. A35-A43, 2017.
- [23] M. I. Olmedo *et al.*, "Multiband carrierless amplitude phase modulation for high capacity optical data links," *Journal of Lightwave Technology*, vol. 32, no. 4, pp. 798-804, 2014.

5.3 Performance Evaluation of Various Training Algorithms for ANN Equalization in Visible Light Communications with an Organic LED

This chapter is a version of the published manuscript:

Z.N. Chaleshtori, P.A. Haigh, P. Chvojka, S. Zvanovec, and Z. Ghassemlooy, “Performance Evaluation of Various Training Algorithms for ANN Equalization in Visible Light Communications with an Organic LED,” In 2019 2nd West Asian Colloquium on Optical Wireless Communications (WACOWC), pp. 11–15, 2019, IEEE.

Connection to my Ph.D. thesis:

As mentioned in [chapter 3](#) due to slow charge transport characteristics, which is depends upon the manufacturing process, materials and the physical dimensions, the OLEDs B_{mod} limited in range of a few kHz. Thus, resulting in a bandwidth bottleneck in optical transmission systems and reduced data throughput. In the literature, equalization techniques have been presented to overcome the bandwidth bottleneck in OVLC systems. The working principle of an ANN is based on mapping the input-output sequence from the received data and a known dataset, and by checking the system’s success using a test data. Since the learning algorithm significantly affects the ANN performance, the effect of various learning algorithms and a number of neurons in the hidden layer and quantify the link performance are investigated.

Performance Evaluation of Various Training Algorithms for ANN Equalization in Visible Light Communications with an Organic LED

Zahra Nazari Chaleshtori¹, Paul A. Haigh², Petr Chvojka¹, Stanislav Zvanovec¹, Zabih Ghassemlooy³

¹Department of Electromagnetic Field, Czech Technical University in Prague, Prague, Czech Republic, 16627

²School of Engineering, Newcastle University, Newcastle upon Tyne, NE1 7RU, UK

³Optical Communications Research Group, Faculty of Engineering and Environment, Northumbria University, Newcastle upon Tyne, NE1 8ST, UK

{nazarzah; petr.chvojka; xzvanovec}@fel.cvut.cz, paul.haigh@newcastle.ac.uk, z.ghassemlooy@northumbria.ac.uk

Abstract—This paper evaluates the effect of training algorithms in an artificial neural network (ANN) equalizer for a feedforward multi-layer perceptron configuration in visible light communication systems using a low bandwidth organic light source. We test the scaled conjugate-gradient, conjugate-gradient backpropagation and Levenberg-Marquardt back propagation (LM) algorithms with 5, 10, 20, 30, and 40 neurons. We show that, LM offers superior bit error rate performance in comparison to other training algorithms based on the mean square error. The training methods can be selected based on the trade-off between complexity and performance.

Keywords—Artificial neural network equalizer; Equalization; Organic LEDs; Visible light communications

I. INTRODUCTION

Recently, visible light communications (VLC) have attracted significant attention as a complementary access network to the radio frequency (RF) based wireless systems in order to meet the growing demand for mobile data. In VLC systems, which utilizes the visible wavelength band (i.e., 370–780 nm) for transmission of data, both inorganic white light emitting diodes (LEDs) and organic LEDs (OLEDs) can be used [1, 2]. OLEDs offer several advantages over the conventional LEDs, such as large and arbitrarily shaped photoactive areas, mechanical flexibility, and ultra-low-cost wet processing methods but at the cost of much reduced modulation bandwidth B_{mod} (i.e., a few hundred kHz) [1-3]. As such, there is a growing interest in OLED-based VLC (OVLC) in certain applications such as display technologies, infrastructure-to-device (I2D) and device-to-device (D2D) communications, smart televisions, etc. [4].

In smart devices with OLED displays [5] pixels can be individually intensity modulated for data transmission, which can be received using the built-in camera of another smartphone (i.e., D2D communications) [6, 7]. A great deal of attention on the implementation of OLEDs in high-resolution displays and applications in low-cost future solid-state lighting are good reasons to extend the use of OVLC technology [8].

The optoelectronics devices (i.e., in this case OLED), with a typical luminous efficiency of 40-60 lm/W (120 lm/W in inorganic LEDs [9]) the low B_{mod} due to slow charge transport characteristics, depending upon the manufacturing process,

materials and the physical dimensions [10], leads to a bandwidth bottleneck in optical transmission systems (i.e., much reduced data throughput) [1]. To overcome the bandwidth bottleneck in OVLC, a number of techniques have been investigated including equalization, signalling schemes and the optimum driver circuits [11].

A review of OVLC systems is provided in [12] which shows that using different organic devices, modulation schemes and digital signal processing techniques the achievable data rate R_b can be increased significantly from 550 kb/s [9] to > 50 Mb/s [13]. For instance, the first notable R_b of 10 Mb/s was achieved by adopting a polymer LED (PLED) with a B_{mod} of 270 kHz using on-off keying (OOK) in combination with a least mean square (LMS) equalizer [14]. The same R_b was achieved using orthogonal frequency-division multiplexing (OFDM) in [15]. Next, through low-temperature thermal annealing and crystallisation of the polymer, a slight marginal improvement in B_{mod} (i.e., 350 kHz) was reported, which was used in OVLC in combination with an artificial neural network (ANN) to achieve a R_b of 20 Mb/s [16]. In [4], using wavelength-division multiplexing (WDM) (i.e., red/orange, blue and green devices) and an ANN equalizer an aggregated link capacity of ~55 Mb/s was reported. Recently, a 51.6 Mb/s VLC link employing a monochromic OLED modulated by an offset-quadrature amplitude modulation (QAM)-based OFDM signal with bit- and power-loading and a joint linear minimum mean-square-error (LMMSE) based decision feedback equalizer (DFE) was reported [13], which is the highest single-wavelength transmission speed reported in OVLC so far.

In the literature, ANN equalization has been reported as an effective method to compensate for the limitation in R_b due to limited B_{mod} of OLEDs [17-19]. Note that, the working principle of an ANN is based on mapping the input-output sequence from the received data and a known dataset, and by checking the system's success using a test data [20]. Since the learning algorithm significantly affects the ANN performance, in this paper we investigate the effect of various learning algorithms and a number of neurons in the hidden layer and quantify the link performance in terms of the bit error rate (BER).

The rest of the paper is organized as follows. In Section II, ANN equalization is introduced. In Section III the results are discussed. Finally, conclusions are given in Section IV.

II. EQUALIZATION

Equalizers represent one of the most effective techniques to compensate multipath induced inter-symbol interference (ISI) in band-limited communication systems. Generally, equalizers can be classified into two categories; analog and digital with different complexity and performance [11]. Although an analog domain equalizer is simple, based on a high pass resistor-capacitor (RC) filter [21] can result in attenuation of low-frequency components, and hence, the baseline wander (BLW) phenomenon [1]. In [22], an OVLC using an OLED with B_{mod} of 150 kHz and an RC equalizer at a R_b of 2.15 Mb/s was reported.

On the other hand, digital equalizers such as LMS or recursive least squares (RLS)-based feedforward and DFE and ANN offer significant system performance improvement at the cost of increased complexity [1, 2]. The ANN takes loose inspiration from the human brain, which uses synapses and neurons to learn and compute. ANNs retain the neurons for computation and use tapped delay lines (in a transversal configuration) as the inputs. ANNs solve nonlinear problems via the neurons, which are divided into a parallel structure where the inputs to each neuron are scaled by an adaptive adjustable contribution of the synaptic weights of each input. Increasing the number of neurons boosts the ANN learning capacity while increasing complexity [23].

The structure of the model, the type of activation function, and the learning algorithm affect neural-network model implementation [20, 23]. The block diagram in Fig. 1 illustrates the fundamental model of a neuron, which forms the basis for designing a large family of NNs [24]. The neural model includes an externally applied bias b_k , which has the effect of increasing or lowering the contribution of each weighted input to the activation function. The output of the k^{th} neuron is given by [24, 25]:

$$y_k = \varphi(v), \quad (1)$$

where $v = u_k + b_k$ and u_k is the summed weighted contribution of the inputs defined as:

$$u_k = \sum_{j=1}^n w_{kj} x_j, \quad (2)$$

where x_1, x_2, \dots, x_n are the input signals, and $w_{k1}, w_{k2}, \dots, w_{kn}$ are the weights of neuron k . Several activation functions are introduced in [24] including threshold function, piecewise linear function, and log-sigmoid function, however, any differentiable formulation may be used. In the following, a log-sigmoid function is considered for the hidden layer output and a linear function at the ANN output as is typical in the literature [3]. An example of the log-sigmoid function, employed in this work, is defined by [24]:

$$\varphi(v) = \frac{1}{1 + \exp(-av)}, \quad (3)$$

where a is the slope parameter of the log-sigmoid function.

In general, there are four fundamentally different network architectures that can be used as an equalizer (i) feedforward single-layer; (ii) feedforward multilayer; (iii) feedback single-layer; and (iv) feedback multilayer networks. In a multi-layer configuration, the neurons are organized as follows; an input-layer consisting of an observation vector of incoming samples, a hidden layer where the processing occurs and an output layer. A recurrent (feedback) ANN is different to a feedforward NN in that has at least one feedback loop, see [24], which generally results in improvement in non-linear mapping at the cost of potential error propagation.

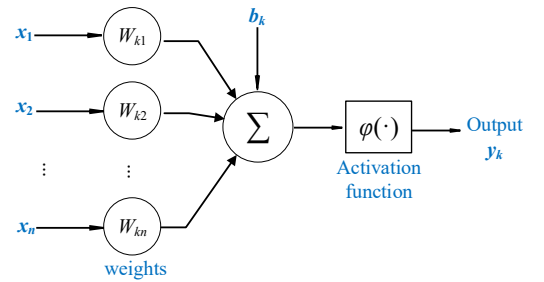


Fig. 1. The neural network model

For channel equalization, the multilayer perceptron (MLP), the functional link ANN (FLANN) and radial basis function (RBF) ANN are known as the popular choice of ANN [25, 26]. RBF and FLANN provide greater error performance, at the cost of increased computational complexity [25].

ANNs require a training sequence to adjust the neuron weights in order to map the input-output sequence of the system under test. For early stopping, algorithms update the neuron weights until the error between the equalized data and the target data does not exceed an objective error. It is also possible to allow ANN to run its training algorithm for objective epochs or seconds [3]. There are a number of training algorithms (see Table 1) that could be used, which are also available in the Matlab™ [27, 28]. One of the most popular ones is Levenberg-Marquardt back-propagation (LM) [25]. The conventional form of the conjugate-gradient (CG) training algorithm requires a time-consuming line search but a modified version of it (i.e., conjugate-gradient (SCG)) introduced by Møller [29] avoids the use of a line search [24].

When comparing against other digital equalisation techniques, ANNs offer several advantages: (i) *generalization* - due to input-output mapping, as opposed to ISI estimation, complex decision boundaries are created and hence, even when an error or bit sequence not included in the training sequence can be estimated [25]; and (ii) *evidential response* - to reject ambiguous patterns in classification, where a NN can provide information of particular pattern selected as well as the confidence in the decision made [24]. ANNs have been palpable in communication systems as a result of their flexibility and

learning capability. There are a large number of algorithms, which could be used for determining the network parameters and for training NNs. It is noticeable that the training algorithm and the network topology affect the performance of the NN [28]. Therefore, in this paper, we investigate the effect of the various network types and number of neurons in the hidden layer on the learning performance of the NN using LMBP, SCG, and conjugate gradient backpropagation (CGP) algorithms for feedforward networks.

The training algorithms and their main features are summarized in Table I [27, 28].

TABLE I. THE TRAINING ALGORITHMS [27, 28]

Algorithm	Feature - Method used to update weight and bias values
Levenberg–Marquardt LM	Levenberg-Marquardt optimization.
Conjugated gradient descent CGB	Conjugate gradient backpropagation with Powell-Beale restarts.
SCG	Scaled conjugate gradient method.
CGP	Gradient backpropagation with Polak-Ribière updates.
Resilient backpropagation RP	Resilient backpropagation algorithm.
Quasi-Newton algorithm OSS	One-step secant method.
BFG	BFGS quasi-Newton method.

III. EQUALIZATION RESULTS

In this work, a feed-forward multi-layer NN equalizer for an OOK-OVLC link is investigated. The schematic system block diagram is shown in Fig. 2. At the transmitter (Tx), a pseudo binary data pattern with a length of 10^6 is used for intensity modulation of the OLED. Note, OLED is modelled as a low pass filter with B_{mod} of 100 kHz. The optical signal propagating along the channel of 0.15 m long is converted back into an electrical signal using an optical receiver which consists of the photodetector and a trans-amplifier, and processing was carried out in the Matlab domain. The matched filter used as the detection type and synchronization with the transmitted data is carried out before being passed through a low pass filter (LPF) then downsampling the signal is applied to ANN equalizer in order to overcome the bandwidth limitation of OLED. The output of ANN passed through the threshold detector for comparison with the transmitted signal as shown in Fig. 2. The inclusion of a low pass filter is to perform the combined functions of noise, and anti-alias filtering, whereas

downsampling is used to reduce the number of sample points passed to the NN. Note, the procedure for training algorithms in multilayer perceptron NN is classified according to following steps (i) define the network structure - the network, activation functions is selected and the network parameters are initialized; (ii) define parameters associated with the training algorithm such as error goal, maximum number of epochs (iterations); and (iii) the training algorithm. The key system parameters adopted in this work are listed in Table II.

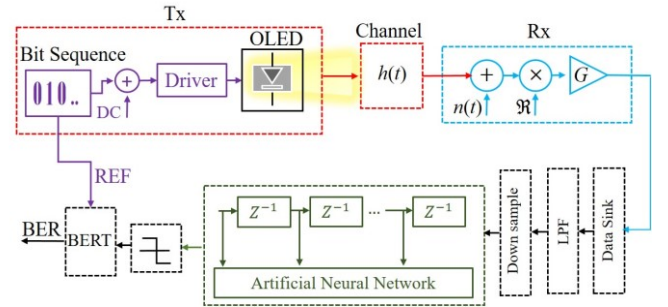


Fig. 2. The scheme of the OVLC with the post-detection ANN equalizer

Figs. 3(a)-(d) show the BER as a function of the energy/bit to noise ratio E_b/N_0 for training algorithms of LM, SCG, and CGP for MLP-ANN adopted in this work. Note, we have used a single hidden layer and a training length of 1000 bits for a range of number of neurons (i.e., 10, 20, 30, and 40). As in Fig. 3, for all cases, the LM algorithm offers the best BER performance compared to CGP and SCG. E.g., for 40 neurons and a BER of 10^{-4} , which is below the 7% forward error correction (FEC) limit of 3.8×10^{-3} , the E_b/N_0 penalties are much higher than 10 dB for SCG and CGP compared to the LM. Despite the storage requirement for LM and its long processing time compared to SCG and CGP it offers lower mean square errors (MSE), e.g., the MSE values are 7×10^{-15} , 3×10^{-5} and 5.3×10^{-6} for LM, SCG and CGP, respectively with enhanced performance as the number of neurons increases.

The effect of varying the number of neurons on the BER performance for LM algorithm is depicted in Fig. 4, which shows that 40 neurons in the hidden layer offer the best performance. E.g., at a BER of 10^{-3} the E_b/N_0 penalties are 12.5, 17.5, 18.5, and 19.5 dB for 30, 20, 10 and 5 neurons, respectively compared with 40 neurons. Note, that the BER performance of SCG and CGP also improved with increasing number of neurons.

TABLE II. THE SYSTEM PARAMETERS

Parameter	Value
Link	
OLED bandwidth	100 kHz
Propagation length	0.15 m
Photodetector active area diameter	ϕ 1 mm
ANN Equalizer	
Network structure	MLP
Activation functions	log-sigmoid
Training algorithms	LM, SCG, CGP
Error goal	10^{-20}
Number of epochs	100
Training length	1000 bits
Number of neurons	5, 10, 20, 30, and 40

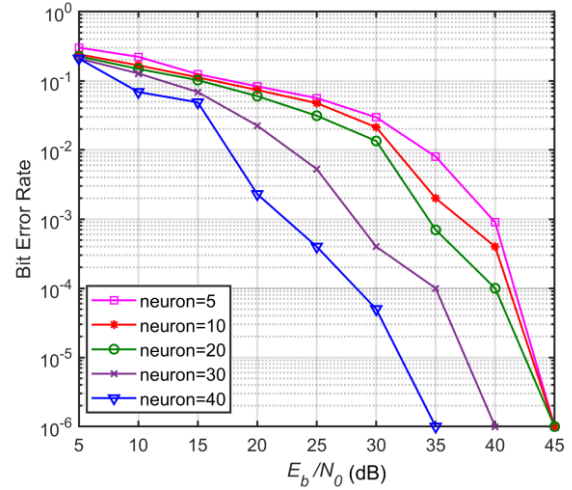


Fig. 4. BER as a function of E_b/N_0 for a range number of neurons (5, 10, 20, 30, 40) for LM training algorithm

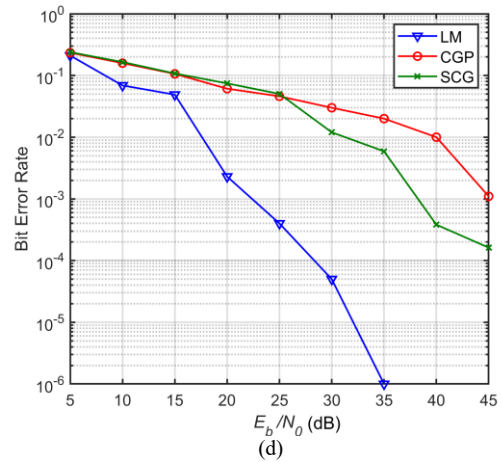
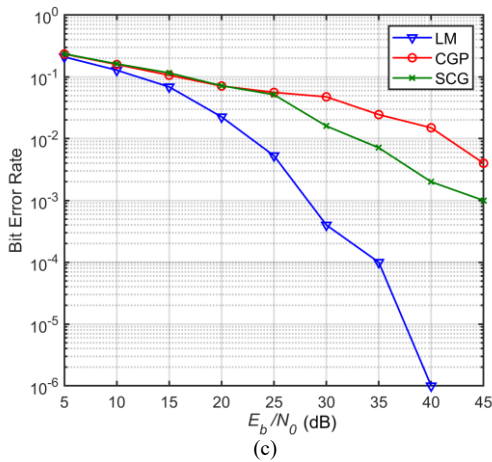
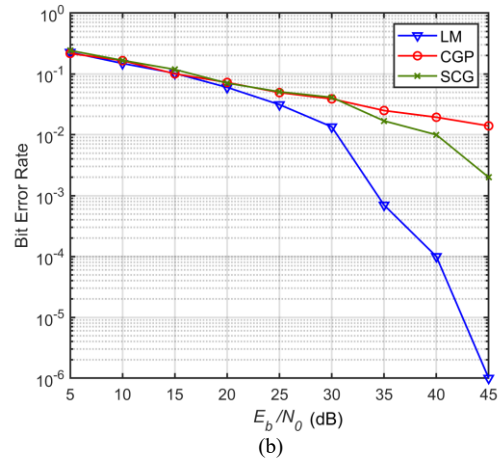
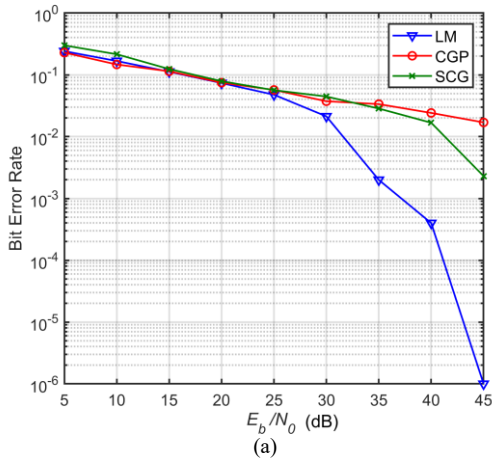


Fig. 3. BER performance against E_b/N_0 for LM, CGP and SCG training algorithms used in MLP-ANN equalizer with one hidden layer. The training length is 1000 bits, and the number of neurons used are (a) 10, (b) 20, (c) 30, and (d) 40.

IV. CONCLUSION AND FUTURE OUTLOOK

The widespread use of OLED-based devices in mobile devices, televisions and cameras with OLED pixels offers a tremendous benefit in modern technology that comes from OLED merits including very less stack thickness (100-500 nm), having large photoactive areas at a low cost, and low power consumption. It is a strong incentive to device-to-device communication growth. ANN equalizer has been popular to overcome OLED bandwidth restriction. In this paper, the effect of various learning algorithms, activation functions and numbers of neurons in the hidden layer were investigated. The structure of architectures and the training methods were selected based on the trade-off between complexity and performance. We investigated a range of training algorithms of LM, SCG and CGP as a part of the ANN equalization for OVLC systems, and showed that for a range of neurons the LM algorithm offered the best BER performance compared to CGP and SCG. In addition, LM algorithm offered the lowest mean square errors. In general, for networks with many neurons we showed that between the CG algorithms, SCG performed the best since it uses a low memory space and therefore performing faster than LM.

ACKNOWLEDGEMENT

The work is supported by the European Union's Horizon 2020 research and innovation programme under the Marie Skłodowska-Curie grant agreement no 764461 (VISION), the Czech Republic funded project GACR 17-17538S, and the UK EPSRC research grant EP/P006280/1: Multifunctional Polymer Light-Emitting Diodes with Visible Light Communications (MARVEL).

REFERENCES

- [1] Z. Ghassemlooy, L. N. Alves, S. Zvanovec, and M.-A. Khalighi, *Visible Light Communications: Theory and Applications*. CRC Press, 2017.
- [2] P. A. Haigh *et al.*, "Organic visible light communications: Recent progress," in *2014 16th International Conference on Transparent Optical Networks (ICTON)*, 2014, pp. 1-5.
- [3] P. A. Haigh, Z. Ghassemlooy, S. Rajbhandari, and I. Papakonstantinou, "Visible light communications using organic light emitting diodes," *IEEE Communications Magazine*, vol. 51, no. 8, pp. 148-154, 2013.
- [4] P. A. Haigh *et al.*, "Wavelength-multiplexed polymer LEDs: Towards 55 Mb/s organic visible light communications," *IEEE Journal on Selected Areas in Communications*, vol. 33, no. 9, pp. 1819-1828, 2015.
- [5] P. H. Pathak, X. Feng, P. Hu, and P. Mohapatra, "Visible light communication, networking, and sensing: A survey, potential and challenges," *IEEE communications surveys & tutorials*, vol. 17, no. 4, pp. 2047-2077, 2015.
- [6] R. Boubezari, H. Le Minh, Z. Ghassemlooy, and A. Bouridane, "Novel detection technique for smartphone to smartphone visible light communications," in *2016 10th International Symposium on Communication Systems, Networks and Digital Signal Processing (CSNDSP)*, 2016, pp. 1-5.
- [7] R. Boubezari, H. Le Minh, Z. Ghassemlooy, and A. Bouridane, "Smartphone camera based visible light communication," *Journal of Lightwave Technology*, vol. 34, no. 17, pp. 4121-4127, 2016.
- [8] N. Thejokalyani and S. Dhoble, "Novel approaches for energy efficient solid state lighting by RGB organic light emitting diodes—A review," *Renewable and Sustainable Energy Reviews*, vol. 32, pp. 448-467, 2014.
- [9] P. A. Haigh *et al.*, "Exploiting equalization techniques for improving data rates in organic optoelectronic devices for visible light communications," *Journal of lightwave technology*, vol. 30, no. 19, pp. 3081-3088, 2012.
- [10] C. W. Tang and S. A. VanSlyke, "Organic electroluminescent diodes," *Applied physics letters*, vol. 51, no. 12, pp. 913-915, 1987.
- [11] P. A. Haigh, Z. Ghassemlooy, and I. Papakonstantinou, "1.4-Mb/s white organic LED transmission system using discrete multitone modulation," *IEEE Photonics Technology Letters*, vol. 25, no. 6, pp. 615-618, 2013.
- [12] Z. N. Chaleshtori, P. Chvojka, S. Zvanovec, Z. Ghassemlooy, and P. A. Haigh, "A Survey on Recent Advances in Organic Visible Light Communications," in *2018 11th International Symposium on Communication Systems, Networks & Digital Signal Processing (CSNDSP)*, 2018, pp. 1-6.
- [13] H. Chen, Z. Xu, Q. Gao, and S. Li, "A 51.6 Mb/s Experimental VLC System Using a Monochromic Organic LED," *IEEE Photonics Journal*, vol. 10, no. 2, pp. 1-12, 2018.
- [14] P. A. Haigh *et al.*, "Visible light communications: real time 10 Mb/s link with a low bandwidth polymer light-emitting diode," *Optics express*, vol. 22, no. 3, pp. 2830-2838, 2014.
- [15] S. T. Le *et al.*, "10 Mb/s visible light transmission system using a polymer light-emitting diode with orthogonal frequency division multiplexing," *Optics letters*, vol. 39, no. 13, pp. 3876-3879, 2014.
- [16] P. A. Haigh *et al.*, "A 20-Mb/s VLC link with a polymer LED and a multilayer perceptron equalizer," *IEEE Photonics Technology Letters*, vol. 26, no. 19, pp. 1975-1978, 2014.
- [17] P. Haigh, "Using Equalizers to Increase Data Rates in Organic Photonic," Doctor of Philosophy, University of Northumbria, 2014.
- [18] H. Le Minh, Z. Ghassemlooy, A. Burton, and P. A. Haigh, "Equalization for organic light emitting diodes in visible light communications," in *2011 IEEE GLOBECOM Workshops (GC Wkshps)*, 2011, pp. 828-832.
- [19] S. Rajbhandari, "Application of wavelets and artificial neural network for indoor optical wireless communication systems," Northumbria University, 2010.
- [20] Y. Sari, "Performance evaluation of the various training algorithms and network topologies in a neural-network-based inverse kinematics solution for robots," *International Journal of Advanced Robotic Systems*, vol. 11, no. 4, p. 64, 2014.
- [21] H. Le Minh *et al.*, "100-Mb/s NRZ visible light communications using a postequalized white LED," *IEEE Photonics Technology Letters*, vol. 21, no. 15, pp. 1063-1065, 2009.
- [22] H. Le Minh, Z. Ghassemlooy, A. Burton, and P. A. Haigh, "Equalization for organic light emitting diodes in visible light communications," in *GLOBECOM Workshops (GC Wkshps)*, 2011 IEEE, 2011, pp. 828-832.
- [23] A. H. Sayed, *Fundamentals of adaptive filtering*. John Wiley & Sons, 2003.
- [24] S. Haykin, S. Haykin, S. Haykin, and S. Haykin, "Neural networks and learning machines. vol. 3 Pearson," *Upper Saddle River, NJ, USA*, 2009.
- [25] K. Burse, R. N. Yadav, and S. Shrivastava, "Channel equalization using neural networks: A review," *IEEE transactions on systems, man, and cybernetics, Part C (Applications and Reviews)*, vol. 40, no. 3, pp. 352-357, 2010.
- [26] P. Haigh, "Using equalizers to increase data rates in organic photonic devices for visible light communications systems," University of Northumbria, 2014.
- [27] S. Haykin and N. Network, "A comprehensive foundation," *Neural networks*, vol. 2, no. 2004, p. 41, 2004.
- [28] V. Vacic, "Summary of the training functions in Matlab's NN toolbox," *Computer Science Department at the University of California*, 2005.
- [29] M. F. Møller, "A scaled conjugate gradient algorithm for fast supervised learning," *Neural networks*, vol. 6, no. 4, pp. 525-533, 1993.

5.4 Coverage of a Shopping Mall with Flexible OLED-based Visible Light Communications

This chapter is a version of the published manuscript:


Z.N. Chaleshtori, S. Zvanovec, Z. Ghassemlooy, H.B. Eldeeb, and M. Uysal, “Coverage of a Shopping Mall with Flexible OLED-based Visible Light Communications,” *Optics Express*, vol. 28(7), pp. 10015–10026, 2020.

Connection to my Ph.D. thesis:

Organic electronics can be mechanically flexible providing a potential of curved OLED panels/displays production. The use of such OLED devices is being growing in public places such as shopping malls, which provides us with a significant potential of facilitate simultaneously illumination, display, and data communication. In addition, the use of curved OLED in VLC for different indoor scenarios has not been reported in the literature yet, showing the necessity of channel modeling of the flexible OLED-based VLC. Therefore, the flexible OLED-based VLC channel is modelled by considering the reflectance properties of the materials and objects in the room with respect to the visible range. Numerical models for the channel have been developed in this work, which followed a 2-term power series model. The results showed that, in an empty room the average optical path losses are lower by 5 and 4 dB compared with the furnished room, where the full and half-circular OLEDs were used, respectively. In addition, for an empty room with full and half-circular OLEDs, R_b of 10 and 3.7 Mb/s were achieved at distance of 6 m, respectively. In a furnished room with full and half-circular OLEDs, R_b of 1.02 and 0.46 Mb/s were recorded for a distance of 6 m, respectively.



Coverage of a shopping mall with flexible OLED-based visible light communications

ZAHRA NAZARI CHALESHTORI,^{1,*} STANISLAV ZVANOVEC,¹ ZABIH GHASSEMLOOY,²  HOSSIEN B. ELDEEB,³ AND MURAT UYSAL³

¹Department of Electromagnetic Field, Faculty of Electrical Engineering, Czech Technical University in Prague, Prague 16627, Czech Republic

²Optical Communications Research Group, Faculty of Engineering and Environment, Northumbria University, Newcastle-upon-Tyne NE1 8ST, UK

³Department of Electrical and Electronics Engineering, Ozyegin University, Istanbul 34794, Turkey
*nazarzah@fel.cvut.cz

Abstract: Visible light communications (VLC) can utilize light-emitting diodes (LEDs) to provide illumination and a safe and low-cost broadcasting network simultaneously. In the past decade, there has been a growing interest in using organic LEDs (OLEDs) for soft lighting and display applications in public places. Organic electronics can be mechanically flexible, thus the potential of curved OLED panels/displays devices. This paper provides unique characteristics of a flexible OLED-based VLC link in a shopping mall. We show that, for curved OLED the radiation pattern displays a symmetry, which is wider than Lambertian. A number of scenarios of VLC system with flexible OLED are analyzed. Numerical models for the delay spread and optical path loss are derived, which followed a 2-term power series model for both empty and furnished rooms. We show that using a full-circular OLED for both empty and furnished rooms offers a uniform distribution of emitted power for the same transmission link spans. The link performance using full and half-circular OLED in an empty room shows that the average optical path losses are lower by 5 and 4 dB, compared with the furnished room.

© 2020 Optical Society of America under the terms of the [OSA Open Access Publishing Agreement](#)

1. Introduction

Visible light communications (VLC) provide illumination and wireless data transmission through the free space at the same time via intensity modulation of the light source [1,2]. In VLC, both the conventional silicon-based light-emitting diodes (LEDs) and organic-based LEDs (OLEDs), which are widely used as lamps and panels in homes, public places and offices, can be adopted [3,4]. In this work, we only consider OLEDs, where the emissive electroluminescent layer is a film of organic compounds, are thinner, lighter and more flexible than the crystalline layers in LEDs or liquid crystal display (LCD) devices [5]. With improved technologies and reduced fabrication and manufacturing costs, OLEDs offer an advantage over the conventional LEDs and other lighting technologies including self-emission, brighter with rich colors, biodegradable, wide beam angle, simple and flexible structure, with no need for backlighting and large active areas [6,7]. However, OLEDs are costly to produce with shorter lifetimes (in particular blue organics) and can be damaged by water. In addition, OLEDs have a low modulation bandwidth B_{mod} of hundreds of kHz compared with solid-state LEDs (a few MHz), which are due to the carrier lifetime and the parasitic resistor-capacitor (RC) effects [8]. An exciting feature of OLED panels is the potential of using flexible substrates to make lights that can be curved, rolled or folded.

Note, in VLC wavelength-dependence channel modeling, it is important to consider the reflectance properties of the materials and objects within the indoor environments. To determine channel impulse response (CIR) of VLC systems, a number of research activities have been reported, which emphasize the use of inorganic LEDs. For instance, in [9], to find CIR of the

VLC system in an empty room, Monte Carlo ray-tracing method was adopted considering up to 3 reflections. However, the majority of published works do not consider the wavelength dependency of the channel. Works in [10,11] used recursive calculation methods [12] to determine CIR of an empty room without considering wavelength dependency. In [13], Barry's model by including wavelength-dependent white LED characteristics and spectral reflectance of indoor reflectors was generalized and up to 4 reflections are considered to model indoor multipath dispersion characteristics for VLC. Next, in [14], Barry's model was compared with channel modeling results obtained using a commercial optical and illumination design software Zemax [15] and the approach yielded the same CIR as in [13]. In this approach, a larger number of reflections and the wavelength-dependency of the materials can be included and it has been endorsed as a reference channel model for upcoming standards such as IEEE 802.15.7r1 [16]. In [17], for VLC a three-dimensional (3D) simulation environment using a CAD software was model based on Monte Carlo algorithm. In [18], flexible OLED lighting panel radiation pattern and its impact on the VLC channel were investigated. It was shown that, compared with Lambertian source, OLEDs are more flexible in terms of the radiation pattern control offering reduced root mean square (RMS) delay spread and the average optical path loss (OPL) of 8.8% and 3 dB, respectively.

The use of curved OLED with a wider beam pattern than Lambertian for VLC for different indoor scenarios has not been reported in the literature yet. Additionally, as the development of organic technology is being increased at applications of large display panels and pixels used in mobile devices, there is a significant potential to facilitate simultaneously illumination, display with text message on it, and data communication via the display of screens provided in shopping malls. In this paper, a flexible OLED used in a shopping mall is investigated by the means of characterizing its illumination profile, spectrum and B_{mod} . For simulating the channel-specific features, we have adopted ray tracing. The specific channel models in terms of OPL and RMS delay spread are derived for four scenarios within the shopping mall. A full and half-circular OLED are placed around the pillar in an empty and a furnished room with different size of a transmitter (Tx) and varied locations of a receiver (Rx). In addition, the performance of an OLED-based VLC link is investigated in terms of the bit error rate (BER). Using full and half-circular OLEDs in an empty room, data rates R_b of 10 Mb/s and 3.7 Mb/s are achieved over a line of sight (LOS) path of 6 m, respectively. The data rate is dropped to 1.02 Mb/s and 0.46 Mb/s in a furnished room, respectively.

The rest of the paper is organized as follows. In Section 2, the principle of the VLC channel and OLED specifics are described. Section 3 represents the main features of the simulation and Section 4 discusses the results. Finally, conclusions are given in Section 5.

2. Principle of VLC

2.1. Channel characterization

The physical indoor VLC channel includes the effects of both LOS, where the LED is aligned directly with the Rx, and non-LOS (NLOS), where the signal is captured via reflections from walls, ceiling, etc., [19]. The regenerated electrical signal at the output of the optical Rx is given as [1]:

$$y(t) = \gamma \cdot x(t) \otimes h(t) + n(t), \quad (1)$$

where $x(t)$ is the emitted optical intensity, γ is the photodetector (PD) responsivity in (A/W), $h(t)$ is the CIR and \otimes denotes convolution. $n(t)$ represents the noise, which includes the quantum noise from the optical signal, background radiation noise caused by the photons reception from ambient light and noise from the Rx such as the dark current noise and the thermal noise. The background radiation noise can be modeled as the signal independent additive white Gaussian noise (AWGN) with one-sided power spectral density N_0 due to its high intensity. The background radiation

induced noise limits the received signal-to-noise ratio (SNR) since it is the dominant noise source [20]. The CIR of the indoor channel can be written as $\sum_{i=1}^N \eta_i \delta(t - \tau_i)$, where $\delta(t)$ is Dirac delta function, τ_i is the time delay of the i^{th} ray, η_i is the gain path of the i^{th} ray and N is the number of received rays [1]. We consider three criteria to quantify the limitation on the transmission rate through the free space channel; channel gain and corresponding OPL = $-10 \log_{10} \left(\int_{-\infty}^{\infty} h(t) dt \right)$ in dB, channel mean excess delay τ and the RMS delay spread τ_{RMS} , which are given as [14]:

$$\tau = \frac{\int_0^{\infty} t \times h(t) dt}{\int_0^{\infty} h(t) dt}, \quad (2)$$

$$\tau_{\text{RMS}} = \sqrt{\frac{\int_0^{\infty} (t - \tau)^2 \times h(t) dt}{\int_0^{\infty} h(t) dt}}. \quad (3)$$

The optical radiation pattern profile determines the spatial intensity distribution of light emitted from the light source. The luminous intensity defined in terms of the angle of irradiance θ is given as [1]:

$$I(\theta) = \frac{m_L + 1}{2\pi} I(0) \cos^{m_L}(\theta) \quad \theta = \left[-\frac{\pi}{2}, \frac{\pi}{2} \right], \quad (4)$$

where $I(0)$ is the center luminous intensity of the LED and m_L is Lambertian order, which is defined in terms of the Tx semi-angle $\theta_{1/2}$ as [1]:

$$m_L = -\frac{\ln(2)}{\ln[\cos(\theta_{1/2})]}. \quad (5)$$

2.2. OLEDs

2.2.1. Structure of OLEDs

OLED display devices use organic carbon-based films, sandwiched together between two charged electrodes; one is a metallic cathode (aluminum or silver) and the other is a transparent anode (indium tin oxide (ITO)), see Fig. 1 [21]. The organic materials can be long-chain polymers (i.e., PLEDs) or small organic molecules (i.e., SMOLEDs) in a crystalline phase. Note, OLEDs have a low-pass filter transfer function with the cut-off frequency given by [1]:

$$f_c = \frac{1}{2\pi RC_o}, \quad (6)$$

where R is the effective resistance of the OLED and $C_o = \frac{A_t \epsilon_0 \epsilon_r}{d}$ is the plate capacitance, A_t is the OLED photoactive area, d is the OLED thickness, and ϵ_0 and ϵ_r are the permittivities of free space and relative dielectric constant of the organic layer, respectively. Evidently, a larger area photoactive will have a lower B_{mod} and hence a limitation on the maximum R_b in OVLC systems. Flexibility and lower production cost of non-rigid OLEDs make them the light source for future applications. The curved or rolled OLED panels/displays can be used in wearable products (such as wearable smart watches and computers), mobile phones, TVs, vehicles, trains, etc.

2.2.2. Characterization of a flexible OLED

A flexible OLED (UNISAGA, the size of $200 \times 50 \text{ mm}^2$) was characterized in terms of the beam pattern and the spectrum profile, which were then used as the inputs for further simulations. Figure 2(a) illustrates the measured normalized optical spectrum of a flexible OLED at different bias currents I_B [22], which shows the peak wavelengths of 620 nm (Red), 553 nm (Green), 454

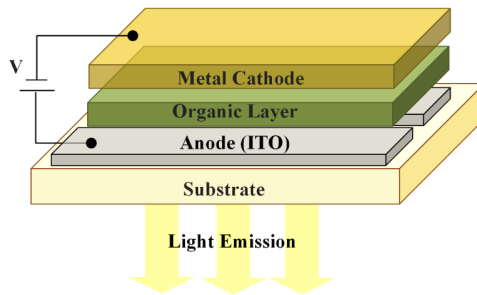


Fig. 1. OLED structure

nm and 480 nm (Blue). The intensity profiles of a flexible OLED for three different configurations are depicted in Fig. 2(b), showing symmetry around 0° but not fitting Lambertian radiation pattern (the solid blue line for $m_L = 1$). Note, the radiation angle $\theta_{1/2}$ ranges are 58°, 65°, 75°, and 90° for the flat, quadrature-circle, half-circle and three quadrature-circle of light panels, respectively. Note that, non-Lambertian emitters can also be considered by Monte Carlo approaches [23]. Instead of a typical Lambertian profile, in the simulation we have used the measured radiation pattern for the curved OLED, which is wider than Lambertian pattern.

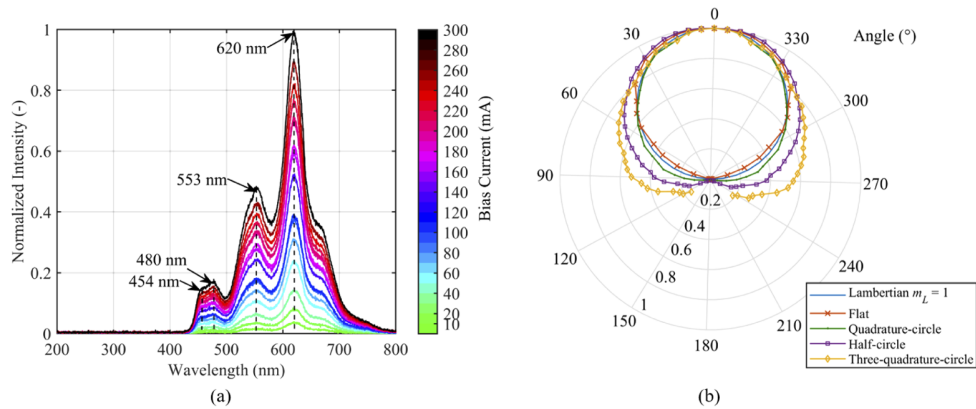


Fig. 2. Characteristics of the flexible OLED adopted in the work: (a) the normalized optical spectrum of the flexible OLED. The peak wavelengths is marked and the legend color scale represents I_B [22]. (b) The intensity pattern of OLED panel bent in different curvature such that we have a quadrature, half and three-quadrature-circle of lighting.

3. Modeling flexible OLED-based VLC within the mall scenario

Figure 3 illustrates the steps adopted in this work for channel modeling. First, an indoor environment or a 3D scene such as office, hospital, store, etc., with specified geometry, shape and with objects is created. This is followed by including the main system parameters for reflection coefficients of different surfaces, and location of light sources and detectors. We have adopted the non-sequential ray tracing feature of Zemax to specify the number of rays, the detected power and the path lengths for each ray. The output data are then imported to Matlab for processing to determine the CIR.

The organic light sources are being widely used in large area including shopping malls, airport, etc, because of flexibility, smooth lighting, etc. Thus the reason why a shopping mall is being

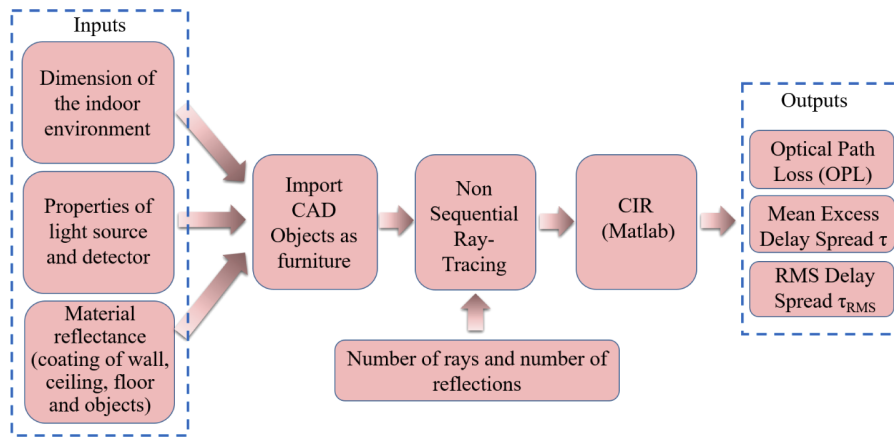


Fig. 3. The major steps followed in the channel modeling methodology.

considered in this work, which can be adopted in other application areas. Figure 4(a) shows a $10 \times 10 \times 3 \text{ m}^3$ size store with a number of objects. Note, the use of curved OLED on the pillar, which is composed of 38 OLED panels 64-chip and with a chip radiating power of 4.1 mW and a total power of 10 W. The size of OLED was set as $2 \times 0.5 \text{ m}^2$. In the model, we adopted measured beam patterns for the curved OLED, see Fig. 5. The reflectance values as a function of the wavelength for a range of surfaces, materials, etc., are shown in Fig. 6, which is adopted from [13,24]. Note that, the specular reflection case is used when materials have specified regular surfaces, which reflect the rays in particular directions and hence the use of Phong model [17,25]. Although specular reflections can occur from shiny objects, in nature (e.g., shopping mall area), where materials have irregular surfaces and rays are reflected in all directions, the resultant reflection pattern is mostly diffuse in nature that can be modeled as Lambertian [13,26,27]. Therefore, the reflections from materials are assumed to be purely diffuse. The Rx is positioned at the height of 1.3 m above the floor level (i.e., the holding position of mobile by people) while the user is facing OLED and its location is varied on the diagonal, which stretches from the corner to the middle of the room. The distance between the Tx and the Rx can be within the range of $0.5 \text{ m} < d_{\text{LOS}} < 6 \text{ m}$. Note, the dimension of the user considered is $25 \times 50 \times 180 \text{ cm}^3$.

We have considered 4 scenarios of (i) a full-circular OLED panel around the pillar in an empty (S_1) and a furnished room (S_2), see Fig. 4(b); and (ii) a half-circular OLED panel (size of $1 \times 0.5 \text{ m}^2$) in an empty room (S_3) and in a furnished room (S_4), see Fig. 4(c). Here, we have adopted Monte Carlo analysis and Sobol sampling as the random ray-tracing methods. The number of reflections was set based on the simulation of particular ray propagation, where the normalized intensity dropped to 10^{-3} . All other key system parameters are given in Table 1.

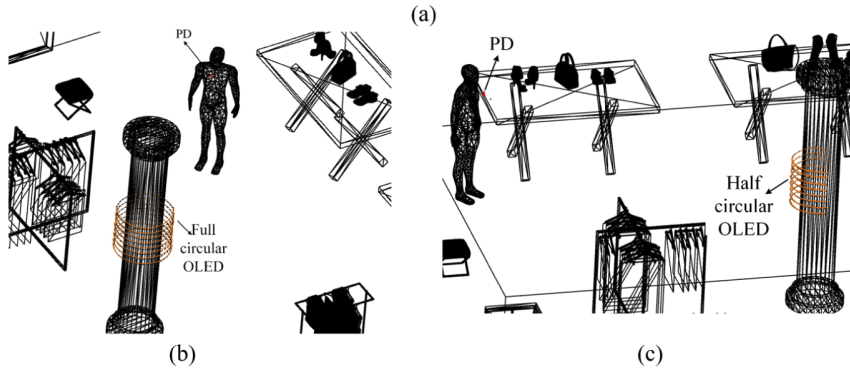
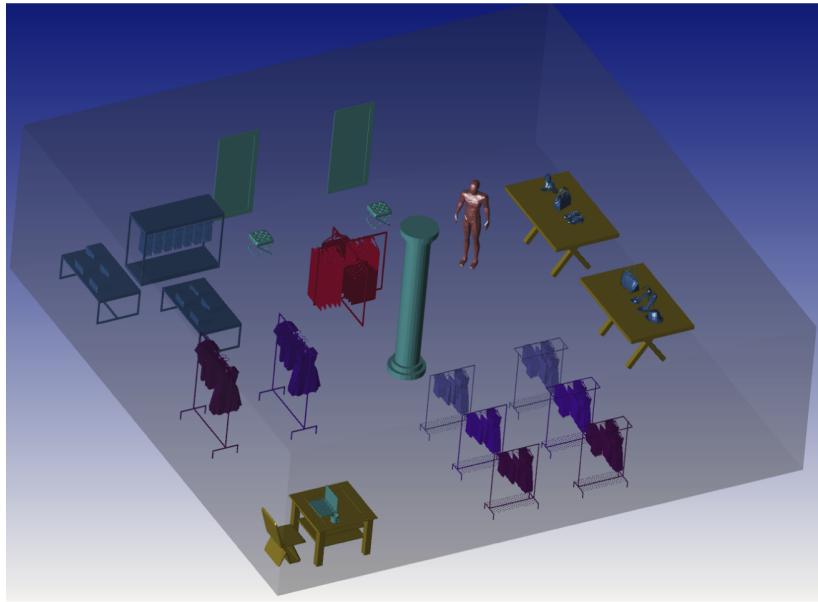


Fig. 4. (a) The three-dimensional indoor environment in Zemax and proposed scenarios; showing the location of curved OLED giving (b) a full-circular lighting and (c) a half-circular lighting.

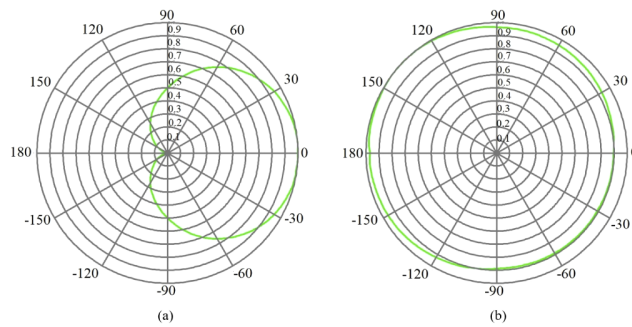


Fig. 5. Emission pattern of the light source used in simulation for: (a) a half-circular OLED and (b) a full-circular OLED.

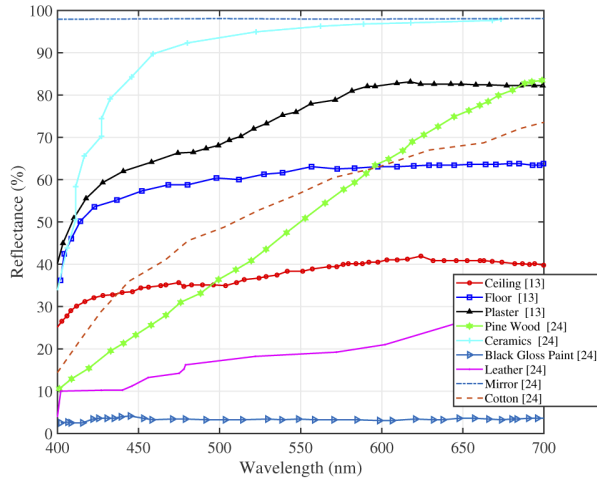


Fig. 6. Spectral reflectance of various materials used in simulation [13,24].

Table 1. System and Simulation Parameters

Item	Parameter	Value
Room	Size	10 × 10 × 3m ³
	Radius of pillar	33 cm
Reflections specifications	Type of reflections	Purely diffuse
	Number of reflections	4
	Material reflectance	Wavelength-dependent
Coating material	Walls and pillar	Plaster
	Desks and chair	Pine wood
	Couch, shoes, and bags	Leather
	Laptop	Black gloss paint
	Coffee cup	Ceramics
	Clothes	Cotton
Tx	Dimension	2 × 0.5m ²
	Type	Flexible OLED
	Bandwidth	50 kHz
	Power of lighting	10 W
	Number of OLED panels	38
	Number of chip per each panel	64
	Power of each chip	4.1 mW
Location on pillar	Fixed (Middle of store)	
Channel	Length d_{LOS}	1 m to 6 m
	Resolution time	0.2 ns
Rx	Active area of PD	1 cm ²
	FOV angle	90°
	Responsivity	0.4 A/W
	N_0	10 ⁻²¹ W/Hz

4. Results

The results from analyzes are discussed in this section.

4.1. CIR characteristics

The channel OPL can be used to specify the required emitting power of light source to meet the BER target. At first we make a comparison of inorganic LED and OLED sources with the results shown in Fig. 7. As can be seen, for the LED, OPL is increased by ~ 5 dB compared with S₄. In addition, τ_{RMS} for S₄ is considerably lower than LED-based VLC. Note, the main purpose, however, was to provide comparison of the utilization of curved OLEDs.

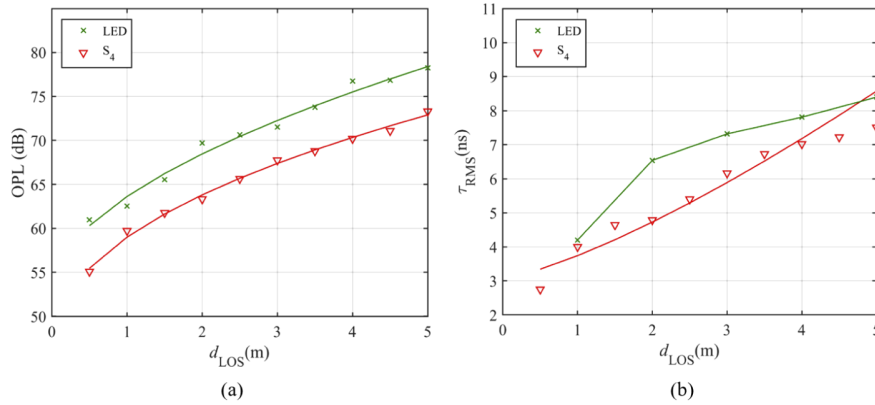


Fig. 7. Comparison of inorganic LED with half-circular OLED (i.e., S₄) in the furnished room in term of: (a) OPL and (b) τ_{RMS}.

Figure 8(a) shows OPL distributions of the curved OLED sources for S₁ and S₂. The OPL increases with the LOS path reaching maximum values of 69 and 74 dB at d_{LOS} of 6 m for S₁ and S₂, respectively. For S₂, OPL is higher compared with S₁ due to the lower reflection coefficients of the objects within the room. It can be seen that, for d_{LOS} > 4 m, there is a huge difference in the received power between the empty and furnished rooms. E.g., the OPL penalties are 2.6, 3.8

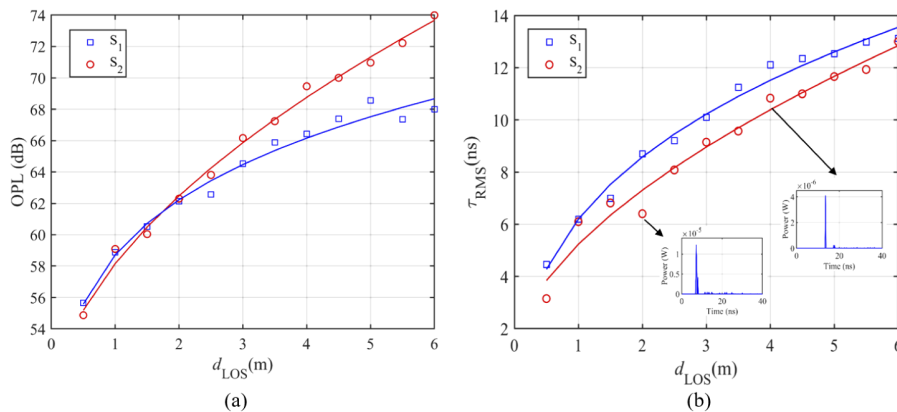


Fig. 8. Comparison of empty and furnished room where a full-circular OLED is employed (i.e., S₁ and S₂) in term of: (a) OPL and (b) τ_{RMS}. The CIR plots for distance of 2 m and 4 m are shown in inset.

and 4.9 dB for d_{LOS} of 4, 5 and 6 m, respectively. As an example, CIR plots for d_{LOS} of 2 and 4 m are shown in insets of Fig. 8(b) depicting τ_{RMS} as a function of d_{LOS} for S_1 and S_2 . Note, τ_{RMS} increases with d_{LOS} reaching maximum values of 13.55 and 12.85 ns at the corner for S_1 and S_2 , respectively.

Figure 9 shows OPL and the delay spread as a function of d_{LOS} for S_3 and S_4 when using a half-circular OLED in empty and furnished rooms, which are higher and lower, respectively, compared with Fig. 8 for a given d_{LOS} . In an empty room, OPL reaches the maximum of 71 dB, which is lower than the value corresponding to S_4 (75 dB). As a result of the comparison between scenarios of S_2 and S_4 OPL decreases at the cost of increasing τ_{RMS} , where a full-circular OLED is employed in a furnished room compared with a half-circular OLED. The OPL penalty improvement is approximately 1.6 dB.

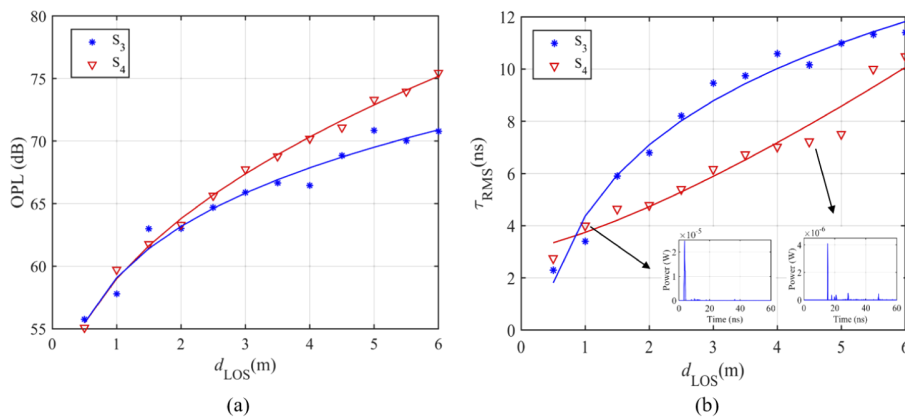


Fig. 9. Comparison of empty and furnished room where a half-circular OLED is employed (i.e., S_3 and S_4) in term of: (a) OPL and (b) τ_{RMS} . The CIR plots for distance of 1 m and 4.5 m are shown in inset.

Based on numerical modeling, we have derived empirical models for d_{LOS} and τ_{RMS} . For all cases the delay spread is obtained by fitting a 2-term power series model, which is given as:

$$\tau_{RMS} = t_1 d_{LOS}^{t_2} + t_3, \quad (7)$$

where t_1 , t_2 and t_3 for the scenarios considered here are summarized in Table 2. In addition, for all cases using the 2-term power series models we have:

$$OPL = o_1 d_{LOS}^{o_2} + o_3, \quad (8)$$

where the parameters o_1 , o_2 and o_3 are given in Table 3. Note, the main aim of this paper is to investigate the behavior/trends of OPL and τ_{RMS} and show that the empirical parameters, which are valid for the specific room size, can vary based on the number of objects in the room and the room-size.

Table 2. Numerical modeling parameters for τ_{RMS} in all proposed scenarios (S_1, S_2, S_3, S_4).

Scenario	t_1	t_2	t_3
S_1	6.2500	0.4381	1.156×10^{-9}
S_2	5.1972	0.5017	7.462×10^{-9}
S_3	4.5961	0.5481	1.468×10^{-12}
S_4	0.6643	1.3132	3.0756

Table 3. Numerical modeling parameters for OPL in all proposed scenarios (S₁, S₂, S₃, S₄).

Scenario	σ_1	σ_2	σ_3
S ₁	29.59	0.1618	29.13
S ₂	9.568	0.5378	48.59
S ₃	29.07	0.1905	30.00
S ₄	13.43	0.4414	45.56

4.2. System performance

The BER performance of the proposed system with non-return-to-zero (NRZ) on-off keying (OOK) is shown in Fig. 10. Also shown is the 7% forward error correction (FEC) BER limit of 3.8×10^{-3} . For S₁, the BER plots are below the FEC limit for d_{LOS} up to 6 m with R_b of 10 Mb/s. For S₂, BER values lower than the FEC are achieved at d_{LOS} of < 4 m with R_b of up to 10 Mb/s. In addition, R_b values are 3.04 and 1.02 Mb/s for d_{LOS} of 5 and 6 m, respectively for S₂. Figure 10(b) depicts the BER for S₃ and S₄, where S₃ shows improved performance over a longer distance compared with S₄. It can be seen that, for S₃ the BER remains just below the FEC limit for $d_{\text{LOS}} < 4$ m and at d_{LOS} of 5 and 6 m the achieved R_b values are 7.05 and 3.7 Mb/s, respectively. For S₄, the BER is also below the FEC limit for d_{LOS} of < 3 m with R_b of 10 Mb/s. Additionally, R_b values are 4.82, 1.48 and 0.46 Mb/s for d_{LOS} of 4, 5 and 6 m, respectively.

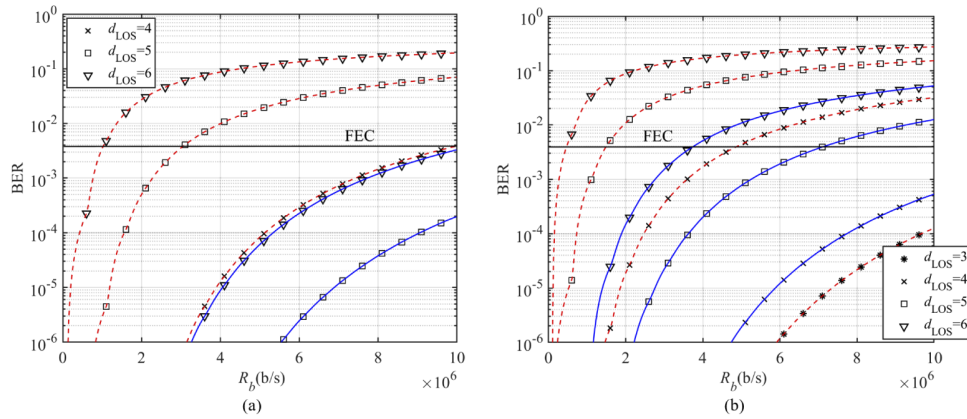


Fig. 10. The BER performance versus R_b for different d_{LOS} in cases of: (a) S₁ (solid blue line), S₂ (dashed red line) and (b) S₃ (solid blue line), S₄ (dashed red line).

Figure 11 illustrates the channel capacity C versus the transmit optical power P_E for a range of d_{LOS} at R_b of 4 Mb/s and B_{mod} of 50 kHz for S₁-S₄. It can be seen that, C increases with respect to P_E . E.g., for S₂, at d_{LOS} of 3 m we observe C of 4.46 and 17.83 Mb/s at P_E of 10 and 20 W, respectively. Obviously, for the same P_E a significant drop in C can be seen with increased d_{LOS} ; e.g., for S₁, at P_E of 10 W, C drops from 23.78 to 1.23 Mb/s for d_{LOS} of 2 and 6 m, respectively. For S₁, it is observed that for $d_{\text{LOS}} < 3$ m and $P_E > 20$ W, C is higher than 100 Mb/s. For S₃ and S₄, we observe the same trend for C as in Fig. 11(a), see Fig. 11(b). It can be seen that, for the same d_{LOS} , almost similar channel capacity can be achieved with lower emitted optical power in the case of S₂ compared with S₄ as the light source dimension increases. E.g., at d_{LOS} of 3 m, C of 10 Mb/s can be achieved for power levels of 15 and 22 W for S₂ and S₄, respectively. As a result of the comparison between all scenarios; e.g., at a given P_E of 20 W and d_{LOS} of 4 m, we have C of 15.58, 4.71, 7.11 and 2.28 Mb/s for S₁ to S₄, respectively. Therefore, there is a

significant drop in C for the case of furnished room compared with an empty room, regardless of using a full or a half-circular OLED.

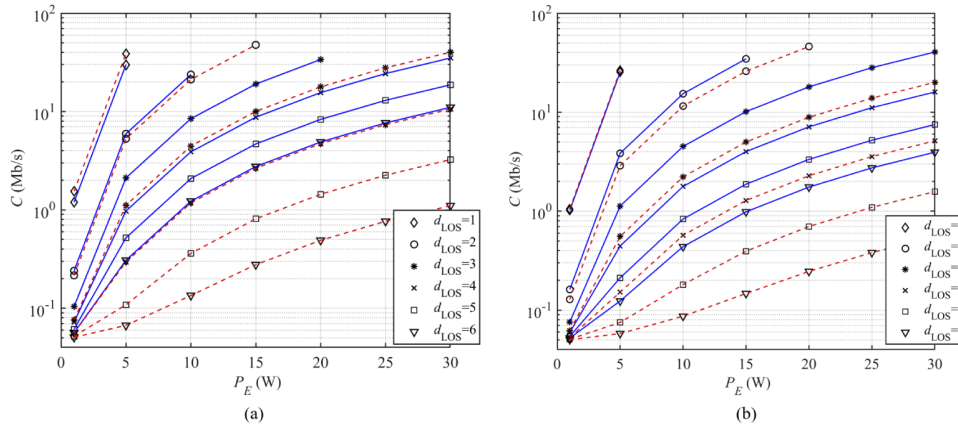


Fig. 11. The channel capacity versus P_E for different d_{LOS} at R_b of 4 Mb/s and B_{mod} of 50 kHz for: (a) S₁ (solid blue line), S₂ (dashed red line) and (b) S₃ (solid blue line), S₄ (dashed red line).

5. Conclusion

In this paper, we proposed a flexible OLED as the Tx in a VLC system to cover the shopping mall. We carried out the characterization of the OLED in terms of the spectrum profile and optical irradiation pattern as part of the simulation modeling of the light source. The beam pattern of a curved OLED was found to be symmetrical about the origin while being wider than Lambertian radiation pattern. This feature offers the benefit of maintaining the same SNR over a given transmission radius of curved OLED. The increasing use of flexible OLED in thin-film devices (such as wearable devices, mobile phones, TVs) acts as a good motivator to investigate the performance of a VLC system based on these devices. The results of utilizing a full-circular OLED for both empty and furnished rooms showed a uniform distribution of emitted power for the same transmission link spans. We showed that for full and half-circular OLEDs adopted in an empty room, the link performance improved with the average OPL penalties of 5 and 4 dB compare with the corner of a furnished room. The numerical models of τ_{RMS} were derived, which followed a 2-term power series model for both the empty and furnished rooms. In addition, the OPL profile models were derived for all proposed scenarios. Furthermore, the link's BER performance and the channel capacity were investigated. For an empty room with full and half-circular OLEDs, R_b of 10 and 3.7 Mb/s were achieved at d_{LOS} of 6 m, respectively. In addition, in a furnished room with a full-circular OLED, R_b of 10, 3.04 and 1.02 Mb/s were recorded for d_{LOS} of 4, 5 and 6 m, respectively, which are two times higher than the values when using a half-circular OLED (i.e., 4.82, 1.48 and 0.46 Mb/s). As a result, for a given d_{LOS} the same channel capacity can be obtained with lower emitted optical power using a full-circular light source compared with a half-circular OLED.

Funding

H2020 Marie Skłodowska-Curie Actions (VisIoN 764461).

Disclosures

The authors declare no conflicts of interest.

References

1. Z. Ghassemlooy, L. N. Alves, S. Zvanovec, and M.-A. Khalighi, *Visible light communications: theory and applications* (CRC press, 2017).
2. Z. Ghassemlooy, W. Popoola, and S. Rajbhandari, *Optical wireless communications: system and channel modelling with Matlab®* (CRC press, 2019).
3. B. Lin, Z. Ghassemlooy, C. Lin, X. Tang, Y. Li, and S. Zhang, "An indoor visible light positioning system based on optical camera communications," *IEEE Photonics Technol. Lett.* **29**(7), 579–582 (2017).
4. S. Schmid, T. Richner, S. Mangold, and T. R. Gross, "Enlighting: An indoor visible light communication system based on networked light bulbs," in *2016 13th Annual IEEE International Conference on Sensing, Communication, and Networking (SECON)*, (IEEE, 2016), pp. 1–9.
5. B. Geffroy, P. Le Roy, and C. Prat, "Organic light-emitting diode (oled) technology: materials, devices and display technologies," *Polym. Int.* **55**(6), 572–582 (2006).
6. J. Clark and G. Lanzani, "Organic photonics for communications," *Nat. Photonics* **4**(7), 438–446 (2010).
7. J. Ráfols-Ribé, P.-A. Will, C. Hänisch, M. Gonzalez-Silveira, S. Lenk, J. Rodríguez-Viejo, and S. Reineke, "High-performance organic light-emitting diodes comprising ultrastable glass layers," *Sci. Adv.* **4**(5), eaar8332 (2018).
8. Z. H. Kafafi, *Organic electroluminescence* (CRC Press, 2018).
9. H. Chun, C.-J. Chiang, and D. C. O'Brien, "Visible light communication using oleds: Illumination and channel modeling," in *2012 International Workshop on Optical Wireless Communications (IWOW)*, (IEEE, 2012), pp. 1–3.
10. H. Nguyen, J.-H. Choi, M. Kang, Z. Ghassemlooy, D. Kim, S.-K. Lim, T.-G. Kang, and C. G. Lee, "A matlab-based simulation program for indoor visible light communication system," in *2010 7th International Symposium on Communication Systems, Networks & Digital Signal Processing (CSNDSP 2010)*, (IEEE, 2010), pp. 537–541.
11. T. Komine and M. Nakagawa, "Performance evaluation of visible-light wireless communication system using white led lightings," in *Proceedings. ISCC 2004. Ninth International Symposium on Computers And Communications (IEEE Cat. No. 04TH8769)*, vol. 1 (IEEE, 2004), pp. 258–263.
12. J. R. Barry, J. M. Kahn, W. J. Krause, E. A. Lee, and D. G. Messerschmitt, "Simulation of multipath impulse response for indoor wireless optical channels," *IEEE J. Select. Areas Commun.* **11**(3), 367–379 (1993).
13. K. Lee, H. Park, and J. R. Barry, "Indoor channel characteristics for visible light communications," *IEEE Commun. Lett.* **15**(2), 217–219 (2011).
14. F. Miramirkhani and M. Uysal, "Channel modeling and characterization for visible light communications," *IEEE Photonics J.* **7**(6), 1–16 (2015).
15. Zemax OpticStudio 18.9, <https://www.zemax.com/products/opticstudio>.
16. M. Uysal, F. Miramirkhani, O. Narmanlioglu, T. Baykas, and E. Panayirci, "Ieee 802.15. 7r1 reference channel models for visible light communications," *IEEE Commun. Mag.* **55**(1), 212–217 (2017).
17. S. P. Rodríguez, R. P. Jiménez, B. R. Mendoza, F. J. L. Hernández, and A. J. A. Alfonso, "Simulation of impulse response for indoor visible light communications using 3d cad models," *J Wireless Com Network* **2013**(1), 7 (2013).
18. H. Chen and Z. Xu, "Oled panel radiation pattern and its impact on vlc channel characteristics," *IEEE Photonics J.* **10**(2), 1–10 (2018).
19. S. Long, M.-A. Khalighi, M. Wolf, Z. Ghassemlooy, and S. Bourennane, "Performance of carrier-less amplitude and phase modulation with frequency domain equalization for indoor visible light communications," in *2015 4th International Workshop on Optical Wireless Communications (IWOW)*, (IEEE, 2015), pp. 16–20.
20. Z. Wang, Q. Wang, W. Huang, and Z. Xu, *Visible light communications: Modulation and signal processing* (John Wiley & Sons, 2017).
21. J. Kalinowski, *Organic Light-Emitting Diodes: Principles, Characteristics & Processes* (CRC press, 2018).
22. Z. N. Chaleshtori, A. Burton, Z. Ghassemlooy, and S. Zvanovec, "A flexible oled based vlc link with m-cap modulation," in *2019 15th International Conference on Telecommunications (ConTEL)*, (IEEE, 2019), pp. 1–6.
23. H. B. Eldeeb, F. Miramirkhani, and M. Uysal, "A path loss model for vehicle-to-vehicle visible light communications," in *2019 15th International Conference on Telecommunications (ConTEL)*, (IEEE, 2019), pp. 1–5.
24. ASTER Spectral Library-Version 2.0, <http://speclib.jpl.nasa.gov>.
25. S. Lee, J. K. Kwon, S.-Y. Jung, and Y.-H. Kwon, "Evaluation of visible light communication channel delay profiles for automotive applications," *J Wireless Com Network* **2012**(1), 370 (2012).
26. C. R. Lomba, R. T. Valadas, and A. de Oliveira Duarte, "Efficient simulation of the impulse response of the indoor wireless optical channel," *Int. J. Commun. Syst.* **13**(7-8), 537–549 (2000).
27. C. R. Lomba, R. T. Valadas, and A. de Oliveira Duarte, "Experimental characterisation and modelling of the reflection of infrared signals on indoor surfaces," *IEE Proc.: Optoelectron.* **145**(3), 191–197 (1998).

5.5 Utilization of an OLED-Based VLC System in Office, Corridor, and Semi-Open Corridor Environments

This chapter is a version of the published manuscript:





Z.N. Chaleshtori, Z. Ghassemlooy, H.B. Eldeeb, M. Uysal, and S. Zvanovec, "Utilization of an OLED-Based VLC System in office, Corridor, and Semi-Open Corridor Environments," 2020, IEEE.

Connection to my Ph.D. thesis:

This work emphasizes on the evaluation of an attractive feature of OLEDs, which is the mechanically flexible potential for utilizing in VLC system. Here the use of flexible substrate-based OLED for VLC system in a furnished office and the impact of the beam pattern of curved OLED, which is symmetrical and wider than Lambertian, are investigated. New results are presented for the VLC system performance in terms of RMS delay spread and BER for the link using both flat and half-circular OLEDs. We demonstrated a data rate of 4 Mb/s using both the curved and flat OLEDs for the transmitter's half-angle within the range of $\pm 90^\circ$ and $\pm 53^\circ$, respectively, with a BER below the FEC. Moreover, since OLEDs are being producing in different shapes and sizes, we decided to investigate VLC channel characteristics when large OLED panels are used as Tx in corridor and semi-open corridors when the user is moving on a straight path along the corridor. It was shown that, OPL in the empty corridor and semi-open corridor are lower compared with the furnished rooms, e.g., for empty corridor and semi-open corridor there was a drop in OPL by 4.4 and 6.1 dB for a link span of 10 m when OLED is positioned on outer-wall of shops. We showed that, when OLED is positioned on the outer wall of shops, the channel gain enhanced in contrast to them being located on inner shop wall, e.g., the channel gain enhanced by 5.2 and 4.8 dB at 10 m for furnished corridor and furnished semi-open corridor, respectively. Additionally, channel gain was enhanced for the furnished corridor in comparison with semi-open corridor, e.g., there was a channel gain enhancement for the furnished corridor by 1.7 and 2.4 dB at distances of 10 and 15 m in comparison with the furnished semi-open corridor.

Article

Utilization of an OLED-Based VLC System in Office, Corridor, and Semi-Open Corridor Environments

Zahra Nazari Chaleshtori ^{1,*} , Zabih Ghassemlooy ² , Hossien B. Eldeeb ³ , Murat Uysal ³ and Stanislav Zvanovec ¹ 

¹ Department of Electromagnetic Field, Faculty of Electrical Engineering, Czech Technical University in Prague, 16627 Prague, Czech Republic; xzvanove@fel.cvut.cz

² Optical Communications Research Group, Faculty of Engineering and Environment, Northumbria University, Newcastle-upon-Tyne NE1 8ST, UK; z.ghassemlooy@northumbria.ac.uk

³ Department of Electrical and Electronics Engineering, Ozyegin University, 34794 Istanbul, Turkey; hossien.eldeeb@ozu.edu.tr (H.B.E.); murat.uysal@ozyegin.edu.tr (M.U.)

* Correspondence: nazarzah@fel.cvut.cz

Received: 12 November 2020; Accepted: 28 November 2020; Published: 1 December 2020



Abstract: Organic light emitting diodes (OLEDs) have recently received growing interest for their merits as soft light and large panels at a low cost for the use in public places such as airports, shopping centers, offices, and train or bus stations. Moreover, the flexible substrate-based OLEDs provide an attractive feature of having curved or rolled lighting sources for the use in wearable devices and display panels. This technology can be implemented in visible light communications (VLC) for several applications such as visual display, data communications, and indoor localization. This article aims to investigate the use of flexible OLED-based VLC in indoor environments (i.e., office, corridor and semi-open corridor in shopping malls). We derive a two-term power series model to be match with the root-mean-square delay spread and optical path loss (OPL). We show that, for OLED positioned on outer-wall of shops, the channel gain is enhanced in contrast to them being positioned on the inner-wall. Moreover, the channel gain in empty environments is higher compare with the furnished rooms. We show that, the OPL for a 10 m link span are lower by 4.4 and 6.1 dB for the empty and semi-open corridors compared with the furnished rooms, when OLED is positioned on outer-wall of shops. Moreover, the channel gain in the corridor is higher compared with the semi-open corridor. We also show that, in furnished and semi-open corridors the OPL values are 55.6 and 57.2 dB at the center of corridor increasing to 87.6 and 90.7 dB at 20 m, respectively, when OLED is positioned on outer-wall of shops.

Keywords: flexible OLED; visible light communications; optical path loss; delay spread

1. Introduction

Visible light communications (VLC) with its huge available bandwidth [1] and its dual functionality, i.e., illumination and safe and low-cost communications [2], has a great potential for different high data rate fixed and mobile applications [3]. The VLC technology has many advantages include inherent security, energy efficiency, healthy for human, and unregulated bandwidth [4,5]. These features make it attractive for numerous applications in different fields including indoor networking [6], vehicular communication [7], medical applications [8], Internet access for vehicles and in airplane cabins [9], and positioning systems [10].

At the receiver (Rx) side, a single photodetector (PD) is usually used, which converts the incident optical power to the electrical power. To enhance the performance, the single PD can be replaced by an angle diversity Rx, which contains multiple PDs oriented in different directions as reported in [11].

For further improvement, the field of view angles of these PDs can be optimized to increase the received signal-to-noise-ratio (SNR) as reported in [12,13]. Optical cameras have been recently introduced to capture data [14,15], resulting in interesting VLC systems applications. It is also possible to utilize the organic PDs with more synthetic flexibility [16], however the limited spectral responsivity range is the drawback. VLC relies on the use of light-emitting diodes (LEDs), organic LEDs (OLEDs) as well as white laser diodes (LDs) as the light source [17]. Owing to OLEDs attractive advantages, including transparent displays, rich color, low power consumption and large active areas [18,19], there has been a growing interest in using OLEDs for soft lighting and display applications in public places [20]. The main differences between OLEDs and the LEDs are (i) the modulation bandwidth of OLEDs, which increases linearly with the drive current, is lower than silicone LEDs (i.e., kHz compared to MHz); and (ii) OLEDs have wider radiation patterns compared with non-organic LEDs, which influences the optical path loss (OPL). This work emphasizes on utilizing OLEDs for VLC systems, where the potential of flexible light sources could be used in office and public indoor environments.

Numerous efforts have been made in modeling VLC channel in order to determine the channel impulse response (CIR) and its characteristics in terms of the average OPL and the root-mean-square (RMS) delay spread. The achievable SNR for a given transmit power can be calculated by OPL obtained from CIR [21]. In addition, the RMS delay spread provides a good estimate of how susceptible the channel is to inter-symbol interference (ISI), thus leading to transmission data rate R_b restriction [18,21]. That is why quantifying channel characteristics is vital; hence, a number of studies have been done so far. For instance, in [22], the CIR of an empty room was evaluated using Monte Carlo (MC) ray tracing at the visible wavelength range where the surface materials reflectance were not wavelength-dependent. However, in [23] the VLC channel was investigated including wavelength-dependent reflectance of materials. In [24], the modified MC ray tracing approach was used for analyzing the CIR as a function of the wavelength using a simplified matrix model. In [25], a three-dimensional (3D) model based on MC algorithm using a CAD software was presented for the VLC system. A simulation of VLC channel by the use of OpticStudio[®] simulator produced by Zemax [26] was reported in [27,28], which was endorsed by the IEEE 802.15.7r1 Task Group. In addition, the use of OpticStudio[®] for validation of the channel modelling was reported in [29]. Recently, utilizing OLEDs in VLC systems has captured attention. In [30], it is claimed that the use of curved OLED in VLC system for an empty room offers lower RMS delay spread and the average OPL values of 8.8% and 3 dB, respectively compared with Lambertian source. The impact of reflections using flat and half-circular OLEDs in a furnished office was investigated [31]. The recorded results in [31] reveals the ability of OLED based VLC system to achieve R_b of 4 Mb/s with a bit-error-rate (BER) below the forward error correction BER limit. In [32], investigating of a flexible OLED-based VLC link in a shopping mall was reported, in both empty and furnished rooms using both full and half-circular OLEDs. The results indicated that, the OPL in an empty room is about 5 dB less than the furnished room.

Currently OLED panels are more costly than LEDs; however, with advances made in fabrication and manufacturing as well as the wider use of OLED-based lights the cost will be reduced as was the case with the non-organic LEDs a few years ago. Since, OLEDs come in different shapes and size, we have decided to investigate their characteristics when used as a transmitter (Tx) in VLC systems. This work emphasizes on the evaluation of an attractive feature of OLEDs, which is the mechanically flexible potential for utilizing in VLC system. The simulation was carried out to determine the impact of the symmetrical beam pattern of curved OLEDs, which is wider than Lambertian, on the VLC channel. In this work, we consider a VLC system in a typical office, corridor, and semi-open corridor environments with and without furniture. In the office environment, the user (i.e., the Rx), is moving along a circular path while holding a mobile phone. In corridor and semi-open corridors, the user is then moving on a straight path along the corridor. We investigate the proposed system optical features and show a new numerical model for the RMS delay-spread and OPL for the channel. We provide statistics for the BER performance and compared it for curved and flat OLED-based VLC systems.

The rest of the paper is organized as follows. In Section 2, the features of simulation and scenarios are described. Section 3 discusses the results. Finally, conclusions are given in Section 4.

2. Simulation

2.1. Simulation Features

To determine the detected optical power and path lengths from the Tx to the Rx, non-sequential ray-tracing approach was used in the 3D environment. It evolves the specification and location of the Tx and the Rx, features of the CAD models of objects, wavelength-dependent reflectance of surfaces (wall, ceiling, floor, and objects), and transmission/reflection coefficient of glass windows. Next, the captured output data of the OpticStudio® is processed in MATLAB to obtain the CIR expressed as given by [27,32]:

$$h(t) = \sum_{i=1}^N P_i \delta(t - \tau_i), \quad (1)$$

where P_i and τ_i are the power and the propagation time of the i th ray, respectively. δ is Dirac delta function and N is the number of rays received at the Rx. Note, a number of reflections from the floor, ceiling, walls, and other objects are considered until the normalized intensity of rays after intercepting an object drops to 10^{-3} .

The spatial intensity distribution of light emitted from the light source is determined by the optical radiation pattern profile. The luminous intensity defined in terms of the angle of irradiance ϕ is given as [1]:

$$I(\phi) = \frac{m_L + 1}{2\pi} I(0) \cos^{m_L}(\phi), \quad \phi = \left[-\frac{\pi}{2}, \frac{\pi}{2}\right] \quad (2)$$

where $I(0)$ is the center luminous intensity of the OLED and m_L is Lambertian order, which is defined in terms of the Tx semi-angle $\phi_{1/2}$ as [1]:

$$m_L = -\frac{\ln(2)}{\ln[\cos(\phi_{1/2})]}. \quad (3)$$

As inputs of the simulator, the measured characteristics of a flexible OLED from UNISAGA with a size of $200 \times 50 \text{ mm}^2$, see Figure 1a, were used. The measured beam pattern of the flexible OLED for flat and a half-circular configuration is depicted in Figure 1b, showing symmetry but not fitting with Lambertian radiation pattern (the solid line for $m_L = 1$). A close match between the simulated and the measured beam patterns can be seen in Figure 1b. The measured spectrum profile of the flexible OLED is presented in Figure 1c, showing the red, green, and two blue components at 620, 553 and 454 and 480 nm, respectively.

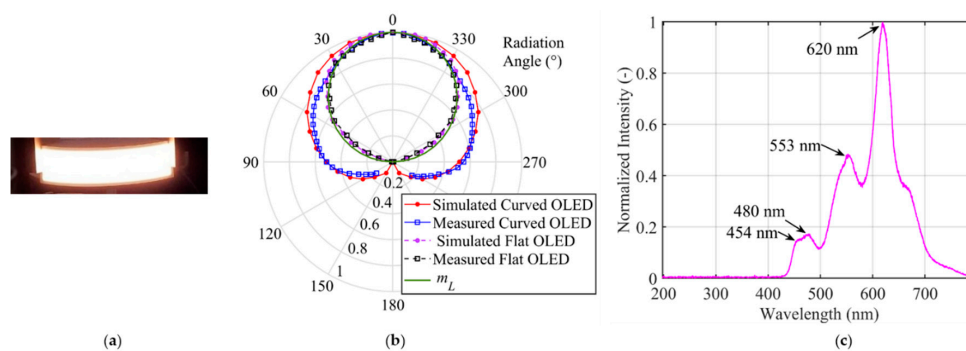


Figure 1. The flexible organic light emitting diodes (OLED) panel and its characteristics adopted in the simulation: (a) photograph, (b) the emission pattern of light source modeled for a flat and curved OLED, which is closely matched with the measured data, and (c) the normalized optical spectrum where the peak wavelengths are marked.

2.2. Scenarios

Figure 2 shows the analyzed example of an office environment designed with the size of $10 \times 10 \times 3 \text{ m}^3$ and a number of objects within. Here, a curved OLED with the size $1 \times 0.5 \text{ m}^2$ is mounted on the wall with a curvature radius of 32 cm. In the office environment, the scenario is to move the Rx over a semi-circular path, where the radius d is 2 m. An angle of radiation θ with respect to the normal from the center point of OLED (i.e., $-90^\circ < \theta < 90^\circ$) is given, see Figure 3. The Rx height is assumed to be 1 m above the floor to represent people holding mobile phones while sitting at their desks. In simulation, we have not considered the synchronization. However, in real time systems synchronization protocols defined by the standards will be adopted, which does not affect the transmission characteristics of the proposed system.

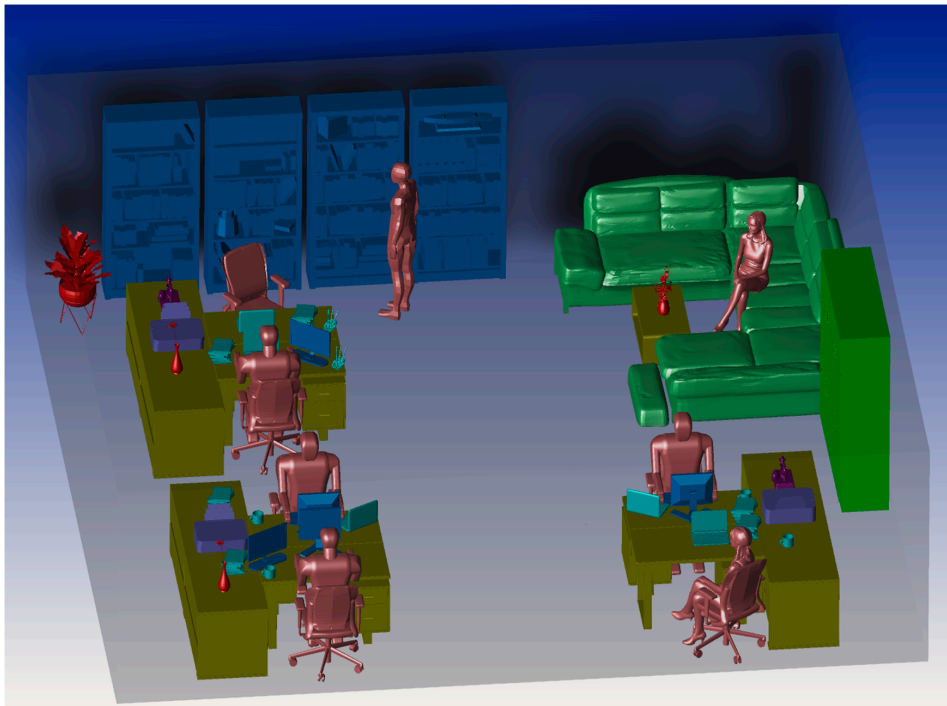


Figure 2. The three-dimensional office environment.

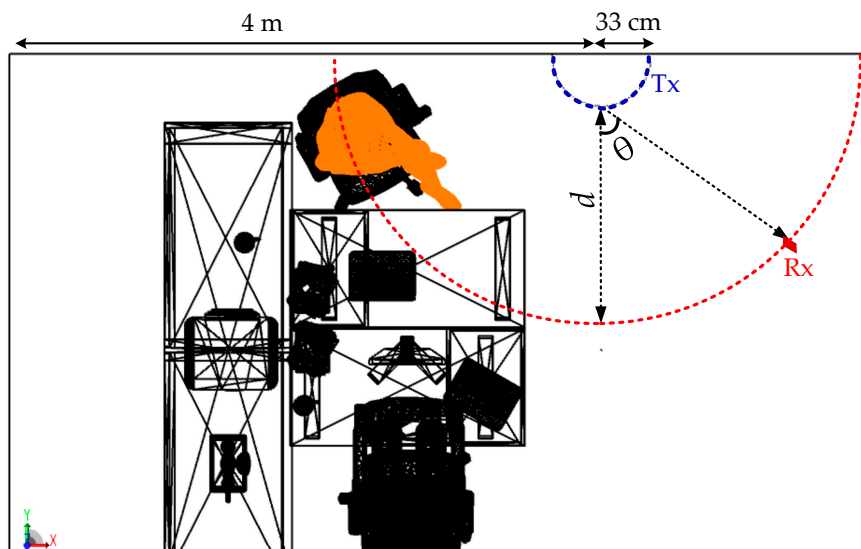


Figure 3. The proposed scenario which shows the location of receiver (Rx) and transmitter (Tx) giving a half-circular lighting.

Figures 4a and 5a then show the 3D corridor and semi-open corridor environments inside a shopping mall, respectively, in which OLED acts as a light source. The semi-open corridor is typical especially for upper floors of the shopping mall, so we have chosen an example when the user walks on the first floor, having shop windows on one side and an open space on the other side. The user is moving on the straight path along the corridor (shown by the red dashed-lines in Figures 4b,c and 5b,c). The Rx is positioned at the height of 1.3 m above the floor level (i.e., the holding position of mobile by people). The user is moving along the shop windows at a distance of 2 m on the path denoted as d_y from -20 to 20 m, where Tx is placed at 0 m position. For both empty and furnished corridor and semi-open environments, we have considered two scenarios of (case1), where the OLED panel is located on the inner shop wall behind the glass window and (case2) on the wall or shop window inside the corridor, see Figures 4b,c and 5b,c. All the key system parameters adopted in this work, including the reflectance values of surfaces and the transmission coefficient of the glass windows, are given in Table 1.

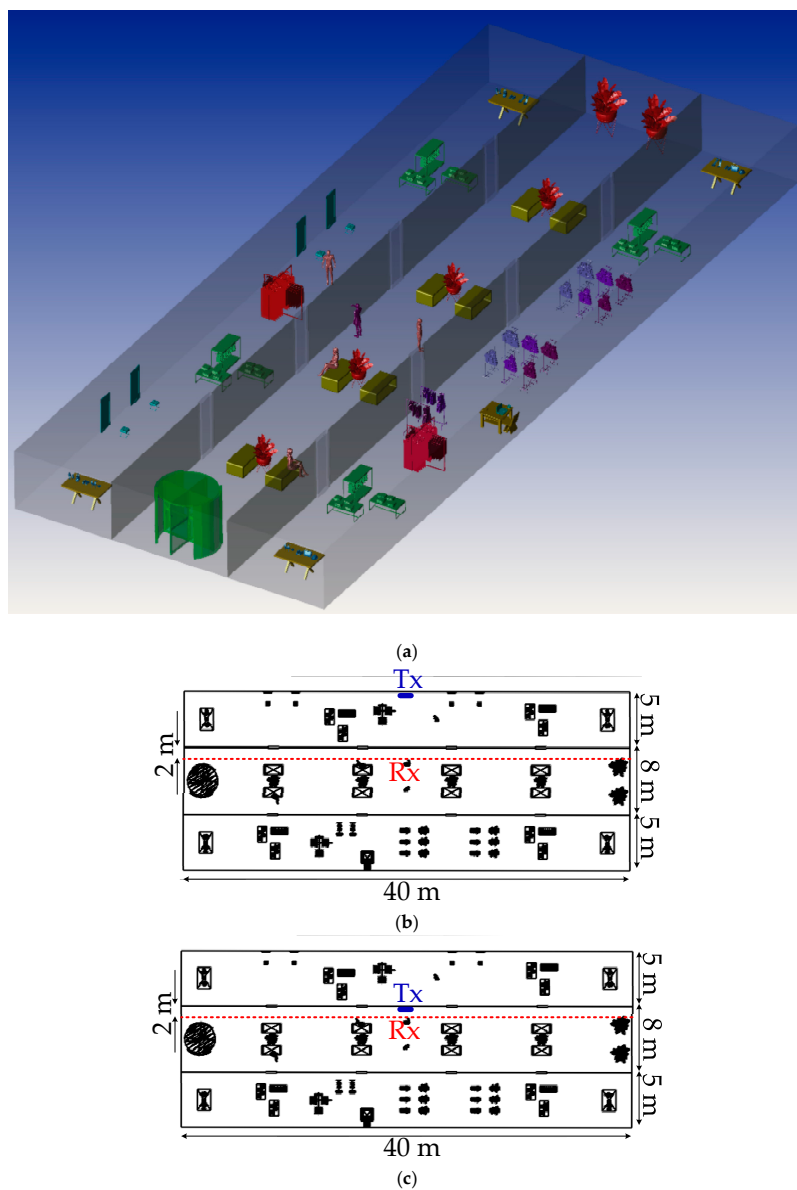


Figure 4. (a) The three-dimensional corridor environment and proposed scenarios which show the location of Rx and Tx, (b) case1 where Tx is located on inner shop wall behind window, and (c) case2 on wall or shop window inside the corridor.

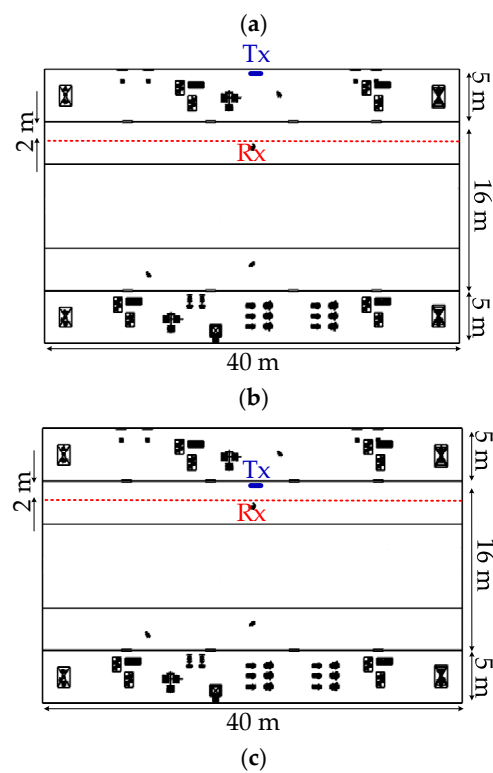
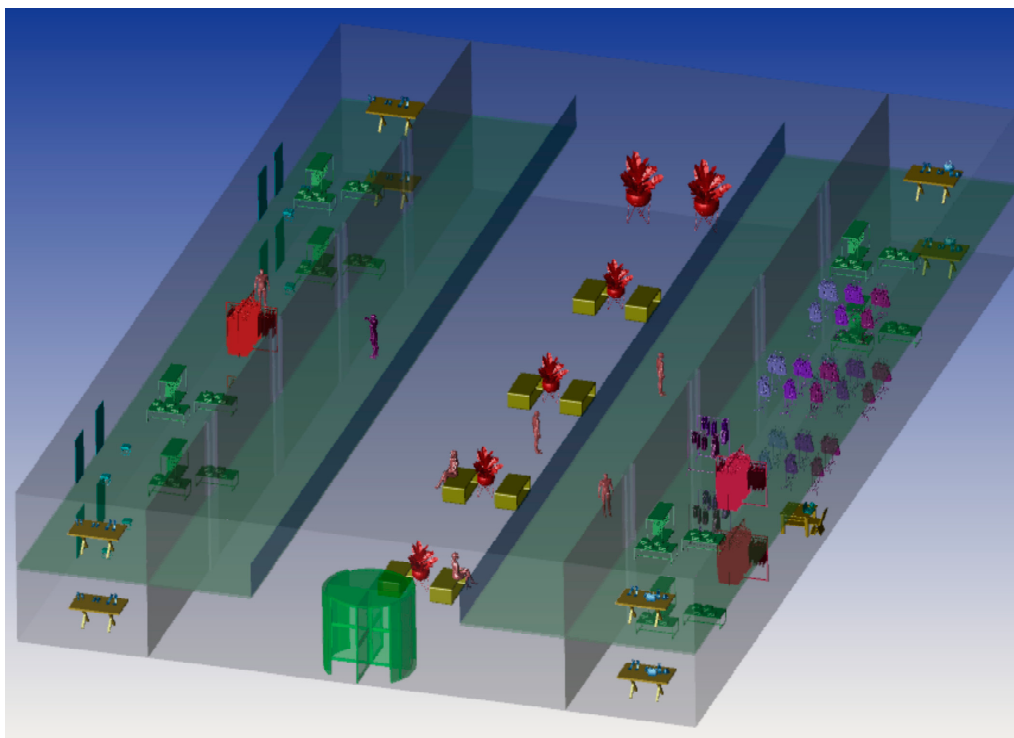


Figure 5. (a) The three-dimensional semi-open corridor environment and proposed scenarios which show the location of Rx and Tx, (b) where Tx is located on inner shop wall behind window (case1), and (c) on wall or shop window inside the corridor (case2).

Table 1. The system parameters.

Item	Parameter	Value
Surface material refractivity in % (RGB)	Chair, sofa (leather)	24 18.8 16.3
	Coffee cup (ceramics)	97.1 96.2 92.3
	Human clothes (cotton)	67 58 45.6
	Plant (leaf)	14 5.9 8.2
	Desk, book shelf, book (pine wood)	70 51 33.1
	Laptop, PC, printer, and telephone (black gloss paint)	3.4 3.2 3.2
Transmission coefficient in % (RGB)	Glass windows	88 90 87
Room size	Office	$10 \times 10 \times 3 \text{ m}^3$
	Corridor	$18 \times 40 \times 3 \text{ m}^3$
	Semi-open corridor	$26 \times 40 \times 3 \text{ m}^3$
Tx	Dimension	$1 \times 0.5 \text{ m}^2$
	Type	Flexible
	Bandwidth	50 kHz
	Power of lighting	10 W
	Number of OLED panels	19
	Number of chip/LED panel	64
	Power of each chip	8.2 mW
	Curvature radius	32 cm
	Location in office	(4, 0.33, 1.5) m
	Location in corridor and semi-open corridor	case1: (0.1, 20, 1.5) m case2: (4.9, 20, 1.5) m
Channel	Time resolution	0.2 ns
Rx	Active area of PD	1 cm^2
	Responsivity	0.4 A/W
	FOV	90°
	Incident angle	0°
	One sided noise power spectral density N_o	10^{-19} W/Hz

3. Results

3.1. Comparison of Flat and Curved OLED Based System Performance

For intensity modulation/direct detection (IM/DD) optical transmission systems, the electrical SNR is defined as

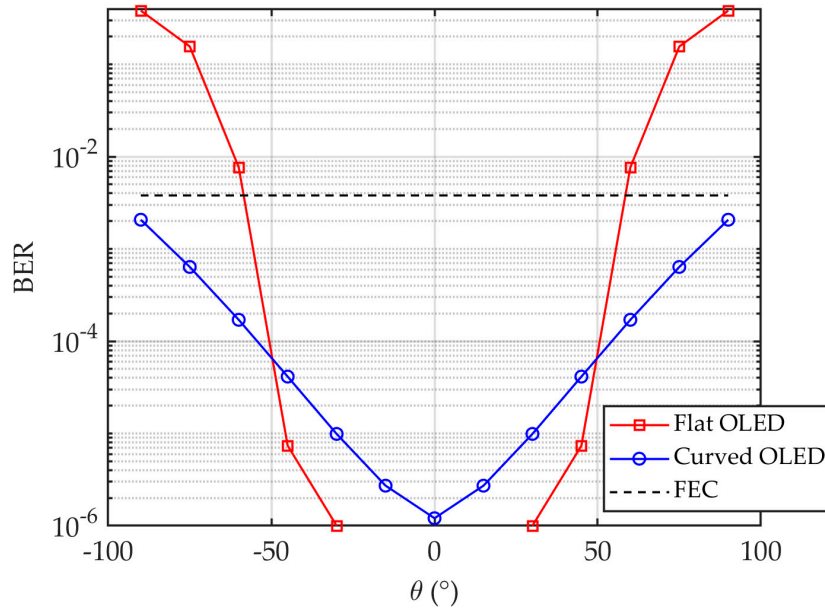
$$\text{SNR} = \frac{(\gamma P_R)^2}{R_b N_o} = \frac{(\gamma H(0) P_E)^2}{R_b N_o}, \quad (4)$$

where γ is the photodetector's responsivity in (A/W), P_E and P_R are the emitted and received optical power, respectively, and $N_o/2$ is double-sided power spectral density. Considering a link with non-return-to-zero (NRZ) on-off keying (OOK), the BER is given as [33]:

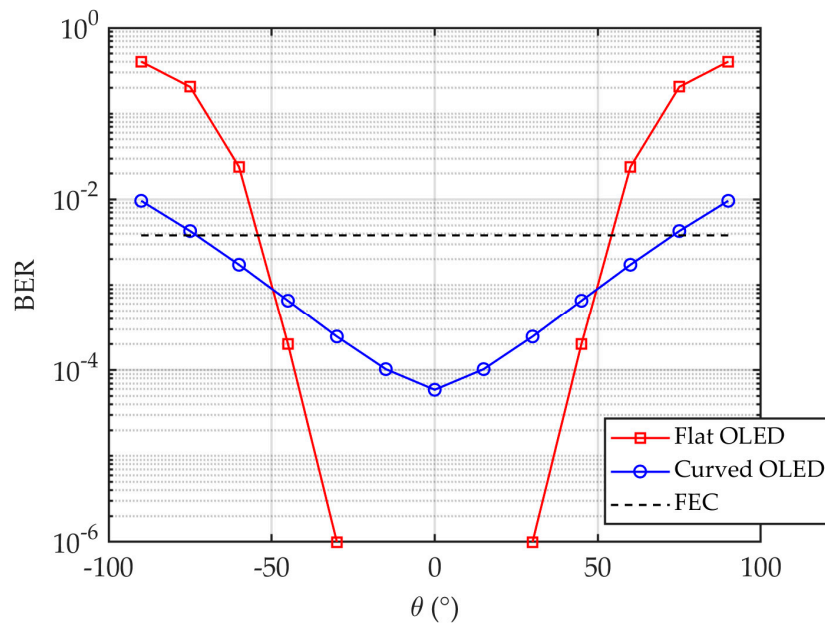
$$\text{BER} = \frac{1}{2} \text{erfc}\left(\sqrt{\frac{\text{SNR}}{2}}\right). \quad (5)$$

Figure 6 shows the plots of the BER for flat and curved OLEDs at R_b of 4 and 6 Mb/s along with the 7% forward error correction (FEC) BER limit of 3.8×10^{-3} [1] for an office. Note, for 4 Mb/s the BER is below the FEC limit for curved OLED. As illustrated, the BER plot displays a symmetry about the origin (i.e., at θ of 0°) because of the same achievable SNR that is maintained across the entire face of OLED. It is obvious that, for the curved OLED the BER is improved over a wider θ compared with the flat OLED. Note, for the flat OLED with $-30^\circ < \theta < 30^\circ$ the BER values are $< 10^{-6}$. At R_b of

4 Mb/s, the BER remains below the FEC limit for θ within the range of $\pm 90^\circ$ and $\pm 53^\circ$ for the curved and flat OLEDs, respectively. However, for R_b of 6 Mb/s, θ drops by 15° and 4° for the curved and flat OLEDs, respectively.



(a)



(b)

Figure 6. The bit-error-rate (BER) for flat and curved OLEDs at R_b of: (a) 4 Mb/s, and (b) 6 Mb/s for an office.

3.2. Channel Characteristics

The channel gain $H(0)$ defines the achievable SNR for a given incident power. To quantify the data rate, $H(0)$ and the optical signal attenuation $OPL = -10\log_{10}(H(0))$ caused by reflections and transmission in the free space are obtained [21,34]. The RMS delay spread is commonly used to define

the time dispersion along the propagation path. The channel mean excess delay τ and the RMS delay spread τ_{RMS} are given as [27,31].

$$\tau = \frac{\int_0^{\infty} t \times h(t) dt}{\int_0^{\infty} h(t) dt}, \tag{6}$$

$$\tau_{RMS} = \sqrt{\frac{\int_0^{\infty} (t - \tau)^2 \times h(t) dt}{\int_0^{\infty} h(t) dt}}. \tag{7}$$

Figure 7 depicts the τ_{RMS} plot for the flat and curved OLEDs in an office. The angle θ is shown in Figure 7 to identify the Rx's location on the semi-circular path with the radius d . τ_{RMS} increases with θ reaching the maximum value of 5 and 10.7 ns at θ of 90° for the curved and flat OLEDs, respectively. It is obvious that, for the curved OLED, there is a slight change in τ_{RMS} by about 0.8 ns with respect to θ . However, τ_{RMS} has changed about 7.3 ns for the flat OLED. Note, there is a significant increase in τ_{RMS} for $\theta > 40^\circ$ for the flat OLED.

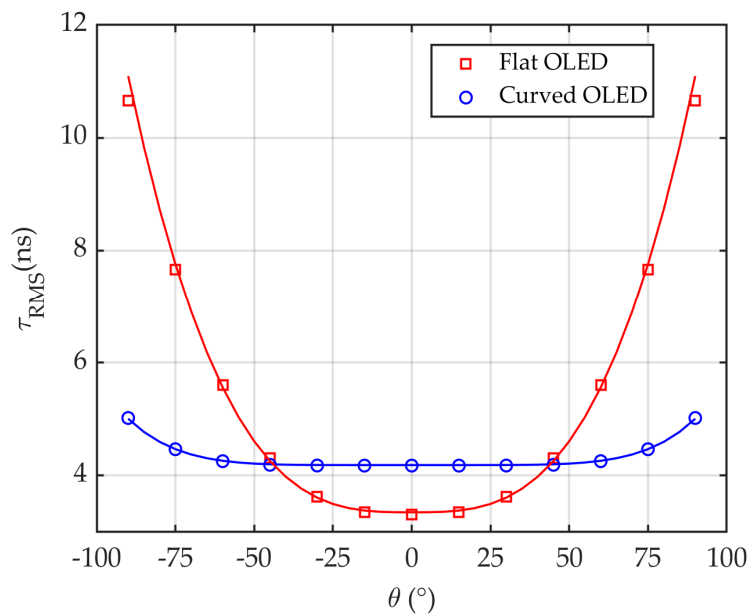


Figure 7. Comparison of a flat and curved OLEDs employed in the office in term of τ_{RMS} .

Using a non-linear approximation algorithm for both cases, a two-term power series model can be derived from simulations for τ_{RMS} as a function of θ given by

$$\tau_{RMS} = p_1\theta^{p_2} + p_3, \tag{8}$$

where p_1, p_2 and p_3 are summarized in Table 2. Note, the empirical parameters can vary based on the number of objects in the room and the size of the specified confined space.

Table 2. Numerical modeling parameters for τ_{RMS} in the case of using flat and curved OLEDs in office.

OLED Type	p_1	p_2	p_3
Curved	8.707×10^{-10}	4.589	4.172
Flat	1.765×10^{-5}	2.875	3.312

Figure 8 shows the azimuthal dependence of the OPL distributions for flat and curved OLEDs for the proposed scenario in an office. OPL increases with θ reaching a maximum of 60.4 and 70.2 dB at θ of 90° for curved and flat OLEDs, respectively. Note, up to ~ 14 dB drop in the channel gain can be seen for the flat OLED when θ changes from 0° to 90° , which is considerably higher compared with the reduced ~ 2 dB channel gain for curved OLED. It can be seen that, for the flat OLED and $\theta < 30^\circ$ there is an improvement in OPL by ~ 1.8 dB compared with the curved OLED. However, for $\theta > 45^\circ$, there is high received power enhancement for the curved OLED compared with the flat OLED, e.g., OPL penalties for flat OLED are 5 and 10 dB for θ of 75° and 90° , respectively. In addition, for both cases OPLs can be determined as the 2-term power series models as

$$\text{OPL} = a_1\theta^{a_2} + a_3, \quad (9)$$

where the derived parameters a_1 , a_2 and a_3 are shown in Table 3.

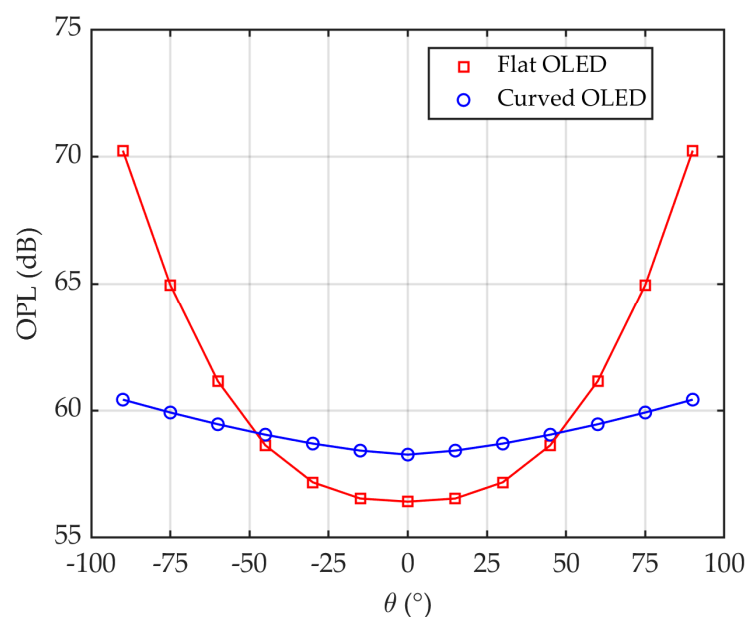
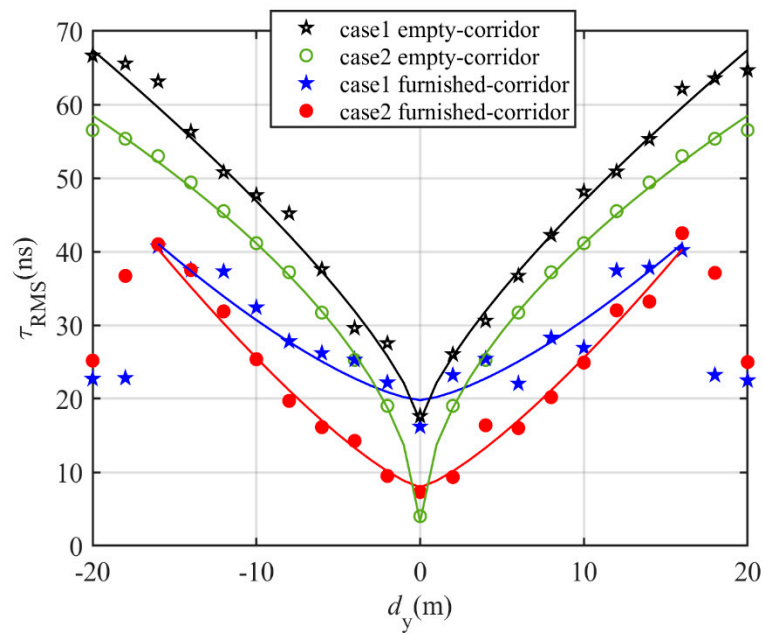


Figure 8. Comparison of a flat and curved OLEDs employed in the office in term of optical path loss (OPL).

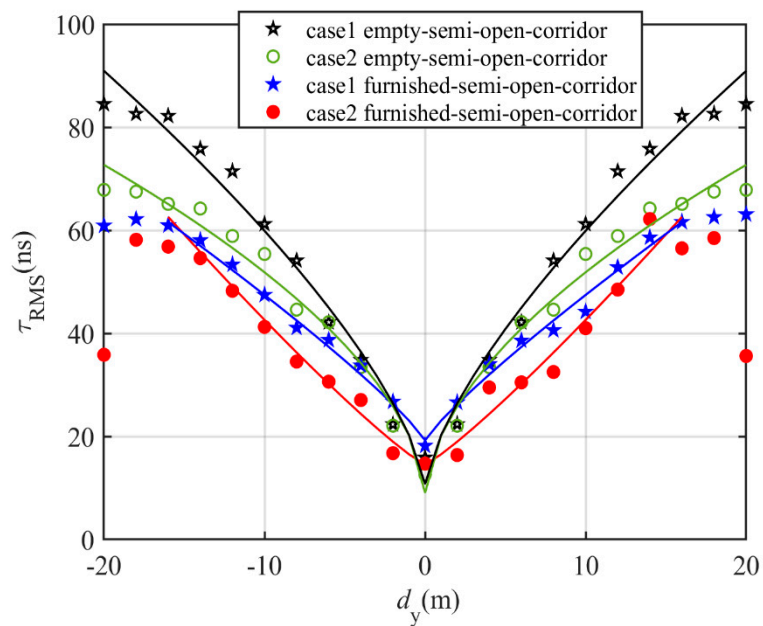
Table 3. Numerical modeling parameters for OPL in the case of using flat and curved OLEDs in office.

OLED Type	a_1	a_2	a_3
Curved	0.2964×10^{-2}	1.465	58.26
Flat	9.315×10^{-5}	2.646	56.42

Figures 9 and 10 illustrate the channel characteristics for both open and semi-open corridor when OLED are mounted on the inner shop wall behind the glass window and on the wall or shop window inside the corridor while the user is moving along the corridor in terms of OPL and τ_{RMS} . As can be seen, both OPL and τ_{RMS} plots show symmetry about the center of the indoor environment with minimum values at the center. Note, τ_{RMS} for furnished rooms is lower than the empty room for both corridor and semi open-corridor; e.g., in a semi-open corridor and case1, the τ_{RMS} values are 42.5 and 52.7 ns at 8 m and 52.2, 66.6 ns at 12 m for furnished and empty, respectively.

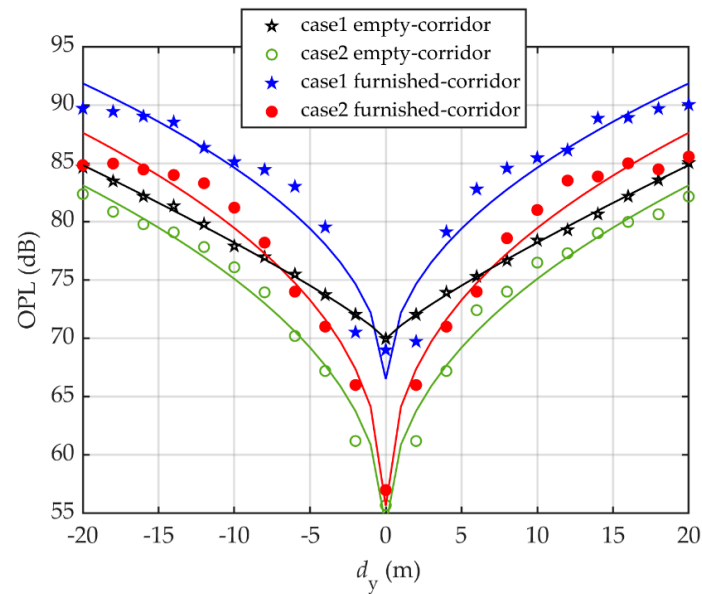


(a)

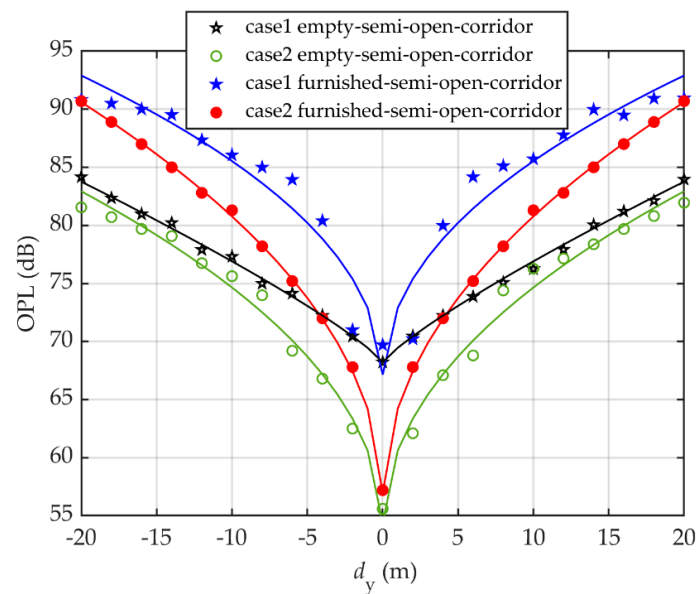


(b)

Figure 9. Channel characteristics in term of τ_{RMS} for both: (a) corridor, and (b) semi-open corridor environment; when OLED are mounted on the inner shop wall behind the glass window (case1) and on the wall or shop window inside the corridor (case2) while the user is moving along the corridor.



(a)



(b)

Figure 10. Channel characteristics in term of OPL for both: (a) corridor, and (b) semi-open corridor environment; when OLED are mounted on the inner shop wall behind the glass window (case1) and on the wall or shop window inside the corridor (case2) while the user is moving along the corridor.

In furnished environments, τ_{RMS} increases with the distance reaching the maximum value of 40 and 60 ns at a distance of 16 m for the corridor and semi-open corridor, respectively. In all environments, τ_{RMS} drop significantly for case2 compared with case1. Note, in both furnished environments, there is a huge drop in τ_{RMS} for case2 compared with case1 for d_y up to 10 m; however, for $d_y > 10$ m τ_{RMS} for case2 reaches the corresponding value of case1. E.g., in a furnished corridor, for case2, τ_{RMS} values are lower than case1 by 13, 6 and 2 ns at $d_y = 0, 8$ and 14 m, respectively. However, in an empty corridor τ_{RMS} for case2 drop by 11, 5 and 5 ns at $d_y = 0, 8$ and 14 m, respectively.

Note, positioning OLEDs behind the window will result in decreased received optical power compare with when located on the outer-wall of shops inside the corridor; i.e., OPL for case2 is lower than case1 in all empty and furnished indoor environments. For instance, in a furnished semi-open

corridor for case1, OPL penalties of 6.5, 4.8, 3.4, and 1.6 dB at 5, 10, 15, and 20 m, respectively, can be seen in comparison to case2. Additionally, for both cases, OPL in the corridor is lower compared with the semi-open corridor. e.g., in furnished environments and case2, OPL in the corridor reaches the maximum of 87.6 dB, which is lower than the value corresponding to the semi-open corridor (i.e., 90.7 dB). Note, the channel gain for both cases in furnished environments for $d_y < 4$ m remains the same; however, for case1 and $d_y > 4$ m, the OPL penalty of the furnished semi-open corridor is ~ 1 dB in contrary with the furnished corridor. For case2, there is a drop in OPL for the furnished corridor by 1.7 and 2.4 dB at d_y of longer distances of 10 and 15 m in comparison with the furnished semi-open corridor.

In addition, the channel gain enhancement in an empty corridor in contrary with furnished one is 5 dB at 5 m reaching 7 dB at 15 m for case1. However, for case2 it remains around 4 dB for $d_y > 4$ m. In addition, the channel gain enhancement in an empty semi-open corridor in contrary with furnished one are 7.2 and 5 dB at 5 m increasing to 9.1 and 7 dB at 15 m for case1 and case2, respectively.

Using a non-linear approximation algorithm for both cases in all environment, a two-term power series model have been derived from simulations for τ_{RMS} and OPL as a function of d_y given by

$$\tau_{\text{RMS}} = r_1 d_y^{r_2} + r_3, \quad (10)$$

$$\text{OPL} = l_1 d_y^{l_2} + l_3, \quad (11)$$

where the derived values of $r_1, r_2, r_3, l_1, l_2,$ and l_3 are summarized in Tables 4 and 5.

Table 4. Numerical modeling parameters for τ_{RMS} in both corridor and semi-open corridor.

Environment	r_1	r_2	r_3
case1 empty-corridor	5.32	0.7519	16.83
case2 empty-corridor	11.26	0.5358	2.446
case1 furnished-corridor	0.409	1.424	19.79
case2 furnished-corridor	0.890	1.296	7.947
case1 empty-semi-open corridor	9.777	0.7035	10.5
case2 empty-semi-open corridor	11.9	0.5637	8.267
case1 furnished-semi-open corridor	3.860	0.864	19.214
case2 furnished-semi-open corridor	2.020	1.143	14.513

Table 5. Numerical modeling parameters for OPL in both corridor and semi-open corridor.

Environment	l_1	l_2	l_3
case1 empty-corridor	1.160	0.852	69.95
case2 empty-corridor	7.893	0.446	53.01
case1 furnished-corridor	6.379	0.469	65.823
case2 furnished-corridor	10.010	0.403	54.130
case1 empty-semi-open corridor	1.265	0.838	68.190
case2 empty-semi-open corridor	6.946	0.480	53.670
case1 furnished-semi-open corridor	6.453	0.470	66.451
case2 furnished-semi-open corridor	8.039	0.485	56.180

4. Conclusions

In this paper, we investigated the performance of OLED-based VLC system and the channel characteristics in office, corridor, and semi-open environments. The measured beam pattern profile of the curved OLED was closely matched with the simulation result. We showed that, when a flat OLED was used in an office, τ_{RMS} increased significantly by 7.3 ns compared with 1 ns for the curved OLED. In the office, contrary to the flat OLED, the curved OLED showed improved BER performance over a wider range of θ . A data rate of 4 Mb/s was achieved using both the curved and flat OLEDs for θ within the range of $\pm 90^\circ$ and $\pm 53^\circ$, respectively. A two-term power series model was found to

match τ_{RMS} and OPL as a function of θ and d_y for the office and corridors, respectively and models' parameters for all three environments with and without furniture were derived. We showed that, when OLED is positioned on the outer wall of shops inside the corridor, the channel gain enhanced in contrast to them being located on inner shop wall, e.g., the channel gain enhanced by 5.2 and 4.8 dB at 10 m for furnished corridor and semi-open corridor, respectively. Moreover, the channel gain in the corridor was higher compared with the semi-open corridor. As a result, for case2, there was an enhancement in the channel gain for the furnished corridor by 1.7 and 2.4 dB at d_y of 10 and 15 m in comparison with the furnished semi-open corridor.

Author Contributions: The contributions of the authors in this paper are the following: conceptualization: Z.N.C., and S.Z.; investigation: Z.N.C., S.Z. and H.B.E.; methodology: Z.N.C., and S.Z.; project administration: S.Z., Z.G.; software: Z.N.C., and H.B.E.; validation: S.Z., Z.G., and M.U. All authors have read and agreed to the published version of the manuscript.

Funding: This work was supported by the European Union's Horizon 2020 Research and Innovation Programme, under the Marie Skłodowska-Curie grant agreement no 764461 (VisIoN).

Conflicts of Interest: The authors declare no conflict of interest. The funders had no role in the design of the study; in the collection, analyses, or interpretation of data; in the writing of the manuscript; or in the decision to publish the results.

References

1. Ghassemlooy, Z.; Alves, L.N.; Zvanovec, S.; Khalighi, M.A. *Visible Light Communications: Theory and Applications*; CRC Press: Boca Raton, FL, USA, 2017.
2. Karunatilaka, D.; Zafar, F.; Kalavally, V.; Parthiban, R. LED based indoor visible light communications: State of the art. *IEEE Commun. Surv. Tutor.* **2015**, *17*, 1649–1678. [[CrossRef](#)]
3. Wu, S.; Wang, H.; Youn, C.H. Visible light communications for 5G wireless networking systems: From fixed to mobile communications. *IEEE Netw.* **2014**, *28*, 41–45. [[CrossRef](#)]
4. Aguiar, L.; de Saa, P.; Guerra, V.; Perez-Jimenez, R. Survey of VLC and OCC Applications on Tourism Industry: Potentials & Challenges. In Proceedings of the 2020 South American Colloquium on Visible Light Communications (SACVC), Santiago, Chile, 1–6 June 2020.
5. Ji, R.; Wang, S.; Liu, Q.; Lu, W. High-speed visible light communications: Enabling technologies and state of the art. *Appl. Sci.* **2018**, *8*, 589. [[CrossRef](#)]
6. Pathak, P.H.; Feng, X.; Hu, P.; Mohapatra, P. Visible light communication, networking, and sensing: A survey, potential and challenges. *IEEE Commun. Surv. Tutor.* **2015**, *17*, 2047–2077. [[CrossRef](#)]
7. Karbalayghareh, M.; Miramirkhani, F.; Eldeeb, H.B.; Kizilirmak, R.C.; Sait, S.M.; Uysal, M. Channel Modelling and Performance Limits of Vehicular Visible Light Communication Systems. *IEEE Trans. Veh. Technol.* **2020**, *69*, 6891–6901. [[CrossRef](#)]
8. Cheong, Y.K.; Ng, X.W.; Chung, W.Y. Hazardless biomedical sensing data transmission using VLC. *IEEE Sens. J.* **2013**, *13*, 3347–3348. [[CrossRef](#)]
9. Quintana, C.; Guerra, V.; Rufo, J.; Rabadan, J.; Perez-Jimenez, R. Reading lamp-based visible light communication system for in-flight entertainment. *IEEE Trans. Consum. Electron.* **2013**, *59*, 31–37. [[CrossRef](#)]
10. Zhuang, Y.; Hua, L.; Qi, L.; Yang, J.; Cao, P.; Cao, Y.; Wu, Y.; Thompson, J.; Haas, H. A survey of positioning systems using visible LED lights. *IEEE Commun. Surv. Tutor.* **2018**, *20*, 1963–1988. [[CrossRef](#)]
11. Nuwanpriya, A.; Ho, S.W.; Chen, C.S. Indoor MIMO visible light communications: Novel angle diversity receivers for mobile users. *IEEE J. Sel. Areas Commun.* **2015**, *33*, 1780–1792. [[CrossRef](#)]
12. Eldeeb, H.B.; Selmy, H.A.; Elsayed, H.M.; Badr, R.I. Interference mitigation and capacity enhancement using constraint field of view ADR in downlink VLC channel. *IET Commun.* **2018**, *12*, 1968–1978. [[CrossRef](#)]
13. Chen, C.; Zhong, W.D.; Yang, H.; Zhang, S.; Du, P. Reduction of SINR fluctuation in indoor multi-cell VLC systems using optimized angle diversity receiver. *J. Lightw. Technol.* **2018**, *36*, 3603–3610. [[CrossRef](#)]
14. Hassan, N.B.; Ghassemlooy, Z.; Zvanovec, S.; Biagi, M.; Vegni, A.M.; Zhang, M.; Luo, P. Non-line-of-sight mimo space-time division multiplexing visible light optical camera communications. *J. Lightw. Technol.* **2019**, *37*, 2409–2417. [[CrossRef](#)]

15. Teli, S.R.; Matus, V.; Zvanovec, S.; Perez-Jimenez, R.; Vitek, S.; Ghassemlooy, Z. Optical Camera Communications for IoT-Rolling-Shutter Based MIMO Scheme with Grouped LED Array Transmitter. *Sensors* **2020**, *20*, 3361.
16. Strobel, N.; Droseros, N.; Köntges, W.; Seiberlich, M.; Pietsch, M.; Schliske, S.; Lindheimer, F.; Schröder, R.R.; Lemmer, U.; Pfannmöller, M.; et al. Color-Selective Printed Organic Photodiodes for Filterless Multichannel Visible Light Communication. *Adv. Mater.* **2020**, *32*, 1908258. [[CrossRef](#)] [[PubMed](#)]
17. Ghassemlooy, Z.; Arnon, S.; Uysal, M.; Xu, Z.; Cheng, J. Emerging optical wireless communications—advances and challenges. *IEEE J. Sel. Areas Commun.* **2015**, *33*, 1738–1749. [[CrossRef](#)]
18. Ghassemlooy, Z.; Popoola, W.; Rajbhandari, S. *Optical Wireless Communications: System and Channel Modelling with Matlab®*; CRC Press: Boca Raton, FL, USA, 2019.
19. Kalinowski, J. *Organic Light-Emitting Diodes: Principles, Characteristics & Processes*; CRC Press: Boca Raton, FL, USA, 2018.
20. Kafafi, Z.H. *Organic Electroluminescence*; CRC Press: Boca Raton, FL, USA, 2018.
21. Ghassemlooy, Z.; Khalighi, M.-A.; Dehao, W. Channel Modeling. In *Visible Light Communications: Theory and Applications*; CRC Press: Boca Raton, FL, USA, 2017; pp. 71–92.
22. Chun, H.; Chiang, C.-J.; O'Brien, D.C. Visible light communication using OLEDs: Illumination and channel modeling. In Proceedings of the 2012 International Workshop on Optical Wireless Communications (IWOW), Pisa, Italy, 22 October 2012; pp. 1–3.
23. Lee, K.; Park, H.; Barry, J.R. Indoor channel characteristics for visible light communications. *IEEE Commun. Lett.* **2011**, *15*, 217–219. [[CrossRef](#)]
24. Ramirez-Aguilera, A.; Luna-Rivera, J.; Guerra, V.; Rabadán, J.; Perez-Jimenez, R.; Lopez-Hernandez, F.J. A generalized multi-wavelength propagation model for VLC indoor channels using Monte Carlo simulation. *Trans. Emerg. Telecommun. Technol.* **2019**, *30*, e3490. [[CrossRef](#)]
25. Rodríguez, S.P.; Jiménez, R.P.; Mendoza, B.R.; Hernández, F.J.L.; Alfonso, A.J.A. Simulation of impulse response for indoor visible light communications using 3D CAD models. *EURASIP J. Wirel. Commun. Netw.* **2013**, *2013*, 7. [[CrossRef](#)]
26. Zemax OpticStudio 18.9. Available online: <http://www.zemax.com/products/opticstudio> (accessed on 10 October 2020).
27. Miramirkhani, F.; Uysal, M. Channel modeling and characterization for visible light communications. *IEEE Photonics J.* **2015**, *7*, 1–16. [[CrossRef](#)]
28. Uysal, M.; Miramirkhani, F.; Narmanlioglu, O.; Baykas, T.; Panayirci, E. IEEE 802.15. 7r1 reference channel models for visible light communications. *IEEE Commun. Mag.* **2017**, *55*, 212–217. [[CrossRef](#)]
29. Eldeeb, H.B.; Uysal, M.; Mana, S.M.; Hellwig, P.; Hilt, J.; Jungnickel, V. Channel modelling for light communications: Validation of ray tracing by measurements. In Proceedings of the 12th IEEE/IET International Symposium on Communication Systems, Networks and Digital Signal Processing (CSNDSP), Porto, Portugal, 20–22 July 2020.
30. Chen, H.; Xu, Z. OLED panel radiation pattern and its impact on VLC channel characteristics. *IEEE Photonics J.* **2017**, *10*, 1–10. [[CrossRef](#)]
31. Chaleshtori, Z.N.; Zvanovec, S.; Ghassemlooy, Z.; Eldeeb, H.B.; Uysal, M. A Flexible OLED VLC System for an Office Environment. In Proceedings of the 12th IEEE/IET International Symposium on Communication Systems, Networks and Digital Signal Processing (CSNDSP), Porto, Portugal, 20–22 July 2020.
32. Chaleshtori, Z.N.; Zvanovec, S.; Ghassemlooy, Z.; Eldeeb, H.B.; Uysal, M. Coverage of a shopping mall with flexible OLED-based visible light communications. *Opt. Express* **2020**, *28*, 10015–10026. [[CrossRef](#)] [[PubMed](#)]
33. Pinho, P. *Optical Communication Technology*; IntechOpen: London, UK, 2017.
34. Proakis, J.G.; Salehi, M. *Digital Communications*; McGraw-Hill: New York, NY, USA, 2001.

Publisher's Note: MDPI stays neutral with regard to jurisdictional claims in published maps and institutional affiliations.



© 2020 by the authors. Licensee MDPI, Basel, Switzerland. This article is an open access article distributed under the terms and conditions of the Creative Commons Attribution (CC BY) license (<http://creativecommons.org/licenses/by/4.0/>).

Conclusion and Future Work

This thesis provided theoretical, analytical and experimental analyses of utilization of OLEDs for VLC systems. The state-of-the-art was presented with an emphasis on the advantages and limitations of OLED devices and their utilization for VLC systems. The thesis is divided into three main parts. The first part proposes measurement setups for optical and electrical characterization of different types of OLEDs within the context of VLC systems. Based on publication [J1], the results showed that, the beam pattern of curved OLED is symmetrical and wider than Lambertian. I derived a numerical model for the beam pattern of curved OLED which follows the three-term Gaussian profile. Following, the use of those OLEDs in VLC system with *m*-CAP modulation was investigated experimentally. In which, the effect of curved OLED radiation pattern on the VLC link has been examined for the first time. The results published in [C3] showed that, the BER performance improved for the curved OLED with the viewing angles greater 40° when the optical receiver moving along a circular path compared to the flat OLED, which is advantageous in D2D communications.

The second part of the thesis was focused on the analysis of the ANN equalizer for the OVLC system. Since the learning algorithm of ANN significantly affects the ANN performance, the effect of various learning algorithms and a number of neurons in the hidden layer and quantify the link performance were investigated [C2].

Finally, the use of flexible OLED in a VLC system in furnished indoor environments (ie., shopping mall, office, corridor and semi-open corridor) was analyzed and showed the merits of adopting curved OLEDs in indoor VLC systems. The simulation was accomplished considering by the reflectance properties of the materials and objects in the room with respect to the visible range. Numerical models for RMS delay spread and OPL were derived, which followed a 2-term power series model.

The results for the shopping mall environment reported in [J2] showed that, in an empty room the average optical path losses are lower by 5 and 4 dB compared with the furnished room, where the full and half-circular OLEDs were used, respectively. In addition, for an empty room with full and half-circular OLEDs, R_b of 10 and 3.7 Mb/s were achieved at a distance of 6 m, respectively. In a furnished room with full and half-circular OLEDs, R_b of 1.02 and 0.46 Mb/s were recorded for a distance of 6 m, respectively. The results published in [C4], [C5] for a furnished office demonstrated a data rate of 4 Mb/s

using both the curved and flat OLEDs for the transmitter's half-angle within the range of $\pm 90^\circ$ and $\pm 53^\circ$, respectively.

[J3] showed the results achieved from VLC channel characteristics when large OLED panels are used as Tx in corridor and semi-open corridors while the user is then moving on a straight path along the corridor. It was shown that, for empty corridor and semi-open corridor there was a drop in OPL by 4.4 and 6.1 dB compared with furnished rooms for a link span of 10 m when OLED is positioned on outer-wall of shops. For OLED positioned on the outer wall of shops, it was shown that the channel gain enhanced in contrast to them being located on inner shop wall, e.g., the channel gain enhanced by 5.2 and 4.8 dB at 10 m for furnished corridor and semi-open corridor, respectively. Additionally, there was a channel gain enhancement for the corridor in comparison with a semi-open corridor, e.g., for the furnished corridor the channel gain enhancements were recorded as 1.7 and 2.4 dB at distances of 10 and 15 m in comparison with the semi-open corridor.

The main suggestions of the author for the future works are as follows:

- At the final stage of the development of OVLC systems, the upcoming work would be focused on D2D communication performed by transmitting and receiving the information data via the smartphone's OLED-based display pixels and the built-in cameras including by user movement and orientation.
- Another work can be analyzing of shadowing impact for D2D communication while one of users is consider as a source of shadowing in the indoor environment. In addition, compensating shadowing impacts on such scenarios can be investigated, for instance PDs with different viewing angles can be operated.
- Considering that the interest in using OLED panels/displays in wearable products such as wearable smart watches/clothes is increasing. Hence, analyzing of D2D communication when Tx is OLED pixel used in wearable products would demonstrate an intention to move towards smart homes.
- The use of OPDs with different specifications in OVLC systems, particularly for single input multiple output (SIMO) and multiple input multiple output (MIMO) systems, would be an important development for OVLC systems. Massively MIMO systems could be implemented to offer D2D communications in the context of smart homes.



References

- [1] M. Uysal and H. Nouri, “Optical wireless communications — an emerging technology,” in *2014 16th International Conference on Transparent Optical Networks (ICTON)*, July 2014, pp. 1–7.
- [2] S. Bloom, E. Korevaar, J. Schuster, and H. Willebrand, “Understanding the performance of free-space optics,” *Journal of optical Networking*, vol. 2, no. 6, pp. 178–200, 2003.
- [3] J. M. Kahn and J. R. Barry, “Wireless infrared communications,” *Proceedings of the IEEE*, vol. 85, no. 2, pp. 265–298, 1997.
- [4] Z. Ghassemlooy, L. N. Alves, S. Zvanovec, and M.-A. Khalighi, *Visible light communications: theory and applications*. CRC press, 2017.
- [5] P. A. Haigh, Z. Ghassemlooy, S. Rajbhandari, and I. Papakonstantinou, “Visible light communications using organic light emitting diodes,” *IEEE Communications Magazine*, vol. 51, no. 8, pp. 148–154, 2013.
- [6] P. Binh and N. Hung, “High-speed visible light communications using znse-based white light emitting diode,” *IEEE Photonics Technology Letters*, vol. 28, no. 18, pp. 1948–1951, 2016.
- [7] P. H. Pathak, X. Feng, P. Hu, and P. Mohapatra, “Visible light communication, networking, and sensing: A survey, potential and challenges,” *IEEE communications surveys & tutorials*, vol. 17, no. 4, pp. 2047–2077, 2015.
- [8] Z. Ghassemlooy, W. Popoola, and S. Rajbhandari, *Optical wireless communications: system and channel modelling with Matlab®*. CRC press, 2019.
- [9] J. Yang, Z. Liu, B. Xue, Z. Liao, L. Feng, N. Zhang, J. Wang, and J. Li, “Highly uniform white light-based visible light communication using red, green, and blue laser diodes,” *IEEE Photonics Journal*, vol. 10, no. 2, pp. 1–8, 2018.
- [10] T.-C. Wu, Y.-C. Chi, H.-Y. Wang, C.-T. Tsai, Y.-F. Huang, and G.-R. Lin, “Tricolor r/g/b laser diode based eye-safe white lighting communication beyond 8 gbit/s,” *Scientific reports*, vol. 7, no. 1, pp. 1–10, 2017.
- [11] B. Lin, Z. Ghassemlooy, C. Lin, X. Tang, Y. Li, and S. Zhang, “An indoor visible light positioning system based on optical camera communications,” *IEEE Photonics Technology Letters*, vol. 29, no. 7, pp. 579–582, 2017.
- [12] P. Luo, M. Zhang, Z. Ghassemlooy, S. Zvanovec, S. Feng, and P. Zhang, “Undersampled-based modulation schemes for optical camera communications,” *IEEE Communications Magazine*, vol. 56, no. 2, pp. 204–212, 2018.
- [13] M.-A. Khalighi, C. J. Gabriel, L. M. Pessoa, and B. Silva, “Underwater visible light communications, channel modeling and system design,” in *Visible Light Communications*. CRC Press, 2017, pp. 337–372.
- [14] D. Krichene, M. Sliti, W. Abdallah, and N. Boudriga, “An aeronautical visible light commu-

- nication system to enable in-flight connectivity,” in *2015 17th International Conference on Transparent Optical Networks (ICTON)*. IEEE, 2015, pp. 1–6.
- [15] D. R. Dhatchayeny, A. Sewaiwar, S. V. Tiwari, and Y. H. Chung, “Experimental biomedical eeg signal transmission using vlc,” *IEEE sensors Journal*, vol. 15, no. 10, pp. 5386–5387, 2015.
- [16] F. R. Gfeller and U. Bapst, “Wireless in-house data communication via diffuse infrared radiation,” *Proceedings of the IEEE*, vol. 67, no. 11, pp. 1474–1486, Nov 1979.
- [17] A. R. Ndjiongue, H. C. Ferreira, and T. M. Ngatched, “Visible light communications (vlc) technology,” *Wiley Encyclopedia of Electrical and Electronics Engineering*, pp. 1–15, 1999.
- [18] Y. Tanaka, S. Haruyama, and M. Nakagawa, “Wireless optical transmissions with white colored led for wireless home links,” in *11th IEEE International Symposium on Personal Indoor and Mobile Radio Communications. PIMRC 2000. Proceedings (Cat. No. 00TH8525)*, vol. 2. IEEE, 2000, pp. 1325–1329.
- [19] IEEE, “IEEE Standard for Local and Metropolitan Area Networks-Part 15.7: Short-Range Wireless Optical Communication Using Visible Light,” *IEEE Std. 802.15.7*, 2011.
- [20] S. Rajagopal, R. Roberts, and S. Lim, “IEEE 802.15.7 visible light communication: modulation schemes and dimming support,” *IEEE Commun. Mag.*, vol. 50, pp. 72–82, 2012.
- [21] B. Geffroy, P. Le Roy, and C. Prat, “Organic light-emitting diode (oled) technology: materials, devices and display technologies,” *Polymer international*, vol. 55, no. 6, pp. 572–582, 2006.
- [22] T. Komine, S. Member, and M. Nakagawa, “Fundamental Analysis for Visible-Light Communication System using LED Lights,” *IEEE Trans. Consum.*, vol. 50, pp. 100–107, 2004.
- [23] T. Komine and M. Nakagawa, “Fundamental analysis for visible-light communication system using led lights,” *IEEE transactions on Consumer Electronics*, vol. 50, no. 1, pp. 100–107, 2004.
- [24] S. Trisno, “Design and analysis of advanced free space optical communication systems,” Ph.D. dissertation, 2006.
- [25] J.-H. Liu, Q. Li, and X.-Y. Zhang, “Cellular coverage optimization for indoor visible light communication and illumination networks,” *J. Commun*, vol. 9, no. 11, pp. 891–898, 2014.
- [26] H. Le Minh, D. O’Brien, G. Faulkner, L. Zeng, K. Lee, D. Jung, Y. Oh, and E. T. Won, “100-mb/s nrz visible light communications using a postequalized white led,” *IEEE Photonics Technology Letters*, vol. 21, no. 15, pp. 1063–1065, 2009.
- [27] P. Haigh, “Using equalizers to increase data rates in organic photonic devices for visible light communications systems,” Ph.D. dissertation, University of Northumbria, 2014.
- [28] A. H. Sayed, *Fundamentals of adaptive filtering*. John Wiley & Sons, 2003.
- [29] Y. Sari, “Performance evaluation of the various training algorithms and network topologies in a neural-network-based inverse kinematics solution for robots,” *International Journal of Advanced Robotic Systems*, vol. 11, no. 4, p. 64, 2014.
- [30] S. S. Haykin *et al.*, “Neural networks and learning machines/simon haykin.” 2009.
- [31] S. Haykin and N. Network, “A comprehensive foundation,” *Neural networks*, vol. 2, no. 2004, p. 41, 2004.
- [32] V. Vacic, “Summary of the training functions in matlab’s nn toolbox,” *Computer Science Department at the University of California*, 2005.
- [33] K. Burse, R. N. Yadav, and S. Shrivastava, “Channel equalization using neural networks:

- A review,” *IEEE transactions on systems, man, and cybernetics, Part C (Applications and Reviews)*, vol. 40, no. 3, pp. 352–357, 2010.
- [34] M. F. Møller, *A scaled conjugate gradient algorithm for fast supervised learning*. Aarhus University, Computer Science Department, 1990.
- [35] S. Zvanovec, P. Chvojka, P. A. Haigh, and Z. Ghassemlooy, “Visible light communications towards 5g,” *Radioengineering*, vol. 24, no. 1, pp. 1–9, 2015.
- [36] K. Lee and H. Park, “Modulations for visible light communications with dimming control,” *IEEE photonics technology letters*, vol. 23, no. 16, pp. 1136–1138, 2011.
- [37] —, “Channel model and modulation schemes for visible light communications,” in *2011 IEEE 54th International Midwest Symposium on Circuits and Systems (MWSCAS)*. IEEE, 2011, pp. 1–4.
- [38] J. Zhao and A. D. Ellis, “A novel optical fast ofdm with reduced channel spacing equal to half of the symbol rate per carrier,” in *Optical Fiber Communication Conference*. Optical Society of America, 2010, p. OMR1.
- [39] S. Yamamoto, K. Yonenaga, A. Sahara, F. Inuzuka, and A. Takada, “Achievement of subchannel frequency spacing less than symbol rate and improvement of dispersion tolerance in optical ofdm transmission,” *Journal of lightwave technology*, vol. 28, no. 1, pp. 157–163, 2009.
- [40] G. Bosco, V. Curri, A. Carena, P. Poggiolini, and F. Forghieri, “On the performance of nyquist-wdm terabit superchannels based on pm-bpsk, pm-qpsk, pm-8qam or pm-16qam subcarriers,” *Journal of Lightwave Technology*, vol. 29, no. 1, pp. 53–61, 2010.
- [41] W.-R. Peng, B. Zhang, K.-M. Feng, X. Wu, A. E. Willner, and S. Chi, “Spectrally efficient direct-detected ofdm transmission incorporating a tunable frequency gap and an iterative detection techniques,” *Journal of Lightwave Technology*, vol. 27, no. 24, pp. 5723–5735, 2009.
- [42] I. Darwazeh, T. Xu, T. Gui, Y. Bao, and Z. Li, “Optical sefdm system; bandwidth saving using non-orthogonal sub-carriers,” *IEEE Photonics Technology Letters*, vol. 26, no. 4, pp. 352–355, 2013.
- [43] F. Wu, C. Lin, C. Wei, C. Chen, Z. Chen, H. Huang, and S. Chi, “Performance comparison of ofdm signal and cap signal over high capacity rgb-led-based wdm visible light communication,” *IEEE Photonics Journal*, vol. 5, no. 4, pp. 7901507–7901507, 2013.
- [44] P. A. Haigh, S. T. Le, S. Zvanovec, Z. Ghassemlooy, P. Luo, T. Xu, P. Chvojka, T. Kanesan, E. Giacomidis, P. Canyelles-Pericas *et al.*, “Multi-band carrier-less amplitude and phase modulation for bandlimited visible light communications systems,” *IEEE Wireless Communications*, vol. 22, no. 2, pp. 46–53, 2015.
- [45] P. A. Haigh, A. Burton, K. Werfli, H. Le Minh, E. Bentley, P. Chvojka, W. O. Popoola, I. Papakonstantinou, and S. Zvanovec, “A multi-cap visible-light communications system with 4.85-b/s/hz spectral efficiency,” *IEEE Journal on Selected Areas in Communications*, vol. 33, no. 9, pp. 1771–1779, 2015.
- [46] P. Chvojka, S. Zvanovec, K. Werfli, P. A. Haigh, and Z. Ghassemlooy, “Variable m-cap for bandlimited visible light communications,” in *2017 IEEE International Conference on Communications Workshops (ICC Workshops)*. IEEE, 2017, pp. 1–5.
- [47] K. Bandara, P. Niroopan, and Y.-H. Chung, “Papr reduced ofdm visible light communication using exponential nonlinear companding,” in *2013 IEEE International Conference on Mi-*

- crowaves, Communications, Antennas and Electronic Systems (COMCAS 2013)*. IEEE, 2013, pp. 1–5.
- [48] X. Zhang, P. Liu, J. Liu, and S. Liu, “An advanced a-law companding algorithm in vlc-ofdm,” in *2014 IEEE 3rd Global Conference on Consumer Electronics (GCCE)*. IEEE, 2014, pp. 721–722.
- [49] Z. Ghassemlooy, C. Ma, S. Guo *et al.*, “Papr reduction scheme for aco-ofdm based visible light communication systems,” *Optics Communications*, vol. 383, pp. 75–80, 2017.
- [50] Z. N. Chaleshtori, P. Chvojka, S. Zvanovec, Z. Ghassemlooy, and P. A. Haigh, “A survey on recent advances in organic visible light communications,” in *2018 11th International Symposium on Communication Systems, Networks & Digital Signal Processing (CSNDSP)*. IEEE, 2018, pp. 1–6.
- [51] P. A. Haigh, F. Bausi, T. Kanesan, S. T. Le, S. Rajbhandari, Z. Ghassemlooy, I. Papakonstantinou, W. Popoola, A. Burton, H. Le Minh *et al.*, “A 20-mb/s vlc link with a polymer led and a multilayer perceptron equalizer,” *IEEE Photonics Technology Letters*, vol. 26, no. 19, pp. 1975–1978, 2014.
- [52] J. Fontanella, C. Andeen, and D. Schuele, “Pressure and temperature derivatives of the low-frequency dielectric constants of lif, naf, nacl, nabr, kcl, and kbr,” *Physical review B*, vol. 6, no. 2, p. 582, 1972.
- [53] P. Haigh, Z. Ghassemlooy, S. Le, F. Bausi, H. Le Minh, F. Cacialli, and I. Darwazeh, “Organic visible light communications: Methods to achieve 10 mb/s,” in *2017 IEEE Photonics Conference (IPC)*. IEEE, 2017, pp. 553–554.
- [54] H. Chen and Z. Xu, “Oled panel radiation pattern and its impact on vlc channel characteristics,” *IEEE Photonics Journal*, vol. 10, no. 2, pp. 1–10, 2017.
- [55] N. Strobel, N. Droseros, W. Köntges, M. Seiberlich, M. Pietsch, S. Schlisske, F. Lindheimer, R. R. Schröder, U. Lemmer, M. Pfannmöller *et al.*, “Color-selective printed organic photodiodes for filterless multichannel visible light communication,” *Advanced materials*, vol. 32, no. 12, p. 1908258, 2020.
- [56] K.-J. Baeg, M. Binda, D. Natali, M. Caironi, and Y.-Y. Noh, “Organic light detectors: photodiodes and phototransistors,” *Advanced materials*, vol. 25, no. 31, pp. 4267–4295, 2013.
- [57] C. Vega-Colado, B. Arredondo, J. C. Torres, E. López-Fraguas, R. Vergaz, D. Martín-Martín, G. Del Pozo, B. Romero, P. Apilo, X. Quintana *et al.*, “An all-organic flexible visible light communication system,” *Sensors*, vol. 18, no. 9, p. 3045, 2018.
- [58] B. Arredondo, B. Romero, J. M. S. Pena, A. Fernández-Pacheco, E. Alonso, R. Vergaz, and C. De Dios, “Visible light communication system using an organic bulk heterojunction photodetector,” *Sensors*, vol. 13, no. 9, pp. 12 266–12 276, 2013.
- [59] P. Peumans, V. Bulović, and S. Forrest, “Efficient, high-bandwidth organic multilayer photodetectors,” *Applied Physics Letters*, vol. 76, no. 26, pp. 3855–3857, 2000.
- [60] T. Hamasaki, T. Morimune, H. Kajii, S. Minakata, R. Tsuruoka, T. Nagamachi, and Y. Ohmori, “Fabrication and characteristics of polyfluorene based organic photodetectors using fullerene derivatives,” *Thin Solid Films*, vol. 518, no. 2, pp. 548–550, 2009.
- [61] Y. Ohmori, T. Hamasaki, H. Kajii, and T. Morimune, “Organic photo sensors operating at high speed utilizing poly (9, 9-dioctylfluorene) derivative and fullerene derivative fabricated by

- solution process,” in *Optical Sensors 2009*, vol. 7356. International Society for Optics and Photonics, 2009, p. 73560W.
- [62] T. Morimune, H. Kajii, and Y. Ohmori, “Photoresponse properties of a high-speed organic photodetector based on copper–phthalocyanine under red light illumination,” *IEEE photonics technology letters*, vol. 18, no. 24, pp. 2662–2664, 2006.
- [63] W.-W. Tsai, Y.-C. Chao, E.-C. Chen, H.-W. Zan, H.-F. Meng, and C.-S. Hsu, “Increasing organic vertical carrier mobility for the application of high speed bilayered organic photodetector,” *Applied Physics Letters*, vol. 95, no. 21, p. 306, 2009.
- [64] P. A. Haigh, Z. Ghassemlooy, H. Le Minh, S. Rajbhandari, F. Arca, S. F. Tedde, O. Hayden, and I. Papakonstantinou, “Exploiting equalization techniques for improving data rates in organic optoelectronic devices for visible light communications,” *Journal of lightwave technology*, vol. 30, no. 19, pp. 3081–3088, 2012.
- [65] H. Chen, Z. Xu, Q. Gao, and S. Li, “A 51.6 mb/s experimental vlc system using a monochromic organic led,” *IEEE Photonics Journal*, vol. 10, no. 2, pp. 1–12, 2017.
- [66] P. A. Haigh, Z. Ghassemlooy, and I. Papakonstantinou, “1.4-mb/s white organic led transmission system using discrete multitone modulation,” *IEEE Photonics Technology Letters*, vol. 25, no. 6, pp. 615–618, 2013.
- [67] H. Le Minh, Z. Ghassemlooy, A. Burton, and P. A. Haigh, “Equalization for organic light emitting diodes in visible light communications,” in *2011 IEEE GLOBECOM Workshops (GC Wkshps)*. IEEE, 2011, pp. 828–832.
- [68] Z. Ghassemlooy, “Oled-based visible light communications,” in *2012 IEEE Photonics Society Summer Topical Meeting Series*. IEEE, 2012, pp. 102–104.
- [69] S. T. Le, T. Kanesan, F. Bausi, P. Haigh, S. Rajbhandari, Z. Ghassemlooy, I. Papakonstantinou, W. O. Popoola, A. Burton, H. Le Minh *et al.*, “10 mb/s visible light transmission system using a polymer light-emitting diode with orthogonal frequency division multiplexing,” *Optics letters*, vol. 39, no. 13, pp. 3876–3879, 2014.
- [70] P. A. Haigh, F. Bausi, H. Le Minh, I. Papakonstantinou, W. O. Popoola, A. Burton, and F. Cacialli, “Wavelength-multiplexed polymer leds: Towards 55 mb/s organic visible light communications,” *IEEE Journal on Selected Areas in Communications*, vol. 33, no. 9, pp. 1819–1828, 2015.
- [71] Z. Ghassemlooy, P. A. Haigh, F. Arca, S. F. Tedde, O. Hayden, I. Papakonstantinou, and S. Rajbhandari, “Visible light communications: 3.75 mbits/s data rate with a 160 khz bandwidth organic photodetector and artificial neural network equalization,” *Photonics Research*, vol. 1, no. 2, pp. 65–68, 2013.
- [72] P. A. Haigh, Z. Ghassemlooy, I. Papakonstantinou, F. Arca, S. F. Tedde, O. Hayden, and E. Leitgeb, “A 1-mb/s visible light communications link with low bandwidth organic components,” *IEEE photonics technology letters*, vol. 26, no. 13, pp. 1295–1298, 2014.
- [73] H. Chen, S. Li, B. Huang, Z. Xu, W. Li, G. Dong, and J. Xie, “A 1.9 mbps ofdm-based all-organic visible light communication system,” in *2016 IEEE International Conference on Communication Systems (ICCS)*. IEEE, 2016, pp. 1–6.
- [74] P. Chvojka, P. Dvorak, P. Pesek, S. Zvanovec, P. A. Haigh, and Z. Ghassemlooy, “Characterization of the organic led based visible light communications,” in *2016 10th International*

- Symposium on Communication Systems, Networks and Digital Signal Processing (CSNDSP)*. IEEE, 2016, pp. 1–4.
- [75] X. Li, H. Chen, S. Li, Q. Gao, C. Gong, and Z. Xu, “Volterra-based nonlinear equalization for nonlinearity mitigation in organic vlc,” in *2017 13th International Wireless Communications and Mobile Computing Conference (IWCMC)*. IEEE, 2017, pp. 616–621.
- [76] S. Zhang, D. Tsonev, S. Videv, S. Ghosh, G. A. Turnbull, I. D. Samuel, and H. Haas, “Organic solar cells as high-speed data detectors for visible light communication,” *Optica*, vol. 2, no. 7, pp. 607–610, 2015.






Author's Publications






List of Author's Publications Related to the Doctoral Thesis

All authors contributed equally unless otherwise stated.

Papers in Peer-Reviewed Journals with Impact Factor:

- [J1] **Z. N. Chaleshtori**, A. Burton, S. Zvanovec, Z. Ghassemlooy, P. Chvojka, “Comprehensive optical and electrical characterization and evaluation of organic light-emitting diodes for visible light communication”, *Optical Engineering*, 59(4), pp. 046106, 2020. 
- [J2] **Z. N. Chaleshtori**, S. Zvanovec, Z. Ghassemlooy, H. B. Eldeeb, and M. Uysal, “Coverage of a shopping mall with flexible OLED-based visible light communications”, *Optics Express*, 28(7), pp. 10015-10026, 2020. 
- [J3] **Z. N. Chaleshtori**, S. Zvanovec, Z. Ghassemlooy, H. B. Eldeeb, and M. Uysal, “Utilization of an OLED-based VLC System in Office, Corridor and Semi-open Corridor Environments”, *Sensors*, 20(23), pp. 6869, 2020. 

Papers and Abstracts in Conference Proceedings Listed in the Web of Knowledge:

- [C1] **Z. N. Chaleshtori**, P. Chvojka, S. Zvanovec, Z. Ghassemlooy, P.A. Haigh, "A Survey on Recent Advances in organic visible light communications," 11th International Symposium on Communication Systems, Networks and Digital Signal Processing (CSNDSP) conference, pp. 1-6, IEEE, 2018. 
- [C2] **Z. N. Chaleshtori**, P. A. Haigh, P. Chvojka, S. Zvanovec, Z. Ghassemlooy, "Performance Evaluation of Various Training Algorithms for ANN Equalization in Organic Visible Light Communications," 2ed West Asian Colloquium on Optical Wireless Communications (WACOWC2019) conference, 2019. 
- [C3] **Z. N. Chaleshtori**, A. Burton, Z. Ghassemlooy, S. Zvanovec, "Flexible OLED based VLC Link with m-CAP Modulation," The 15th International Conference on Telecommunications, Graz, Austria, ConTEL 2019. 
- [C4] **Z. N. Chaleshtori**, S. Zvanovec, Z. Ghassemlooy, H. B. Eldeeb, and M. Uysal, "A Flexible OLED VLC System for an Office Environment," In 12th IEEE/IET International Symposium on Communication Systems, Networks and Digital Signal Processing (CSNDSP), Porto, Portugal, 2020. 
- [C5] **Z. N. Chaleshtori**, S. Zvanovec, Z. Ghassemlooy, "Performance of an Indoor Flexible OLED-based VLC Link," In 27th International Conference on Telecommunications (ICT) (pp. 1-5). IEEE, 2020. 

Citations in Web of Knowledge and Scopus (except self-citations):

Journal Paper [J2]:

- [J2,Cit1] Xiu-min, G.A.O., Yue-feng, L.I.U., Hai-jing, Z.H.A.N.G., Tian-run, Z.H.A.N.G., Da, Y.I.N. and Jing, F.E.N.G., "Nano-imprint structure for organic light emitting device and organic laser", Chinese Journal of Liquid Crystal Displays, 36(2), 2021.
- [J2,Cit2] Eldeeb, H.B., Al-Nahhal, M., Selmy, H.A. and Abd El-Samie, F.E., "Continuous phase modulation with chaotic interleaving for visible light communication systems based on orthogonal frequency division multiplexing", Transactions on Emerging Telecommunications Technologies, 31(10), p.e4100, 2020.

Journal Paper [J3]:

- [J3,Cit1] Li, X., Ghassemlooy, Z., Zvánovec, S. and Haigh, P.A., "A 40 Mb/s VLC System Reusing an Existing Large LED Panel in an Indoor Office Environment", Sensors, 21(5), p.1697, 2021.

[J3,Cit2] Chaudhary, N., Younus, O.I., Alves, L.N., Ghassemlooy, Z., Zvanovec, S. and Le-Minh, H., "An Indoor Visible Light Positioning System Using Tilted LEDs with High Accuracy", *Sensors*, 21(3), p.920, 2021.

Conference Paper [C1]:

[C1,Cit1] Gojanović, Jovana P. "Organic Semiconductors in Optical Communications", 27th Telecommunications Forum (TELFOR). IEEE, 2019.

[C1,Cit2] Manousiadis, Pavlos P., Yoshida, K., Turnbull, Graham A., et al. "Organic semiconductors for visible light communications", *Philosophical Transactions of the Royal Society A-Mathematical, Physical and Engineering Sciences*, 378(2169), pp.20190186, 2020.

[C1,Cit3] Wang, N., Wang, P., Alipour-Fanid, A., Jiao, L. and Zeng, K., "Physical-layer security of 5G wireless networks for IoT: Challenges and opportunities", *IEEE Internet of Things Journal*, 6(5), pp.8169-8181, 2019


Conference Paper [C2]:

[C3,Cit1] Pešek, P., Haigh, P.A., Younus, O.I., Chvojka, P., Ghassemlooy, Z. and Zvánovec, S., "Experimental multi-user VLC system using non-orthogonal multi-band CAP modulation", *Optics Express*, 28(12), pp.18241-18250, 2020.



[C3,Cit2] Ha, Y., Niu, W. and Chi, N., "High spectrum compression scheme based on DNN post equalization for multiband quadrature dual-quaternary coded FTN CAP 49QAM signals in visible light communication system", *Microwave and Optical Technology Letters*, 62(9), pp.3066-3076, 2020.

List of author's publications non-related to the doctoral thesis







Papers in Peer-Reviewed Journals with Impact Factor:

- [J4] **Z.N. Chaleshtori**, A. Gholami, Z.Ghassemlooy, M.Sedghi, "Experimental Investigation of Environment Effects on the FSO Link with Turbulence," *Photonics Technology Letters (PTL)*, 2017. 

Papers and Abstracts in Conference Proceedings Listed in the Web of Knowledge:

- [C6] **Z. N. Chaleshtori**, A. Gholami, Z. Ghassemlooy, S. Zvanovec, "Experimental Investigation of the Effective Spectrum Bandwidth of the FSO Link with Scintillation," 1st West Asian Colloquium on Optical Wireless Communications (WACOWC2018) conference, 2018. 
- [C7] **Z.N. Chaleshtori**, A. Gholami, M.Sedghi, Z.Vali, Z.Ghassemlooy "Experimental Investigation of Scintillation Effect on FSO Channel" in Proc. of 24th International Iranian Conference on Electrical Engineering (ICEE), IEEE, pp. 1629-1633, 2016. 

Zahra Nazarichaleshtori

 22.01.1988  nazarzah@fel.cvut.cz  Prague, Czech Republic  Female
 Researchgate  Google Scholar


EDUCATION

P.h.D. Study in Radioelectronics

 Czech Technical University in Prague (CTU)  Since December 2017

- Thesis: "Organic LED-based Visible Light Communication"
- Under supervision of Prof. Stanislav Zvánovec ([email](#)) and Prof. Zabih Ghassemlooy ([email](#))
- The project is supported by the European Union's Horizon 2020 research and innovation programme under the Marie Skłodowska-Curie grant agreement no 764461 ([VISION](#))

M.Sc. in Electrical Engineering (Electro-Optics)

 Isfahan University of Technology (IUT), Isfahan, Iran  September 2013 – January 2016

- Thesis: "Design, Simulation and Experimental Investigation of environmental effects on a FSO Link"
- Under supervision of Dr. Asghar Gholami ([email](#))

B.Sc. in Electrical engineering - Electronics

 Shahrekord University, Iran  September 2007 – February 2012

- Thesis: "Simulation and Experimental Investigation of an Active and Reactive Power Calculator by AVR"
- Under supervision of Dr. Gholamreza Arab
- Traineeship: Mohajer technical and vocational college of Isfahan, Iran. (PLC Software)

ACADEMIC EXPERIENCES

International Visits

- Researcher at Northumbria University, Newcastle, United Kingdom. (A secondment as a part of VISION project), Instructor: Prof. Zabih Ghassemlooy

Research Assistant

- Research Assistant of Optoelectronics and Optical Communications Research Laboratory, Isfahan University of Technology, Instructor: Dr. Asghar Gholami
- Research Assistant of Optics Laboratory, Isfahan University of Technology, Instructor: Dr. Reza Safian

Teaching Experiences

- Lecturer at Arad Institute, Isfahan, Iran. (AVR Microcontrollers, C++ Programming, Fundamentals of Digital Design, Fundamentals of Robotics and Electronics for high school students)
- Teaching Assistant of AVR Microcontrollers lab, Isfahan University of Technology, Instructor: Dr. Nader Karimi
- Teaching Assistant of AVR Microcontrollers lab, Shahrekord University, Instructor: Dr. Hamed Saghaei

AWARDS AND ACHIEVEMENTS

- **Programming Languages & Microprocessor Programming:** C, C++, AVR (CodeVisionAVR)
- **Computer software:** MATLAB, Zemax Opticstudio, OrCAD, PSpice, Proteus, Altium Designer
- **Practical Skills:** Design of Optical Wireless Systems and Optical Components
- **Typesetting:** LaTeX, Microsoft Office
- **Language:** Persian (Native), English (Fluent), Czech (A2)
- **Leisure Activities:** Swimming, Volleyball